Damage Location and Estimation in Large Space Structures

by

Gregory Brian Twitty

Thesis submitted to the Faculty of the

Virginia Polytechnic Institute and State University

in partial fulfillment of the requirements for the degree of

MASTER OF SCIENCE

in

Electrical Engineering

APPROVED:

Douglas K. Lindner, Chairman

William T. Baumann

John S. Bay

April 1993

Blacksburg, Virginia

Damage Location and Estimation in Large Space Structures

by

Greg B. Twitty
Committee Chairman: Douglas K. Lindner
Electrical Engineering
(ABSTRACT)

This thesis presents a unique method of damage detection in large space structures. The goal is to develop an efficient algorithm which can be automated in an on-line format, and can asses damage in many elements. Theses are goals not realized by current methods. Damage incurred in a structural member is modeled as a linear reduction in that member's modulus of elasticity. The damaged structure's global stiffness matrix is expressed as the healthy global stiffness matrix minus some perturbation matrix. A vector expression of the perturbation matrix allows the percent reduction in damage to be solved for exactly in an equation involving the healthy truss model and a mode identified from the damaged structure. An algorithm for locating and estimating single-element damage is built around this equation. Simulations of the algorithm are performed on two planar truss models.

The vector expression of the damage perturbation is shown to lead to a mode shape – strain energy relationship. From this, it is shown that a smaller truss model can be computed from element stiffness vectors. Damage can then be detected as existing among a small group of elements. Simulations show detection in one group to be independent from damage in other groups. From this information, a dimensionally expanded version of the single-element detection method can be used to exactly locate and estimate damage in many elements simultaneously. This process is presented as a sequential algorithm which meets all of the desired criteria.

ACKNOWLEDGEMENTS

Many people are very deserving of my sincere gratitude for their help and support during the creation of this work. I would like to thank my father, Roy Twitty, who inspired me to return to school. I owe much to my mother and stepfather, Roy and Edith Tanner, for their financial support and motivation over my entire scholastic career. The support and hospitality of Mary and Jackson Siler is also greatly appreciated. I would like to dedicate this work to my wife, Beverly Twitty, who's constant support, patience and sacrifice made this work possible.

I thank Dr. Baumann and Dr. Bay for their patience, their input, and the resources they made available to me. I would like to especially thank my advisor, Dr. Lindner for giving me the opportunity to do research in a unique and fascinating field. His guidance and patience were substantial and greatly appreciated. Under his tutelage, I have learned an immense amount about research and technical literature.

TABLE OF CONTENTS

Page

1.0 Introduction 1

2.0 Survey of Damage Detection Methods 6
2.1 Early Work in Damage Detection 6
2.2 Model Refinement in Damage Detection 7
2.2.1 Optimal Updates 9
2.2.2 Eigenstructure Assignment 13
2.2.3 Sensitivity 16
2.2.4 Submatrix Adjustment 17
2.3 Other Methods 19
2.4 Summary 21

3.0 Healthy and Damaged Truss Models 23
3.1 The Finite Element Method 23
3.1.1 Element Equations of Motion 24
3.1.2 Coordinate Transformation 28
3.1.3 Natural Modes of Vibration 32
3.2 Healthy and Damaged Truss Models 34
3.3 Experimental Truss Models 39

4.0 Mode Identification 43
4.1 Identification Methods 43
4.2 Mode Shape Assurance 51
4.3 Mode Shape Expansion 54

5.0 Location and Estimation of Single-Element Damage 56
5.1 Single-Element Damage Model 56
5.2 Damage Location and Estimation 61
5.3 Simulation Results 65

6.0 Strain Energy 72
6.1 Fractional Modal Strain Energy 72
6.2 Mode Shape – Strain Energy Relationship 82
6.3 Mode Sensitivity 88
6.4 Simulated Healthy-Damaged Mode Comparison 92

7.0 Multi-Element Damage Detection 99
7.1 Detecting Damage in Element Groups 99
7.1.1 Defining Element Groups 99
7.1.2 Eigenvector Assignment Decomposition 101
7.1.3 Damaged Group Location Sub-algorithm 104
7.1.4 Simulation Results 110
7.1.4.1 Computing Element Group Vectors 110
7.1.4.2 Locating Damaged Groups 115
7.2 Location and Estimation of Multi-Element Damage 119
7.2.1 Multi-Element Damage Model 119
7.2.2 Multi-Element Damage Location and Estimation Sub-algorithm .. 124
7.3 Sequential Damage Detection Algorithm 127

8.0 Conclusion 131

References 134

LIST of ILLUSTRATIONS

Figure 1.1: On-Line Damage Detection 3
Figure 2.1: General Model Refinement Algorithm 8
Figure 2.2: Model Refinement Applied to Damage Detection 8
Figure 3.1: One Dimensional Element 26
Figure 3.2: One Dimension-to-Two Dimension Transformation 29
Table 3.1: Planar Truss Parameters 40
Figure 3.3: 3 Bay Planar Truss 41
Figure 3.4: 10 Bay Planar Truss 42
Figure 5.1: Single-Element Damage Location & Estimation Algorithm 63
Figure 5.2: $[\widehat{d}]_f$ for 3 Bay Truss - Element 3 Damaged 50% 68
Figure 5.3: $[\widehat{d}]_f$ for 3 Bay Truss - Element 10 Damaged 50% 68
Figure 5.4: $[\widehat{d}]_f$ for 3 Bay Truss - Elements 3, 14 Damaged 70%, 30% 69
Figure 5.5: $[\widehat{d}]_f$ for 3 Bay Truss - Elements 3, 15 Damaged 40%, 60% 69
Figure 5.6: $[\widehat{d}]_f$ for 10 Bay Truss - Element 14 Damaged 50% 70
Figure 5.7: $[\widehat{d}]_f$ for 10 Bay Truss - Elements 16 Damaged 50% 70
Figure 5.8: $[\widehat{d}]_f$ for 10 Bay Truss - Elements 4, 33 Damaged 40%, 60% 71
Figure 5.9: $[\widehat{d}]_f$ for 10 Bay Truss - Elements 14, 22 Damaged 60%, 40% 71
Figure 6.1: SE_{Hi1} for the 10 Bay Truss 77
Figure 6.2: SE_{Hi2} for the 10 Bay Truss 77
Figure 6.3: SE_{Hi3} for the 10 Bay Truss 78
Figure 6.4: SE_{Hi4} for the 10 Bay Truss 78
Figure 6.5: SE_{Hi5} for the 10 Bay Truss 79
Figure 6.6: SE_{Hi6} for the 10 Bay Truss 79
Figure 6.7: SE_{Hi7} for the 10 Bay Truss 80
Figure 6.8: SE_{Hi8} for the 10 Bay Truss 80
Figure 6.9: SE_{Hi9} for the 10 Bay Truss 81
Figure 6.10: SE_{Hi10} for the 10 Bay Truss 91
Figure 6.11a: ϕ_{H6} vs. ϕ_{D6} for Element 14 Damaged 70% 93
Figure 6.11b: SE_{Hi6} and SE_{Di6} for Element 14 Damaged 70% 93
Figure 6.12a: ϕ_{H10} vs. ϕ_{D10} for Element 14 Damaged 70% 94
Figure 6.12b: SE_{Hi10} and SE_{Di10} for Element 14 Damaged 70% 94

Figure 6.13a: ϕ_{H6} vs. ϕ_{D6} for Element 16 Damaged 70% 95
Figure 6.13b: SE_{Hi6} and SE_{Di6} for Element 16 Damaged 70% 95
Figure 6.14a: ϕ_{H8} vs. ϕ_{D8} for Element 16 Damaged 70% 96
Figure 6.14b: SE_{Hi8} and SE_{Di8} for Element 16 Damaged 70% 96
Table 6.1: Frequency Sensitivity for Element 14 Damaged 70% 98
Table 6.2: Frequency Sensitivity for Element 16 Damaged 70% 98
Figure 7.1: Damaged Group Location Sub-Algorithm 109
Figure 7.2: Inner Product of G_1^m and B_i^m for all i 112
Figure 7.3: Inner Product of G_2^m and B_i^m for all i 112
Figure 7.4: Inner Product of G_3^m and B_i^m for all i 113
Figure 7.5: Inner Product of G_4^m and B_i^m for all i 113
Figure 7.6: Inner Product of G_5^m and B_i^m for all i 114
Figure 7.7: $[E]$ for Elements 8 Damaged 10% 116
Figure 7.8: $[E]$ for Elements 2, 3, 10 Damaged 30%, 40%, 50% 116
Figure 7.9: $[E]$ for Elements 12, 14, 16 Damaged 30%, 40%, 50% 117
Figure 7.10: $[E]$ for Elements 22, 24, 26 Damaged 50%, 30%, 40% 117
Figure 7.11: $[E]$ for Elements 2, 4, 5, 35, 32, Damaged 40%,20%,50%,40%,60% ..118
Figure 7.12: $[E]$ for Elements 4, 5, 23, 44, 45 Damaged 40%,50%,30%,50%,60% .118
Figure 7.13: Multi-Element Damage Location & Estimation Sub-algorithm 126
Figure 7.14: Sequential Damage Detection Algorithm 128

1 INTRODUCTION

The current level of space technology and future projections suggest many new roles for large space truss structures. Communications, remote sensing, image processing, human space exploration, and national defense are some applications for large satellite platforms. Two primary concerns held for large satellite structures is vibration suppression and health monitoring. The high cost of satellite deployment motivates weight reduction, making large structures susceptible to vibration. To meet the mission requirements of these structures, active structure control is often required.

The field of space craft control and vibration suppression has received considerable attention within the last two decades. Of particular importance is structure identification and structure modeling. The performance of vibration control systems is directly related to the accuracy of the structure model. The large volume of research towards model identification and refinement reflects this.

In the harsh environment of space, damage caused by meteorite impacts can severely affect the dynamics of a structure, and the control law by which a vibration control system is based. The field of damage detection has been created to address this issue. With knowledge of the location and extent of damage, the structure's analytical model can be updated for use in a control system. In this way, damage detection can be viewed as a form of model identification or model

refinement.

The random nature of structural damage requires that any damage detection algorithm must periodically monitor the integrity of the structure. A high frequency of monitoring better ensures the functionality of the satellite. However, any satellite down-time caused by monitoring reduces functionality. Hence, because of limited computer resources in orbit, any on-line algorithm must be computationally efficient. This is especially true for large structures with hundreds of degrees of freedom.

The goal of this thesis is to address the issue of damage detection in undamped structures. Two damage detection algorithms will be developed that will detect, locate, and estimate damage in large space trusses with a minimum number of computations. One of the primary considerations around which this material is presented is the desire that any detection algorithm is suitable for use on-line aboard a satellite. This requires that the algorithm developed must be efficient and fully automated, requiring no human interaction. An additional consideration is the ability to accurately assess damage to many elements.

Using the finite element method, damage is modeled as a linear reduction in stiffness of the effected element. Because interpolation functions are used to map a change in the elasticity modulus to a finite element, this work is a flexible platform for the introduction of other materials theory.

The general form of the damage detection problem is illustrated in Figure 1.1. The state of the truss is unknown: healthy or damaged. This is represented by the *healthy* and *damaged* notation. If the truss is damaged, the location and severity of damage is not known. From the given structure, the first step is to identify the natural modes from input and output excitation signals. This can be

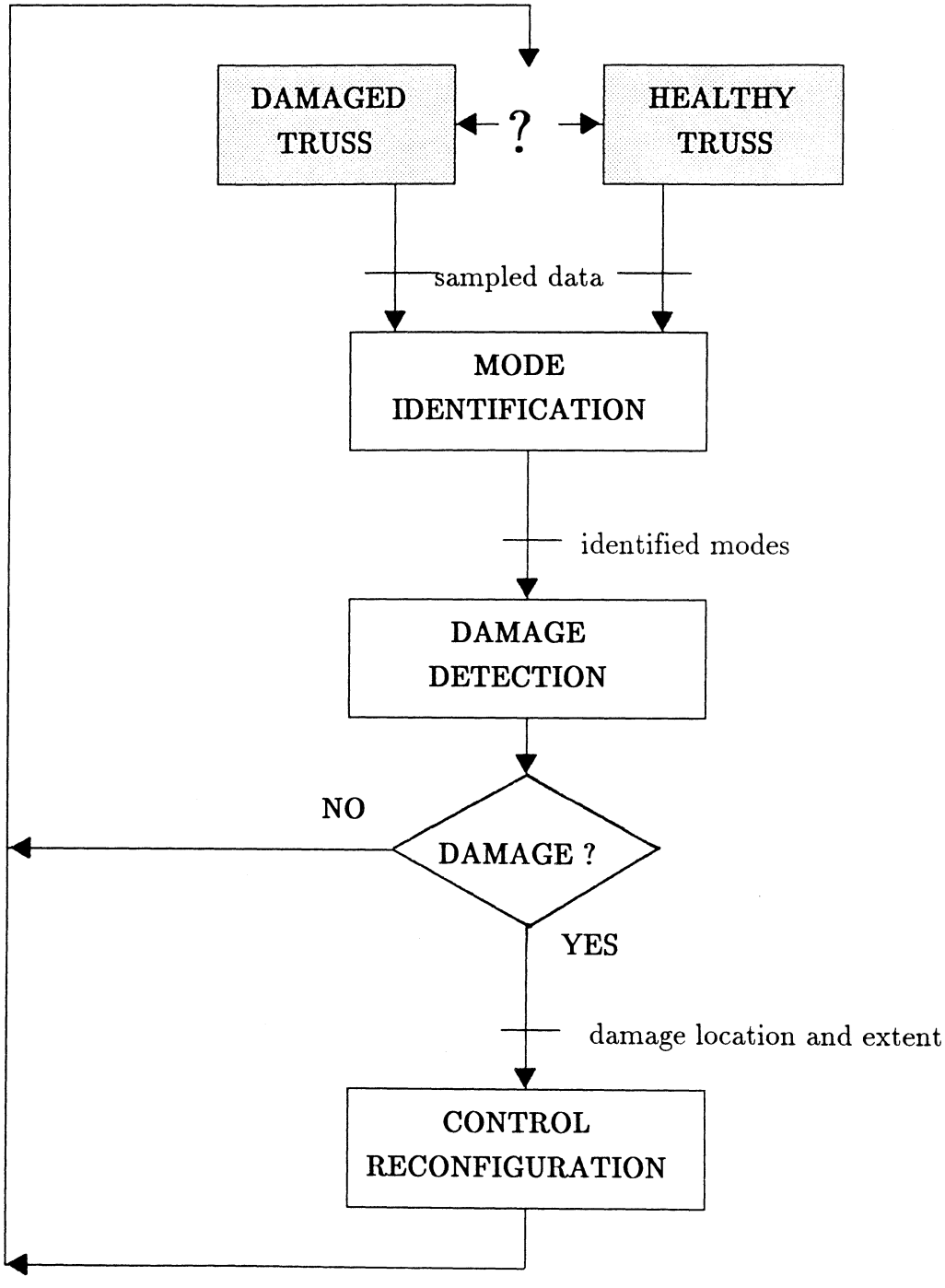

Figure 1.1: On-Line Damage Detection

accomplished from a number of common identification methods. In this thesis, these identified modes will be called *damaged modes.* Damage detection is then performed using the damaged modes as input data. If the truss is damaged, it is desired to estimate the location and extent of the damage, and supply this information to a control reconfiguration procedure.

There are two main approaches evident in damage detection research. Several detection methods are based on model refinement techniques intended for the verification of analytical models. These methods often require a large number of computations that is prohibitive to their use in an on-line format. A second approach is to express the damage in terms of the healthy truss model and the damaged modes. These methods often solve for a large number of unknowns, requiring a least square estimate as a solution. These methods are sensitive to the number of damaged modes available and often incur large amounts of error.

The approach taken in this thesis is similar to the latter. The damage perturbation to the healthy global matrix is expressed as function of known vectors and the unknown damage coefficient . This enables the damage extent to be solved for exactly in an equation involving the healthy truss model and the damaged modes. Because the damage location is unknown, several iterations of this equation are required for each element of the structure. From this data, the damage location and extent can be found exactly. Since each iteration involves few matrix operations, this detection method requires fewer computations than most current published methods. The iterations which correspond to a damaged element are an exact expression of the damage extent. The damage extent can thus be found exactly, were most current methods cannot.

The most significant product of this work is offered as a sequential

algorithm consisting of two sub-algorithms, both of which are based on the above relationship. The first sub-algorithm uses a coarse structure model to locate regions of the structure which contain damaged elements with a small number of iterations. The number of iterations required is proportional to the size of the coarse truss model. The creation of a coarse model is a flexible process, so several models of different size can be used in a nested fashion for greater efficiency. The second sub-algorithm locates and estimates the damage within the defined regions of damage. With few limitations, the sequential algorithm can exactly locate and measure the extent of damage to multiple elements. Current methods only consider single element damage and few attempt to measure damage extent.

The material presented in this thesis is intended to encompass all issues relevant to the development of a detection algorithm. Chapters 2 through 4 cover background material. Chapter 2 is a review of most current literature in the damage detection field. Chapter 3 covers the development of the finite element method for truss structures. The model of the damaged truss that is basis of this thesis is also developed. Chapter 4 discusses mode identification, selection, and expansion.

Chapter 5 develops the first detection algorithm used for single-element damage cases. It is the simpler of the two methods. Chapter 6 introduces strain energy and its relationship to mode sensitivity and damage. This chapter also develops several key relationships on which the second detection algorithm is based. Chapter 7 builds the second algorithm from two sub-algorithms, both of which are derived in a process very similar to that of Chapter 5. This resulting algorithm is well suited to location and estimation of damage to multiple elements in very large structures. Chapter 8 concludes the thesis.

2 SURVEY OF DAMAGE DETECTION METHODS

2.1 EARLY WORK IN DAMAGE DETECTION

This work is briefly presented as a preview to current methods. For various reasons, most of these methods show little or no promise for use on space structures. Only methods using some form of vibrational analysis on complex or multi-element structures were considered. Research directed towards damage effects on local material properties, crack propagation in materials, etc. are not directly applicable to damage detection in large structures and are not included[1].

In the civil field, Kirchner [2] compared the frequency response of buildings with similar design. It was found that the power spectral density computed from acceleration data remained constant over time for a specific structure and sensor location. It was then postulated that a change in the spectrum would indicate the presence of damage, caused possibly by earthquakes. Yao [3] tried to locate damage by examining changes in the damping of buildings computed from vibration identification. Because of the complexity of the location problem, he was only able to suggest artificial intelligence as an approach. To aid in the inspection of offshore drilling platforms, Coppolino [4] used ambient excitation and sensitivity identification to locate damage. The location of damage in key elements was detectable, which suggests detection as function of strain energy.

In the field of airframes, West [5] and Pacia [6] successfully attempted to detect damage in aircraft structures and wings by modal testing through frequency response analysis. Location of damage was only possible after extensive comparison to empirical vibration data.

2.2 MODEL REFINEMENT IN DAMAGE DETECTION

In the application of dynamic structure modeling, the finite element method of which so much of structure research is based, is not exact. The analytical modes corresponding to the initial finite element model are only an approximation of the true modes. To arrive at a more accurate model, some form of *model refinement* is usually performed on the initial finite element model using data from a modal survey [1]. The result is an analytical model whose modes exactly or closely agree with the identified modes. This is a key step in structure modeling, and is a topic of great attention.

Because the damaged structure model differs only slightly from the undamaged structure model, the application of model refinement to damage detection is well suited. The interest is not in identifying a more accurate structure model, but in the change the refinement applies to the original model. It is hoped that this change will contain enough information to locate any damage and estimate its extent.

Most refinement methods use the identified modes and some initial finite element model as inputs [1]. Shown in Figure 2.1, the result of the typical refinement method is the estimated mass matrix $\widehat{M}$ and stiffness matrix $\widehat{K}$. The change in K_{FEM} to arrive at the solution $\widehat{K}$ is the stiffness perturbation matrix

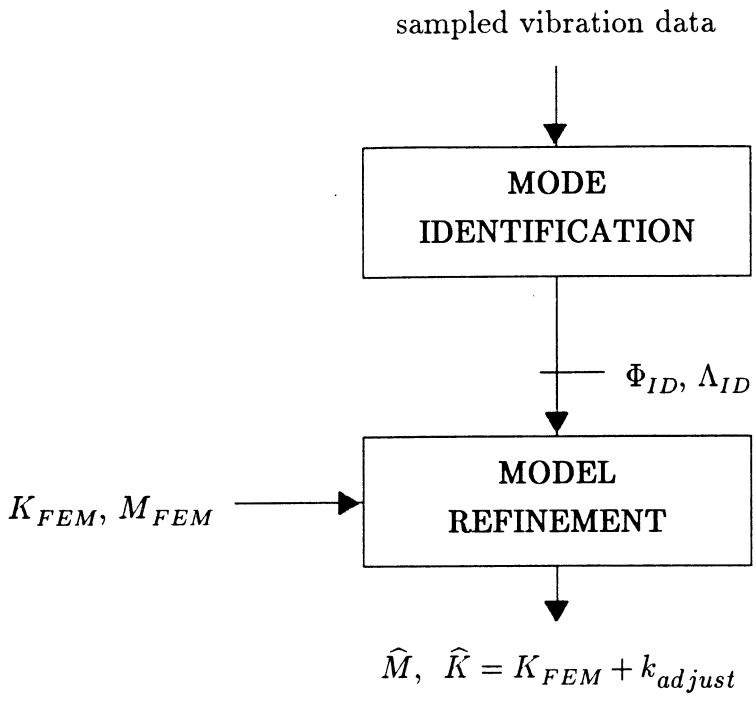

Figure 2.1: General Model Refinement Algorithm

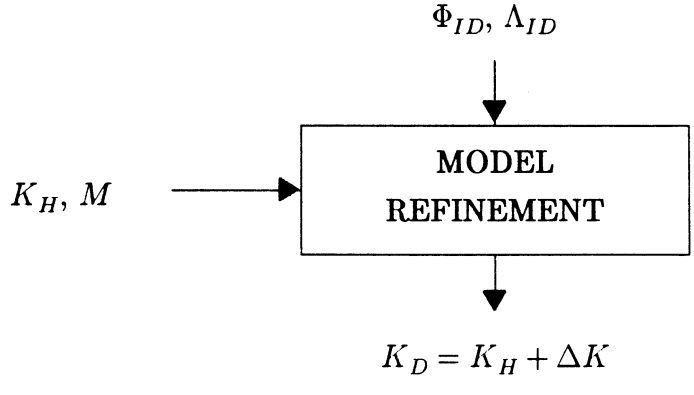

Figure 2.2: Model Refinement Applied to Damage Detection

k_{adjust}.

In the application of refinement methods to damage detection, the identified modes of the damaged truss and the undamaged truss model are the inputs. That is, the matrices M_{FEM} and K_{FEM} derived from the known *healthy* structure are used and are notated as M_H and K_H. Most detection methods based on model refinement assume the mass properties of the structure are unchanged by damage. Hence, the output of interest is only $\widehat{K}$ which is termed K_D for *damaged* stiffness matrix. It is assumed the actual identified modes of the undamaged truss are in agreement with the healthy analytical model.

Because of the large number of refinement techniques, this section will only consider refinement methods that have been applied specifically to the problem of damage detection. In general, refinement methods can be grouped into three major categories: optimal matrix updates, eigenstructure assignment, and sensitivity methods [1].

2.2.1 Optimal Updates

In general, optimal refinement methods use optimization techniques to solve for some adjustment to the stiffness matrix such as k_{adjust}. Constraints are imposed to minimize the number nonzero entries in k_{adjust}, to minimize some norm of k_{adjust}, to ensure k_{adjust} symmetry, and to preserve the scarcity of the stiffness matrix.

Intended for application to aircraft structures, the work of Hajela and Soeiro [7] considers damage detection in load bearing trusses which can be used to approximate wing and fuselage structures. Update of the stiffness matrix is created

by solving an optimization problem by nonlinear programming. Adjustment coefficients for every entry in K_H are solved for while minimizing the total square error of measured (Y_m) verses analytical (Y_a) degrees of freedom modal or static displacements. The error is

$$e = \sum_i \sum_j (Y_{m_{ij}} - Y_{a_{ij}})^2. \tag{2.1}$$

Unique to model refinement is this method's use of static deflections to approximate the higher modes that are unidentifiable. This limits the application to load bearing structures only, of which satellites and space stations are generally not. The difficulty of imposing artificial loads on a satellite structure and measuring the resulting deflections, and the impracticality of on-ground testing before deployment, make this an unlikely candidate for use in space [8].

In a comprehensive study, Smith [9] evaluated current methods in model refinement and formed a damage detection algorithm around the most suitable components. Considerations of computational effort, adjustment matrix symmetry and maintenance of physical coupling reduced a large list of refinement methods to two candidates: Kabe's optimal update method and White & Maytum's submatrix method.

In 1985, Kabe [13] presented an effective stiffness matrix refinement method using a small set of identified modes. An attempt to preserve the geometric load paths in the stiffness matrix is made by the preservation of zeros in the stiffness matrix. To ensure the scarcity of K_{FEM}, Kabe incorporated a unique element-by-element matrix multiplication operation denoted by $\odot$. The stiffness adjustment matrix $[\gamma]$ is applied to K_{FEM} resulting in

$$[K] = [k] \odot [\gamma] \quad => \quad K_{ij} = k_{ij}\gamma_{ij} \tag{2.2}$$

where $[K] = \widehat{K}$ and $[k] = K_{FEM}$. Under this structure, a constrained optimization problem is developed which minimizes ϵ such that

$$\epsilon = \left\| [\widehat{I}] - [\widehat{I}] \odot [\gamma] \right\| \tag{2.3}$$

$$\text{where} \qquad \widehat{I}_{ij} = \begin{cases} 1 \text{ for } k_{ij} \neq 0 \\ 0 \text{ for } k_{ij} = 0 \end{cases} .$$

The constraints imposed include the symmetry of $[\gamma]$ and the satisfaction of an eigenvalue equation. Using Legrange multipliers to include the constraints, the following relation is obtained:

$$\widehat{K} = K_o - 1/4\ [K^2] \odot ([\lambda]\Phi^{\mathrm{T}} + \ \Phi[\lambda]^{\mathrm{T}}) \tag{2.4}$$

where $[K^2] = K_o \odot K_o$

$[\lambda]$ is a matrix of Lagrange multipliers

Φ is a matrix of available mode shapes.

The Lagrange multipliers are solved for with a series of matrix multiplications. Then $\widehat{K}$ can be computed. Because the original analytic mass and stiffness matrices contain information of the structure, few modes are needed as input for acceptable results [9].

In 1976, White and Maytum [14] introduced a mass and stiffness matrix refinement method that uses only measured frequencies. It is assumed the analytical modes are very similar to the identified modes. The adjustment to the stiffness matrix is expressed as a weighted sum of element subgroups containing similar elements. The adjusted stiffness matrix is

$$\widehat{K} = K_{FEM} + \sum_{p=1}^{P} \delta_p [k]_p. \tag{2.5}$$

Here p corresponds to the element subgroup indices. For application to damage detection, White and Maytum assumed the known mass matrix is correct, and that the damaged mode shapes are similar to the healthy mode shapes. The subgroup weights δ_p can then be calculated from the healthy mode shapes, damaged frequencies and an energy matrix which expresses the energy distributed over each healthy mode shape. Information from mode coupling, mode-subgroup potential energy sensitivity, and geometry are used in selecting the element subgroups.

Smith exercised Kabe's update method and White and Maytum's matrix perturbation method on a ten bay planar truss and a ten bay 3-D truss. Damage was modeled by complete removal of one element without effecting the mass matrix. Smith eliminated White & Maytum's method because the creation of element subgroups destroyed the unique contribution of each element to the stiffness matrix. Damage detection was proven impossible.

To locate damage with Kabe's method, the percent adjustment to each entry in the refined stiffness matrix was formed into a matrix. These matrix entries were filtered with two thresholds: one for on-diagonal entries, one for off-diagonal entries. Matrix graph theory was then used to described the zero-nonzero

pattern of the filtered matrix. Because each element is represented uniquely by the matrix graph, damage detection using this result is possible.

This algorithm was shown to successfully locate completely damaged elements in all but a few cases. In one case, damage in elements with small modal energy for the modes used was undetectable. A more sever problem is specific to only certain truss geometries. With the planar truss, diagonal elements created cancellations in the stiffness matrix (zeros). If damage occurs to one of these diagonal elements, Kabe's method will then wrongly preserve these zeros. The update algorithm will then adjust the wrong degrees of freedom, and correct detection is impossible.

2.2.2 Eigenstructure Assignment

An alternative to the computationally intensive optimal update methods are the eignestructure assignment methods presented by Zimmerman and Kaouk [10,11]. Using eigenvalue-eigenvector assignment theory, these methods calculate gain matrices that assign the identified modes to the analytical model. From these feedback gain matrices, mass, damping, or stiffness adjustment matrices are formed. As with applying optimal refinement to damaged detection, constraints on perturbation matrix symmetry are often applied.

Zimmerman and Kaouk's initial work models the perturbation matrices applied to the healthy parameter matrices as matrix triple products. A pseudo-system with feedback control is produced. This system is represented by the three equations

$$M\ddot{x} + D_H\dot{x} + K_H x = B_0 u, \tag{2.6}$$

$$y = C_0 x + C_1 \dot{x}, \text{ and } u = Fy. \tag{2.7}$$

The first (B_0) and third matrix (C_0, C_1) terms can be viewed as the input and output matrices, respectively. The middle matrix terms correspond to the feedback gains required to assign the damaged modes to the pseudo-system. The triple products B_0FC_1 and B_0FC_0 are the perturbation matrices of the damping and stiffness matrices respectively.

Rewriting the eigenvector equation by separating the perturbation matrices, an expression involving only the healthy property matrices and the damaged modal data is obtained:

$$\{d\}_j = (\lambda^2{}_{dj}M_H + \lambda_{dj}D_H + K_H)\phi_{dj} = (\lambda^2{}_{dj}\Delta M + \lambda_{dj}\Delta D + \Delta K)\phi_{dj}. \tag{2.8}$$

For exact damaged modes, any nonzero entries in the vector $\{d\}_j$ correspond to degrees of freedom effected by the damage. Zero entries in $\{d\}_j$ correspond to the orthoginality of the mode shape and a vector, $\{z\}_j$, that is a function of the perturbation matrices. The angle, α, between the two orthogonal vectors is 90° for perfect modal data, and some near 90° value for modes corrupted with measurement error. Zimmerman et al. states that the deviation of α is less sensitive to mode error than the magnitude of $\{d\}_j$ entries themselves [10]. For mode j, vector $\{\alpha\}_j$ is calculated from $\{z\}_j$, $\{d\}_j$, and ϕ_{dj}. Damage is then located by noting the entries of $\{\alpha\}_j$ that are much different than 90°.

For damage estimation, a method for finding the triple product perturbation

ΔK for undamped trusses while M_H remains constant is given. Symmetry of ΔK is ensured and $K_H - \Delta K$ provides an exact damaged truss model when measured modes are exact. From this, no method for estimating damage extent is specified.

Examples on Kabe's model [13] and a 6 bay truss constrained at three degrees of freedom are given. By introducing random error on mode shapes, the use of angle α to locate damage was proved more reliable than by comparing the magnitude of entries of $\{d\}_j$.

Improving upon the method above, Zimmerman and Kaouk [11] present a second pole placement algorithm that ensures triple product matrix symmetry for both ΔK and ΔD. This symmetry is expressed as the nonunique solution of a Riccati equation. Because this is not a sufficient condition, every possible real solution must be considered and filtered for symmetry and definiteness, leaving several suitable solutions. The remaining solutions must be compared for relevance and quality of information for damage detection.

Simulated results from damage in Kabe's model was presented, as well as detection in a cantilevered continuous beam. Because both models were assumed undamped, the simulation results only illustrate this method's accuracy of estimating the stiffness perturbation matrix, and the effect of mode shape expansion. As expected, the accuracy of damage detection was proportional to the number of entries considered for the mode expansion.

2.2.3 Sensitivity

One of the few damage detection methods developed specifically to incorporate inexact modal data and a changing mass matrix is presented by Ricles and Kosmatka [15]. The modal assurance criterion defined by Edwins [16] is used to select the identified modes most similar to those of the analytical model. To locate damage, Ricles and Kosmatka define a residual force vector R_j which is identical to $\{d\}_j$ defined in Eq. (2.8).

For damage estimation, difference in the healthy and damaged modal data is expressed as a first order Taylor series involving the healthy modal data and a transformation of a damage parameter array. That is

$$\Lambda_d = \Lambda_o + T(r_d - r_o) + \epsilon \tag{2.9}$$

where $\Lambda^{\mathrm{T}} = (\omega^2, \phi)^{\mathrm{T}}$

r_d is the damage parameter array

ϵ is an array of testing errors associated with measured mode

T is a sensitivity matrix based on the partial derivative of the damage mode with respect to the initial analytical model matrices M_o and K_o.

The vector difference $(r_d - r_o)$ is initially treated as an array of normally distributed random variables, where the corresponding covariance values are the diagonal entries of the matrix S_{RR}. After analysis of the residual force vector, only elements suspected of damage are assigned a nonzero covariance value in S_{RR}. The

solution of a Taylor series iteration is expressed as

$$r_d = r_o + S^*_{RR}\, T^{\mathrm{T}}\, (T\, S^*_{RR}\, T^{\mathrm{T}} + S_{\epsilon\epsilon})^{-1}(\Lambda_d - \Lambda_o) \tag{2.10}$$

where

$$S^*_{RR} = S_{RR} - S_{RR}\, T^{\mathrm{T}}\, (TS_{RR}\, T^{\mathrm{T}} + S_{\epsilon\epsilon})^{-1}\, TS_{RR}. \tag{2.11}$$

The test error ϵ is also treated as a random variable with a covariance of $S_{\epsilon\epsilon}$.

If the relationship between the stiffness and mass matrices and the structure were exactly linear, Eq. (2.10) would converge in one step. If it is not linear, the series converges to the estimated parameters in r_d. Iterations are terminated when Δr_d falls below some convergence tolerance.

Several simulations of cantilevered 8 bay trusses with point mass loading were exercised. The damage was modeled as a 5% or 10% reduction in stiffness of selected diagonal and longitudinal elements. After location, the reduction of stiffness was estimated within 10% of the true value, even in cases of damage to two and tree elements simultaneously.

2.2.4 Submatrix Adjustment

In 1990, Lim [17] presented a stiffness matrix correction method using incomplete modal test data. By finding scaling coefficients to submatrices by a pseudo-inverse least squares calculation, Lim improves upon White and Maytum's method [14] which often requires several iterations. Submatrices are created by lumping together the stiffness matrices of elements with similar geometry. This dramatically reduces the number of unknown parameters in the stiffness matrix

that must be adjusted. One of Lim's primary goals is to modify this refinement method for use with an analytic model reduced in size by the Guyan method to be compatible with the dimensions of the measured modal data.

Lim [8] applied this refinement method to detection of damage. Rather than creating subgroups, each element is represented as a submatrix, and the corresponding scaling factors are found. By simulating damage on an unconstrained ten bay truss, Lim claims full detection is possible given accurate modal data, even in multi-damage cases. Erroneous modal data requires analysis of mode strain energy to find the modes most sensitive to damage. By weighting the resulting scaling factors by their standard deviation over several modes, Lim found damage detectable only in several select cases. Lim also applies this method to a reduced order model of the ten bay truss, and found detection difficult.

2.3 OTHER METHODS

One of the few methods derived specifically for damage detection is presented by Chen and Garba [18]. Similar to Zimmerman and Kaouk's subspace rotation method for damage location, Chen and Garba define the damage perturbation vector $\{d\}_j$ in Eq. (2.8) as a discrepancy in the distribution between the damaged kinetic energy and healthy kinetic energy. They start by multiplying the eignevector equation by a diagonal matrix $\left[\cdot \phi_{\cdot}\right]$, giving

$$\left[\cdot \phi_{\cdot}\right]_j K_H \phi_j = \omega^2{}_j \left[\cdot \phi_{\cdot}\right]_j M_H \phi_j. \tag{2.12}$$

This equation implies that for a given undamped structure and its modes, the kinetic energy per degree of freedom per mode is equal to the potential energy per degree of freedom per mode.

Chen and Garba assume the mass matrix does not change with damage, and that the damaged mode shapes are close to the the healthy mode shapes. Noting this, the kinetic energy expressed in the right hand side of Eq. (2.12) only changes by a scalar frequency coefficient. As damage occurs, ϕ_j changes locally and K_H remains constant, creating a discrepancy in the equation. This relation can be viewed using the damaged stiffness matrix model of healthy plus perturbation, where the perturbation is

$$\Delta K \phi_j = (\omega^2{}_j M_H - K_H) \phi_j. \tag{2.13}$$

Note that Eq. (2.13) is essentially identical to Eq. (2.8) by Zimmerman and Kaouk

for an undamped structure. Chen and Garba define a connectivity matrix $[C]_j$ as

$$\Delta K \ \phi_j = [C]_j[\Delta k_{ij}]. \tag{2.14}$$

where $[\Delta k_{ij}]$ is a vector of the unknown entries in ΔK. The connectivity matrix $[C]_j$ is a mapping of the entries of mode shape j. The mapping pattern is determined by the geometry of the structure and is the same for all modes. Depending on the number of available modes, $[\Delta k_{ij}]$ can be solved for exactly or by a constrained minimization problem. In the typical case of a small set of identified modes, Eq. (2.14) may have more unknowns than equations, especially for a multi-element damage case. Chen and Garba leave it up to the reader to extract damage location and estimation information from the computed $[\Delta k_{ij}]$.

By applying this detection method to a three dimensional MAST beam, Chen and Garba note that any stiffness change of less than 10% must be ignored due to round off error. First, percent changes in kinetic energy per degree of freedom is analyzed. The modes with the greatest change are chosen for computing $[C]_j$. Physically unrealizable values in $[\Delta k_{ij}]$ are constrained to specific values in the optimization problem and $[\Delta k_{ij}]$ is computed again. The damage in the example was successfully located after several iterations where human analysis was necessary to discard misleading information. Only cases of near 100% damage were considered, and no estimation was attempted. The poor performance of this method when few modes are used suggests cases of less sever damage will be undetectable unless a large set of accurate identified modes are available.

2.4 SUMMARY

Many different approaches to damage detection were presented, each with varying amounts of success in detection. By hypothesizing 100% damage, Smith applies Kabe's update method to the location damage. The degree of freedom connectivity of the elements is the only structure geometry information used. Information of healthy element stiffness and element angle with respect to global coordinates is discarded by only considering the location of the largest changes in the perturbation matrix. This makes Smith's method lass attractive for estimating the extent of damage. In addition, Kabe's update algorithm is extremely computationally intensive.

Zimmerman and Kaouk provide two methods for estimating the damaged model. As an initial step, the subspace rotation method to locate damage is less sensitive to data error than the residual force method used by Ricles and Kosmatka and Chen and Garba. Estimates of ΔK and ΔD were shown to be quite accurate, even for incomplete mode shapes. No methods of estimating damage extent from these matrices was given. However, the best solution of ΔK and ΔD must be chosen out of a nonunique set of solutions making this method difficult to automate.

In an effort to relax the assumptions of exact identified modes and an unchanging mass matrix, Ricles and Kosmatka have developed a detection method that is successful in the location and extent estimation of multi-damage cases. A subset of damaged candidates must first be made. Then many iterations of two matrix equations must be completed to find the damage estimate. Although computationally intensive, this method appears to perform well in experiments

involving actual trusses, but may be diffucult to automate.

Lim's method proved to be very versatile, accurately detecting damage to many elements simultaneously. However, because of the large number of unknowns to be estimated, many modes are required. The number of modes required is dependent on the number and location of damaged elements.

Rather than applying a refinement technique, Chen and Garba attempt to solve for the stiffness parameters of the suspected damaged elements directly. In addition to Lim's method, this is the only method that used all geometric information available form the candidate elements. For cases of multi-damage and small mode sets, this method performs poorly, requiring much data analysis and possibly multi-iterations. Automation of this method would be difficult.

Of all detection methods, the research mentioned in this conclusion seem to hold the most promise for use in an on-line detection scheme. All of this research recognizes the need for strain energy analysis for selection of modes as input. All use a finite element model approximation as the initial healthy model, and all but one assume the mass matrix to be constant.

3 HEALTHY and DAMAGED TRUSS MODELS

The damage location and estimation algrithms in this thesis are based on a finite element model. The first section of this chapter develops a finite element model of a general truss. The second section models the damage in a truss using the finite element method. Two planar trusses that will be used in simulations are presented in the last section.

3.1 THE FINITE ELEMENT METHOD

The finite element model of a truss structure is developed in this section [19]. For a structure of interest, a finite element is created for each structural member. The nodes are assigned to the physical joints which link the structural member together. Each node has two degrees of freedom. Thus no bending moments exist.

It is assumed that:

1. The element material is homogeneous over the length of the element, and the cross sectional area of each element is constant over its length.
2. Elements are uncoupled - no bending moments are applied.
3. All deflections within the elements occur axially.

4. Any displacements imposed on the degrees of freedom are relatively small with respect to the size of the truss.
5. Dynamically, the structure behaves as a linear system.

The dynamics of the resulting finite element model can be described by a series of second order differential equations. Expressing these equations as one matrix equation, it can be written with respect to the nodal displacements as

$$M\ \ddot{q}(t) + K\ q(t) = F(t). \tag{3.1}$$

The vector of the nodal displacements, or degrees of freedom, is $q(t)$. The vector of forces applied to the degrees of freedom is $F(t)$. The mass and stiffness matrices are M and K, respectively. Equation (3.1) is the dynamic model of a truss of dimension n, where n is equal to the number of degrees of freedom.

3.1.1 Element Equations of Motion

This section develops the equations of motion for each element within it's corresponding local coordinates. By using Lagrange's equations of motion, the elements' kinetic energy and potential energy can be expressed in terms of interpolation functions. This will lead to the creation of element mass and stiffness matrices.

Consider element i of a structure viewed in a one dimensional coordinate system in Figure 3.1. Note the prime on the q variables indicate displacements with respect to the local coordinates.

The displacement at any point along the length of the element is described with respect to the two end displacements by the equation

$$q'(x,t) = L_1(x)q'_1(t) + L_2(x)q'_2(t) = L(x)^{\mathrm{T}}q'(t), \tag{3.2}$$

where

$$q'(t) = \begin{bmatrix} q'_1(t) \\ q'_2(t) \end{bmatrix}.$$

The linear interpolation functions are defined as

$$L_1(x) = 1 - \frac{x}{h_i}, \text{ and } \qquad L_2(x) = \frac{x}{h_i}, \tag{3.3}$$

or

$$L(x) = \begin{bmatrix} L_1(x) \\ L_2(x) \end{bmatrix}.$$

From Eq. (3.2), the kinetic energy for element i is

$$T_i(t) = \frac{1}{2}\int_0^{h_i} m_i(x)\left[\frac{\partial q'(x,t)}{\partial t}\right]^2 dx$$

$$= \frac{1}{2}\int_0^{h_i} m_i(x)\ \dot{q}'(t)^{\mathrm{T}}\ L(x)L(x)^{\mathrm{T}}\ \dot{q}'(t)\ dx. \tag{3.4}$$

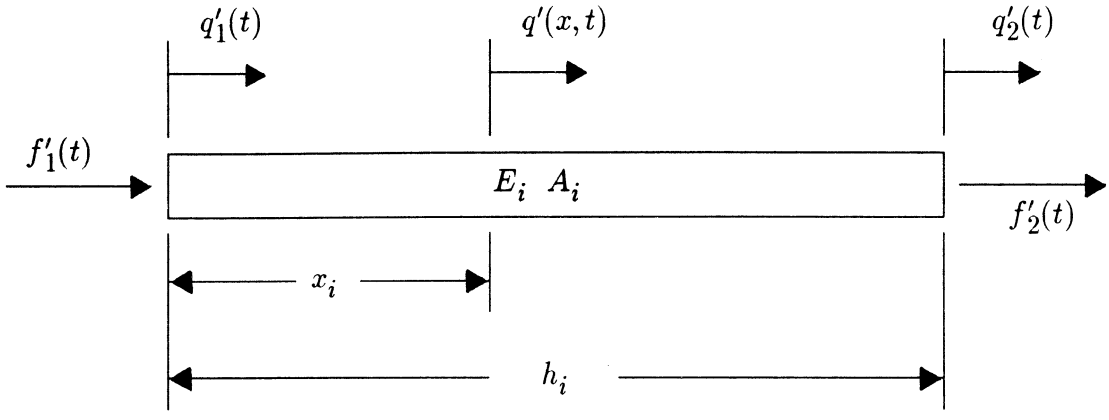

$q'_l(t)$ are local displacements at time t

$f'_l(t)$ are local forces at time t acting on nodes 1 and 2

h_i is the length of element i

E_i is the modulus of elasticity of element i

A_i is the cross sectional area of element i

Figure 3.1: One Dimensional Element

Considering the first assumption, $m_i(x) = \rho A_i$. Equation (3.4) can then be rewritten as

$$T_i(t) = \tfrac{1}{2}\, \dot{q}'(t)^{\mathrm{T}}\, M_i'\, \dot{q}'(t), \tag{3.5}$$

where the element mass matrix in local coordinates is

$$M_i' = \int_0^{h_i} \rho A_i\, L(x) L(x)^{\mathrm{T}} dx. \tag{3.6}$$

Evaluating the integral, the element mass matrix is expressed as

$$M_i' = \frac{\rho A_i h_i}{6} \begin{bmatrix} 2 & 1 \\ 1 & 2 \end{bmatrix}, \tag{3.7}$$

where ρ is the material density assumed constant for all elements. To develop the stiffness matrix, the potential energy of element i is

$$V_i(t) = \tfrac{1}{2} \int_0^{h_i} E_i A_i(x) \left[\frac{\partial q'(x,t)}{\partial x} \right]^2 dx$$

$$= \tfrac{1}{2} \int_0^{h_i} E_i A_i(x)\, q'(t)^{\mathrm{T}}\, L_x(x) L_x(x)^{\mathrm{T}}\, q'(t)\, dt, \tag{3.8}$$

where $L_x(x)$ corresponds to the derivative with respect to x. Again, considering the first assumption, $E_i A_i(x)$ is constant over x. Then

$$V_i = \tfrac{1}{2}\, q'(t)^{\mathrm{T}}\, K_i'\, q'(t), \tag{3.9}$$

where the element stiffness matrix with respect to its local coordinates is

$$K_i' = \int_0^{h_i} E_i A_i \, L_x(x) L_x(x)^{\mathrm{T}} \, dx. \tag{3.10}$$

Evaluating the integral, the element stiffness matrix is

$$K_i' = \frac{E_i A_i}{h_i} \begin{bmatrix} 1 & -1 \\ -1 & 1 \end{bmatrix}. \tag{3.11}$$

Equations (3.7) and (3.11) are the mass and stiffness element matrices, respectively, for element i in that element's local one dimensional coordinate system.

3.1.2 Coordinate Transformation

To relate the two displacements of each element to the truss's global degrees of freedom, two transformations must be made. The first transformation is from the local one dimensional coordinate system of element i to the 2-dimensional global coordinate system for element i with four displacements. In Figure 3.2, the truss's global coordinate system lies on the x and y axes. The orientation of element i with respect to the global coordinate system is described by angle θ_i. The one dimensional displacements can be expressed in relation to the 2-dimensional displacements and angle θ_i via

$$\begin{aligned} q_1' &= \tilde{q}_1 \cos\theta_i + \tilde{q}_2 \sin\theta_i \quad \text{and} \\ q_2' &= \tilde{q}_3 \cos\theta_i + \tilde{q}_4 \sin\theta_i. \end{aligned} \tag{3.12}$$

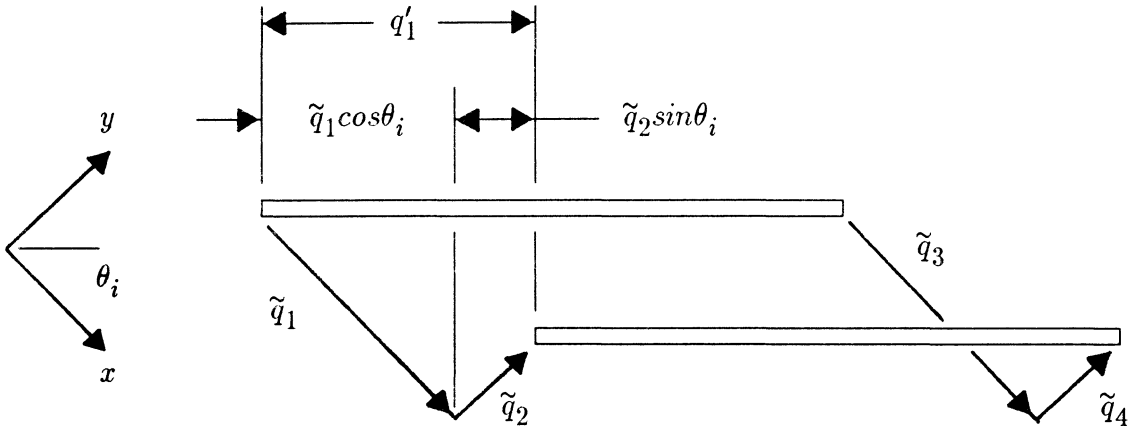

Figure 3.2: One Dimension-to-Two Dimension Transformation

In matrix form, these equations can define a transformation matrix N_i such that

$$q' = \begin{bmatrix} q'_1 \\ q'_2 \end{bmatrix} = \begin{bmatrix} \cos\theta_i & \sin\theta_i & 0 & 0 \\ 0 & 0 & \cos\theta_i & \sin\theta_i \end{bmatrix} \begin{bmatrix} \tilde{q}_1 \\ \tilde{q}_2 \\ \tilde{q}_3 \\ \tilde{q}_4 \end{bmatrix} = N_i^{\mathrm{T}} \, \tilde{q}. \tag{3.13}$$

Now a second transformation is defined which expands the two dimensional local displacements in $\tilde{q}$ to fit into the set of the global displacements. Consider element i connecting nodes l and m. The relationship between the local displacement at nodes l and m and the global displacement indices is defined by the following convention:

$$\tilde{q}_1 = q_{2l-1}\,, \qquad \tilde{q}_2 = q_{2l}\,, \qquad \tilde{q}_3 = q_{2m-1}, \qquad \tilde{q}_4 = q_{2m}. \tag{3.14}$$

This convention is used to create the transformation P_i as

$$q = \left[\, e_{2l-1} \,\middle|\, e_{2l} \,\middle|\, e_{2m-1} \,\middle|\, e_{2m} \,\right] \begin{bmatrix} \tilde{q}_1 \\ \tilde{q}_2 \\ \tilde{q}_3 \\ \tilde{q}_4 \end{bmatrix} = P_i \, \tilde{q}, \tag{3.15}$$

The vector q contains two displacements for every node in the truss. The columns of P_i are unit vectors: e_j is a vector of zeros of length n with a 1 in the j^{th} entry.

Substituting Eqs. (3.5) and (3.13) into Eqs. (3.5) and (3.9), the element

mass and stiffness matrices can be obtained from their respective energy equations. That is

$$T_i = \frac{1}{2}\,\dot{q}'^{\mathrm{T}}\,M_i'\,\dot{q}' = \frac{1}{2}\,\dot{q}'^{\mathrm{T}} P_i N_i\,M_i'\,N_i^{\mathrm{T}} P_i^{\mathrm{T}}\,\dot{q}' \tag{3.16}$$

leads to

$$M_i = P_i N_i\,M_i'\,N_i^{\mathrm{T}} P_i^{\mathrm{T}}, \tag{3.17}$$

and

$$V_i = \frac{1}{2}\,q'^{\mathrm{T}}\,K_i'\,q' = \frac{1}{2}\,q'^{\mathrm{T}} P_i N_i\,K_i'\,N_i^{\mathrm{T}} P_i^{\mathrm{T}}\,q' \tag{3.18}$$

leads to

$$K_i = P_i N_i\,K_i'\,N_i^{\mathrm{T}} P_i^{\mathrm{T}}. \tag{3.19}$$

Each element's mass and stiffness matrix describes that element's contribution to the truss's mass and stiffness properties through superposition. This contribution is unique for every element.

To formulate the global mass and stiffness matrices, the individual matrices are assembled by summation. Considering a structure with a total of N_e elements, the global mass and stiffness matrices are

$$M = \sum_{i=1}^{N_e} M_i \tag{3.20}$$

and

$$K = \sum_{i=1}^{N_e} K_i \tag{3.21}$$

respectively. Matrices M and K contain the mass and stiffness properties of the entire structure approximated by the finite element method. Both are real, symmetric matrices and have dimensions $(n \times n)$ where $n/2$ is the number of degrees of freedom in a planar truss.

3.1.3 Natural Modes of Vibration

A set of vectors and scalars that describe the dynamic behavior of a structure are its natural modes of vibration. Modes are broken up into two sets of parameters: *mode frequencies* and *mode shapes.* For a given structure with the $(n \times n)$ stiffness matrix K and mass matrix M, there exist a set of n eigenvectors, ϕ_j, and eigenvalues, λ_j, that satisfy the equation

$$M^{-1}K\ \phi_j = \omega_j^2 \phi_j, \qquad \text{for } j = \{1,2,\ldots,n\}. \tag{3.22}$$

All ϕ_j are real vectors. The mode frequencies of the structure are ω_j. The mode shapes are ϕ_j and are paired with the corresponding j^{th} mode frequency. The lowest mode frequency is termed the primary frequency or first mode, and is assigned an index of 1. The higher modes are indexed in order of increasing frequency.

A property of mode shapes is their orthoginality with respect to the mass and stiffness matrices. By convention, the mode shapes are normalized with respect to the mass matrix. That is

$$\phi_i^{\mathrm{T}} M \phi_j = \delta_{ij}, \tag{3.23}$$

where δ_{ij} is the Kronecker delta, and

$$\phi_i^{\mathrm{T}} K \phi_j = \delta_{ij} \omega_j^2. \tag{3.24}$$

In the physical sense, mode frequencies define the distinct frequencies of a structure's free response. The mode shape ϕ_j defines the amplitude of the oscillation of each degree of freedom, at the frequency ω_j. For a structure in space, no degrees of freedom are fixed with respect to the global coordinates. This creates a matrix $M^{-1}K$ that is not full rank. The zero eigenvalues of this matrix represent rigid body modes. A two dimensional truss model has two translational and one rotational rigid body modes.

3.2 HEALTHY and DAMAGED TRUSS MODELS

Before any damage has occured to a truss, the truss model is considered *healthy.* Once damage has occured to any elements, the truss model changes to a *damaged* model.

It is assumed the mass matrix is not effected by any damage. The mass matrix will be notated as M for both undamaged and damaged models. Second, the damage is modeled as a linear reduction in stiffness only. Damage then only effects stiffness of some element(s) in a given structure and nothing else.

Noting Eq. (3.10), the stiffness of an element i is completely described by the modulus of elasticity E_i of that element. Damage of element i effects only this parameter, and nothing else. For an arbitrary amount of damage in that element, a new modulus of elasticity can be written

Define: *Damage Coefficient* for element i, d_i,

$$E_{Di} = (1 - d_i)\, E_{Hi}\,, \quad 0 \leq d_i \leq 1, \tag{3.25}$$

where E_{Hi} is the undamaged modulus of elasticity and E_{Di} is the damaged modulus of elasticity. When d_i is near zero, the damaged element has little change in stiffness. When d_i is near unity, the element is highly damaged and has almost no contribution to the stiffness of the structure. Because the damage coefficient can represent damage from null to 100%, it can be assigned to every element in the structure. That is, for every element i, there is a corresponding d_i. For elements assumed to be undamaged, the term $(1 - d_i)$ is equal to unity.

Introduced in Eq. (3.25) is the subscript D which corresponds to a *damaged condition* of the parameter it marks. The subscript H corresponds to an undamaged or *healthy condition.*

Applying Eq. (3.25) to the assembly of the global stiffness matrix defined in Eq. (3.21), a damaged stiffness matrix can be derived. Assume that one arbitrary element l is the only damaged element in a given truss. That is $d_i = 0$ for all $i \neq l$. Then

$$K_D = K_1 + K_2 + \cdots + (1 - d_l)K_l + \cdots + K_{N_e} \tag{3.26}$$

or

$$K_D = K_H - d_l K_l. \tag{3.27}$$

Equation (3.27) expresses damage in element l in terms of the healthy structure.

For damage to many elements, the damaged stiffness matrix is

$$K_D = K_H - \sum_{i=1}^{N_e} d_i K_i \tag{3.28}$$

The representation of the damaged stiffness matrix in terms of the healthy stiffness matrix can be simplified further. Consider the singular value decomposition of the stiffness matrix of element i. Since K_i is a real, symmetric matrix with the rank of one, only one singular vector and singular value are needed to form K_i. The singular value decomposition of K_i yields

$$K_i = U_i \Sigma_i U_i^{\mathrm{T}}. \tag{3.29}$$

Since all but one singular values in Σ_i are zero, this can be written as

$$K_i = u_i \sigma_i u_i^{\mathrm{T}}, \tag{3.30}$$

where u_i is the first singular vector and σ_i is the first singular value. The decomposition in Eq. (3.30) will play an important role below.

Define: Element Stiffness Vector, B_i,

$$B_i = \sqrt{\sigma_i}\, u_i. \tag{3.31}$$

Note $B_i B_i^{\mathrm{T}} = K_i$. Recalling the development of K_i, B_i can be calculated directly from P_i and N_i. To see this, perform symmetric factorization on Eq. (3.11) and substitute into Eq. (3.20), yielding

$$K_i = P_i N_i \begin{bmatrix} 1 \\ -1 \end{bmatrix} \frac{E_{Hi} A_i}{h_i} \begin{bmatrix} 1 & -1 \end{bmatrix} N_i^{\mathrm{T}} P_i^{\mathrm{T}}. \tag{3.32}$$

Then by the definition of the element stiffness vector

$$B_i = \sqrt{\frac{E_{Hi} A_i}{h_i}}\; P_i N_i \begin{bmatrix} 1 \\ -1 \end{bmatrix}. \tag{3.33}$$

Because no two elements can connect the same two nodes, the transformation matrix P_i is unique for every element in the structure. This makes every B_i unique. The element stiffness vector B_i contains all the information contained in K_i. In Eq. (3.33), it is important to note the inclusion of an H subscript defining the healthy modulus for element i. This means that B_i is computed at the point of space structure deployment, and **is not effected by damage**. Thus, the set of B_i for i=$\{1,2,\ldots, N_e\}$ is always known, before and after damage. This idea is crucial to the development of the damage detection algorithm in a later chapter. To represent damage in element i, Eq. (3.26) can be substituted into Eq. (3.33) to yield

$$\sqrt{(1-d_i)}\, B_i = \sqrt{\frac{E_{Di}A_i}{h_i}}\; P_i N_i \begin{bmatrix} 1 \\ -1 \end{bmatrix}, \tag{3.34}$$

where $d_i \neq 1$. Substituting this expression into Eq. (3.33), the damaged stiffness matrix becomes

$$K_D = K_H - \sum_{i=1}^{N_e} B_i d_i B_i^{\mathrm{T}} \tag{3.35}$$

The only unknown parameters of a damaged truss then are the set of all damage coefficients d_i for $i = \{1,2,\ldots,N_e\}$. Embedded in this set of unknowns is the location and severity of all damage. A damage coefficient d_i that is nonzero implies that damage is located in element i. It is the goal of this damage detection research to provide a method for estimating all d_i.

The system equation of a structure with element l damaged is

$$M\ddot{q} + \left(K_H - B_l d_l B_l^{\mathrm{T}}\right) q = \{0\}, \tag{3.36}$$

and more generally for any damage case

$$M\ddot{q} + \left(K_H - \sum_{i=1}^{N_e} B_i d_i B_i^{\mathrm{T}}\right) q = \{0\}. \tag{3.37}$$

These two equations are the base from which two damage detection methods will be derived in later chapters.

Because modes are unique to a model, they are affected by any change in the property matrices due to damage. Introducing the healthy and damage subscripts, the *health modes* are defined as

$$K_H \phi_{Hj} = \omega_{Hj}^2 M \phi_{Hj}, \tag{3.38}$$

and the *damaged modes* are

$$K_D \phi_{Dj} = \omega_{Dj}^2 M \phi_{Dj}$$

or

$$(K_H - \sum_{i=1}^{N_e} B_i d_i B_i^{\mathrm{T}})\ \phi_{Dj} = \omega_{Dj}^2 M \phi_{Dj} \tag{3.39}$$

3.3 EXPERIMENTAL TRUSS MODELS

Two planar truss models used for simulations in future chapters are presented here. Both models are constructed with the same unit box called a *bay*. A bay consists of two vertical, two horizontal, and two diagonal elements. All elements are constructed with the same material, and all have the same cross-sectional area. This particular model has been used by several researchers [7,8,9,10,11,15,18].

Table 3.1 lists the properties of all elements. The 3 bay truss is shown in Figure 3.3 and the 10 bay in Figure 3.4. Note in both trusses, elements are indexed by the same convention.

Table 3.1: Planar Truss Parameters

A_i	element cross-sectional area	0.3657 in^2
E_i	axial elastic modulus	40×10^6 psi
ρ	material density	0.63 lb/in^3
h	bay dimension	196.85 in

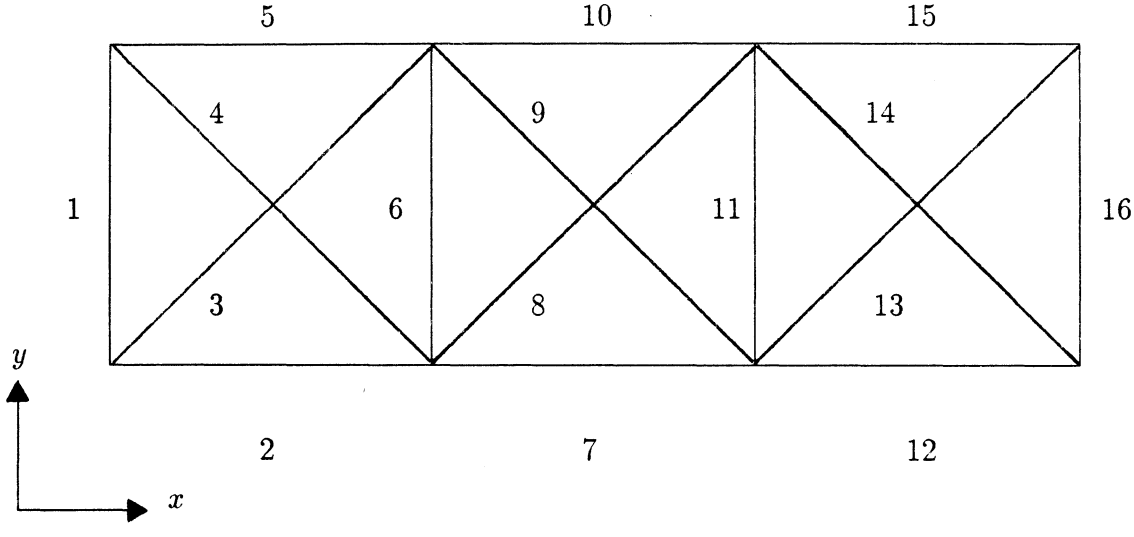

Figure 3.3: 3 Bay Planar Truss

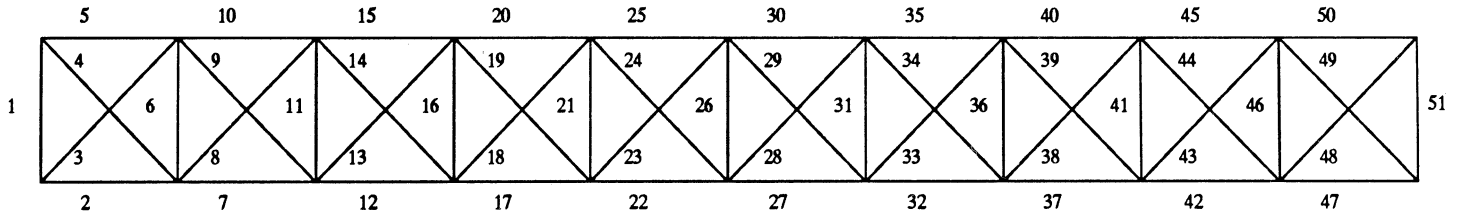

Figure 3.4: 10 bay truss

4 MODE IDENTIFICATION

The primary step in any damage detection method is to perform a modal survey or mode identification. The importance of this topic warrants it's coverage in this thesis. The first section of this chapter discusses a linear system identification method commonly used in modal surveys. The second section presents the modal assurance criteria as a measure of the error in the identified modes. This measurement is used to detect modes with large amounts of error. The last section discusses a mode expansion method which enables incomplete modes to be modified for use in damage detection methods.

4.1 IDENTIFICATION METHODS

The two groupings for mode identification are frequency domain methods and time domain methods. The frequency domain methods began with the introduction of the Fast-Fourier-Transform [23]. Starting with the cross and auto-spectra of both input and output signals, the frequency methods develop a structure transfer function from ensemble averages. To estimate the modal parameters from the transfer function, there are two types of general methods: single-degree-of-freedom methods and multi-degree-of-freedom methods [16,23]. The single-degree-of-freedom techniques assume the structure's dynamics are

dominated by a single mode, a poor assumption for large truss structures which have closely spaced natural frequencies. The multi-degree-of-freedom methods use curve fitting over the frequency range of interest and are not widely used [23].

In the time domain group, the Ibrahim Time Domain method [25] and the Eigensystem Realization Algorithm (ERA) [24] are the two most used identification methods [23]. Because of its popularity, the latter method will be discussed.

Because the time response at each DOF is sampled, the structure's ideal model is a discrete-time, linear, time-invariant system with the n dimensional system equation

$$x_{k+1} = Ax_k + Bu_k \tag{4.1}$$

$$y_k = Cx_k,$$

where B is a $(n \times m)$ input matrix determined by actuator placement, and C is a $(p \times n)$ output matrix determined by sensor placement. For this algorithm to estimate modes of full dimension, m and p must equal n.

Matrix A is the unknown system matrix which is a function of the structure's mass, damping, and stiffness properties. For a given input signal and a given output signal, there exist an infinite number of realizations of A, B, and C that will identically reproduce the system dynamics. The realization produced by this method is of minimum order.

To estimate a realization, this algorithm operates on a Hankel matrix constructed of *Markov parameters* which are defined as

$$J_k = CA^{k-1}B. \tag{4.2}$$

For a discrete-time system, the Markov parameters are identical to the system's impulse response. The primary source of error in the ERA is the estimation of the Markov parameters in the presence of noise [26]. The Markov parameters form the multi-dimensional Finite Impulse Response filter

$$y_k = \left(J_0 z^{-1} + J_1 z^{-2} + \cdots + J_l z^{-l}\right) u_k + v_k \tag{4.3}$$

where v_k is a vector of the added noise in the sensor array and l is the last term before truncation.

Rather than approximating the Markov parameters as the impulse response of the structure, they can be estimated from the cross-correlation between the output and uncorrelated white noise input by the ensemble average

$$J_{k-j-1} = E\left[y_k\, u_j^{\mathrm{T}}\right] \tag{4.4}$$

[27]. Each Markov parameter is of dimension $(p \times m)$.

The Eigensystem Realization Algorithm operates on a Hankel matrix such that

$$H_{rs}(k-1) = \begin{bmatrix} J_k & J_{k+1} & \cdots & J_{k+r} \\ J_{k+1} & J_{k+2} & \cdots & J_{k+r+1} \\ \vdots & \vdots & \ddots & \vdots \\ J_{k+s} & J_{k+s+1} & \cdots & J_{k+s+r} \end{bmatrix}. \tag{4.5}$$

The dimension of H_{rs} is $(rp \times sm)$ where r and s are values chosen by the user. This matrix is identical to the matrix triple product

$$H_{rs}(k) = V_r A^k W_s \tag{4.6}$$

where V_r is defined as the observability matrix of dimensions $(rp \times n)$ and W_s is the controllability matrix of dimension $(n \times ms)$. That is

$$V_r = \begin{bmatrix} C \\ CA \\ CA^2 \\ \vdots \\ CA^{r-1} \end{bmatrix}, \tag{4.7}$$

and

$$W_s = \begin{bmatrix} B & AB & A^2B & \cdots & A^{s-1}B \end{bmatrix}. \tag{4.8}$$

The first step in this algorithm is to build the Hankel matrix $H_{rs}(0)$. The dimensions r and s should be chosen such that the number of independent rows and columns in $H_{rs}(0)$ are larger than the order of the system. This results in the Hankel matrix being of order n. If n is unknown, then the values of r and s should be increased until the rank of $H_{rs}(0)$ stops increasing.

Next, perform singular value decomposition on the Hankel matrix. Because the rank of $H_{rs}(0)$ is n, there are only n nonzero singular values. The singular

value equation is then partitioned to reflect this:

$$H_{rs}(0) = \left[P_d \,\middle|\, P_e \right] \begin{bmatrix} D_d & 0 \\ 0 & 0 \end{bmatrix} \left[\frac{Q_d^{\mathrm{T}}}{Q_e^{\mathrm{T}}} \right] = P_d D_d Q_d^{\mathrm{T}} \tag{4.9}$$

where P_d is an $(rp \times n)$ unitary matrix and Q_d is an $(ms \times n)$ unitary matrix. To compute the realization from the decomposition, Eq. (4.9) is rewritten as

$$H_{rs}(0)\, Q_d D_d^{-1} P_d^{\mathrm{T}} = I_d. \tag{4.10}$$

Next, two matrices are identified such that

$$E_p = \left[\begin{array}{cccc} I_p & \emptyset_p & \cdots & \emptyset_p \end{array} \right], \text{ and } \qquad E_m = \begin{bmatrix} I_m \\ \emptyset_m \\ \vdots \\ \emptyset_m \end{bmatrix}, \tag{4.11}$$

where $\emptyset_l$ is a zero matrix of dimension $(l \times l)$. Then, by definition,

$$J_k = E_p\, H_{rs}(0)\, E_m. \tag{4.12}$$

Substituting Eqs. (4.6) and (4.10) into Eq. (4.12) yields

$$J_k = E_p H_{rs}(0)\, [Q_d D_d^{-1} P_d^{\mathrm{T}}]\, V_r A^k\, W_s\, [Q_d D_d^{-1} P_d^{\mathrm{T}}]\, H_{rs}(0)\, E_m$$

$$J_k = E_p\, H_{rs}(0) Q_d D_d^{-1/2}\, [D_d^{-1/2} P_d^{\mathrm{T}}\, H_{rs}(1)\, Q_d D_d^{-1/2}\,]^k\, D_d^{-1/2}\, P_d^{\mathrm{T}}\, H_{rs}(0)\, E_m$$

$$J_k = \underbrace{E_p\, P_d D_d^{1/2}}\ \underbrace{[D_d^{-1/2} P_d^{\mathrm{T}}\, H_{rs}(1)\, Q_d D_d^{-1/2}\,]^k}\ \underbrace{D_d^{1/2}\, Q_d^{\mathrm{T}}\, E_m} \tag{4.13}$$

$$J_k \;=\; \tilde{C} \qquad\qquad \tilde{A}^k \qquad\qquad \tilde{B}$$

where $\tilde{A} = T^{-1}AT$, $\tilde{B} = T^{-1}B$, and $\tilde{C} = CT$, and T is some unknown transformation matrix. The definitions stated in Eq. (4.13) can be viewed as

$$H_{rs}(k) = V_r A^k\, W_s \;= \tilde{V}_r \tilde{A}^k\, \tilde{W}_s, \tag{4.14}$$

where

$$H_{rs}(0) = \tilde{V}_r \tilde{W}_s = \left[P_d D_d^{1/2}\right]\left[D_d^{1/2}\, Q_d^{\mathrm{T}}\right] \tag{4.15}$$

then

$$H_{rs}(1) = \tilde{V}_r \tilde{A}\, \tilde{W}_s = \left[P_d D_d^{1/2}\right] \tilde{A} \left[D_d^{1/2}\, Q_d^{\mathrm{T}}\right].$$

Solving for $\tilde{A}$ then yields

$$\tilde{A} = D_d^{-1/2} P_d^{\mathrm{T}}\, H_{rs}(1)\, Q_d D_d^{-1/2}. \tag{4.16}$$

To obtain $\tilde{B}$, extract the first m columns of $\tilde{W}_s$, and to obtain $\tilde{C}$, extract the first p rows of $\tilde{V}_r$.

The choice of the factorization of D_p to $D_d^{1/2}$ is not unique. That is, one could write $V_r = P_d$ and $W_s = D_d Q_d$ and would still obtain a valid realization.

The decomposition $[D_d^{1/2} D_d^{1/2}]$ is chosen to create a system that is internally balanced [28]. This implies the system's observability and controllability holds the relationship $V^*V = WW^*$ where

$$V^*V = D_d^{1/2} P_d^* P_d D_d^{1/2} = D^d = D_d^{1/2} Q_d Q_d^* D_d^{1/2} = WW^*. \tag{4.17}$$

To compute the identified mode shapes and frequencies, first consider the eigenvalues and eigenvectors of the system identified. The eigenvalue equation is

$$\tilde{A}\ \Psi = Z\ \Psi \tag{4.18}$$

where Ψ is a matrix of identified eigenvectors and Z is a diagonal matrix of the Z-domain poles, z_j. The discrete poles can be mapped to the S-domain with the function

$$\lambda_j = (ln(z_j) \pm 2\pi ik)\ /t_s \tag{4.19}$$

where t_s is the sample time chosen during data acquisition, $i = \sqrt{-1}$ and k is an integer. The mode shapes are given by

$$\Phi = \tilde{C}\ \Psi \tag{4.20}$$

where Φ is the matrix of mode shapes. Because eigenvectors do not change from the Z-domain to the S-domain, no transformation is required.

Care must be taken when selecting the size of the Hankel matrix and

choosing the sample rate. If the sample frequency is chosen too large, the Hankel matrix must be large to incorporate enough information on the lowest modes. This can create a tremendous computational burden during singular value decomposition.

Errors in the estimated Markov parameters may produce a Hankel matrix that is of larger rank than the true linear system. The result is small, nonzero singular values are produced in lue of zero singular values. Round-off error is also a cause of this. To reduce this effect, a threshold may be applied to filter out the small singular values [24]. If this process produces a P_d matrix that is still larger than the correct system order, noise modes are produced in addition to the true modes. Modal amplitude coherence can be used to detect and filter out these noise modes, and to measure error in the true identified modes.

4.2 MODE SHAPE ASSURANCE

Once the natural modes of vibration have been estimated by an identification algorithm, it is desired to select from them, a set of modes that are good representatives of the damaged structure. That is, a set of modes that are not greatly corrupted by error. This selection process is a key step in a modal survey.

In application, there are many sources of error during mode identification. An incorrect selection of singular values in the ERA will create noise modes. Noise modes are modes with no physical significance, and do not describe the dynamics of the damaged structure. Typically, only the lower frequency modes provide accurate dynamic information. The signal strength of the higher frequency components in the sampled data is very low compared to the lowest frequencies. Noise tends to dominate these measurements. In addition, structural nonlinearities, geometric errors incurred during construction, and local vibrations not considered by the finite element method all contribute to errors in the higher modes [1]. Hence, determining and eliminating these erroneous modes is a necessary step.

To provide a quantitative measure of identified modes, an indicator called the *modal amplitude coherence* is discussed by Juang and Pappa that uses only information from the identification algorithm [24]. The measure is formed by comparing the identified modal amplitude history with a history extrapolated from the initial amplitudes and the identified eigenvalue. The initial amplitudes are defined as

$$\Psi^{-1}B = \left[\begin{array}{c|c|c|c} b_1 & b_2 & \cdots & b_n \end{array}\right]^* \tag{4.21}$$

where Ψ and B are known from the ERA and the columns, b_i, corresponds to the S-domain eigenvalues, s_i. The ideal modal amplitude history is expressed as

$$\widehat{q}_j^* = \left[\; b_j^* \;\middle|\; b_j^* \, e^{t_1 \Delta\tau s_j} \;\middle|\; \cdots \;\middle|\; b_n^* \, e^{t_{s-1} \Delta\tau s_j} \; \right]^* \tag{4.22}$$

where $j = \{1, 2, \ldots, n\}$. The identified amplitude history which represents real measurement data obtained from the decomposition of the Hankel matrix is expressed as

$$\Psi^{-1} D^{1/2} Q^{\mathrm{T}} = \left[\; q_1 \;\middle|\; q_2 \;\middle|\; \cdots \;\middle|\; q_n \; \right]^* . \tag{4.23}$$

The modal amplitude coherence is created by comparing the ideal history $\widehat{q}_j^*$ with the measured history q_j^*. The coherence measure is defined as

$$\gamma_j = \frac{\left| \widehat{q}_j^* q_j \right|}{\left(\left| \widehat{q}_j^* \widehat{q}_j \right| \left| q_j^* q_j \right| \right)^{1/2}} \tag{4.24}$$

where $0 \leq \gamma_j \leq 1$. Under an exact identification, $\gamma_j = 1$ when the eigenvalue s_j and the initial amplitude b_j correspond to the true jth mode. As $\gamma_j \rightarrow 0$, the ideal and identified history become more dissimilar, indicating poor identification, or a noise mode.

Edwins offers the *modal assurance criteria* which is a similar measure that uses the healthy modes as well as the identified modes [16]. This measure was originally developed to compare the analytic mode shapes with the measured mode shapes in the process of model refinement [20]. In the application of damage detection, the structure to be identified is similar dynamically to the healthy structure. Hence, the identified modes often differ only slightly from the healthy modes. The measure is defined as

$$MAC_{ij} = \left[\frac{(\phi_{Dj}^{\mathrm{T}} \phi_{Hi})^2}{(\phi_{Dj}^{\mathrm{T}} \phi_{Dj})(\phi_{Hi}^{\mathrm{T}} \phi_{Hi})} \right]^{1/2} \tag{4.25}$$

where $0 \leq MAC_{ij} \leq 1$. Different from the modal amplitude coherence, this measure will only exactly equal unity if the identified mode j is identical to the healthy mode i, implying no damage. The value of MAC_{ij} is equal to zero when the two mode shapes are orthogonal. Since mode shapes are orthogonal with respect to the mass and stiffness matrices and not always with respect to each other, MAC_{ij} is not always zero. For cases where damage affects the modes shapes very little, the MAC_{ij} are expected to be near unity for all $i = j$. However, as damage increase, MAC_{ij} for $i = j$ decreases and MAC_{ij} for $i \neq j$ tend to increase.

Because of the influence of damage on this measure, its use is limited to the rejection of noise modes. For a given damaged mode j, if MAC_{ij} over all i has no dominant maximum, mode j may be a noise mode. However, this method of mode selection is recognized as being inaccurate under some circumstances [20,24].

4.3 MODE SHAPE EXPANSION

The ideal modal survey will use a full set of signals in which to identify modes. This requires sensors to be located at every degree of freedom. Due to the large number of degrees of freedom, actual structures are usually not fully instrumented. The number of sensors usually is less than 10% of the finite element model order [1]. Two different approaches to deal with this widely recognized problem are the expansion of identified mode shapes and analytical model reduction [1,11]. However, model reduction methods are inadequate for damage detection when damage significantly effects the unmeasured portion of mode shapes [1]. Only modal expansion is applicable to the algorithm developed in this thesis. The orthogonal Procrustes expansion technique will be discussed in this section.

Originally, the development of this expansion method was motivated by research in the model refinement field. Applied to damage detection, this expansion method can be viewed as a search for a linear relationship between the healthy modes and the incomplete identified modes from the damaged structure [11].

If the number of degrees of freedom measured is s and the number of identified modes is p, the expanded or estimated mode shape can be expressed as

$$\widehat{\Phi}'_D = \left[\begin{array}{c} u_m \\ \hline d_m \end{array}\right] = \left[\begin{array}{c} u_H \\ \hline d_H \end{array}\right] P_{op} \tag{4.26}$$

where u_m is a matrix of the s measured components of the identified mode shapes

and u_H is a matrix of the corresponding known, healthy mode shapes. The remaining unmeasured and known components are d_m and d_H, respectively. Note that the resulting damage mode estimates $\widehat{\Phi}'_D$ must be reordered to obtain $\widehat{\Phi}_D$.

The problem is reduced to computing the transformation matrix P_{op}. The problem is stated as

$$\min_{\text{wrt } P_{op}} \left\| u_m - u_H P_{op} \right\|_F \quad \text{subject to} \quad P_{op}^{\mathrm{T}} P_{op} = I_p. \tag{4.27}$$

The solution to this equation is

$$P_{op} = DQ^{\mathrm{T}} \tag{4.28}$$

where D and Q are the unitary matrices produced by the singular value decomposition of the $(p \times p)$ matrix

$$Y = u_H^{\mathrm{T}} u_m = D\Sigma Q^{\mathrm{T}} \tag{4.29}$$

[11]. This implies

$$d_m = d_H P_{op} \tag{4.30}$$

Once d_m is computed, it is reordered with u_m to create the expanded mode. The performance of this technique is dependent upon the severity of the damage.

5 LOCATION and ESTIMATION of SINGLE-ELEMENT DAMAGE

The algorithm developed in this chapter is designed to locate and estimate the damage in a single-element damage scenario. It is developed in two sections. First, a common eigenvector assignment method is used to solve for the damage coefficient. The damage coefficient estimate is computed for every mode and element. Then, a method of searching through the resulting data is developed to locate and estimate the damage. The result is a damage detection method that has few steps and is accurate for single-element damage. Finally, some simulation results are presented.

5.1 SINGLE-ELEMENT DAMAGE MODEL

The algorithm presented in this chapter expresses the location and extent of the damage to one element in terms of the damaged modes and the healthy truss model. Recall Eq. (3.37) and multiply both sides by M^{-1}. For damage occurring only to element l, the equation is simplified to

$$\left(M^{-1}K_H - M^{-1}B_l d_l B_l^{\mathrm{T}}\right)\phi_{Dj} = \omega_{Dj}^2 \phi_{Dj}. \tag{5.1}$$

This provides a relationship between the known parameters K_H, M, ϕ_{Dj}, and ω_{Dj} and the unknown parameters describing the damage, d_l and B_l. To reach the goal of damage location and estimation, an intermediate step is taken by assuming that the location of the damage is known. Thus, the damaged element index l is known as well as the damaged modes, resulting in complete description of Eq. (5.1) except for d_l.

Equation (5.1) holds the same form as an eigenvalue equation to a linear system with feedback gain d_l, where $M^{-1}B_l$ and B_l^{T} are the input and output matrices, respectively. Because of this likeness, an eigenvector assignment technique common in the field of control systems can be used to solve for d_l. To begin, let the matrix T must be a transformation matrix such that

$$TM^{-1}B_l = \begin{bmatrix} B_{cl} \\ 0 \\ \vdots \\ 0 \end{bmatrix}, \tag{5.2}$$

where B_{cl} is a scalar [29]. This transformation is applied to all other terms in Eq. (5.1), resulting in

$$A = TM^{-1}K_H T^{-1},$$

$$\tilde{B}_l^{\mathrm{T}} = B_l^{\mathrm{T}} T^{-1},$$

and

$$\tilde{\phi}_{Dj} = T\phi_{Dj}.$$

Next A and $\tilde{\phi}_{Dj}$ are partitioned compatibly with Eq. (5.2) yielding

$$A = \left[\begin{array}{c} A_1 \\ \hline A_2 \end{array}\right], \quad \text{and} \qquad \tilde{\phi}_{Dj} = \left[\begin{array}{c} \tilde{\phi}_{D1j} \\ \hline \tilde{\phi}_{D2j} \end{array}\right],$$

where, A_1 has dimension $(1 \times n)$ and $\tilde{\phi}_{D1j}$ is a scalar. With these partitions, Eq. (5.1) becomes

$$A_1\tilde{\phi}_{Dj} - B_{cl}d_l\tilde{B}_l^{\mathrm{T}}\tilde{\phi}_{Dj} = \omega_{Dj}^2\tilde{\phi}_{D1j}. \tag{5.3}$$

Now the dimensions of the partitioned matrices are suitable to solve for d_i. The result is

$$d_l = B_{cl}^{-1}\left[\omega_{Dj}^2\tilde{\phi}_{D1j} - A_1\,\tilde{\phi}_{Dj}\right]\left(\tilde{B}_l^{\mathrm{T}}\,\tilde{\phi}_{Dj}\right)^{-1} \tag{5.4}$$

This equation is significant in that knowing the location of damage and one damaged mode in a single-element damage scenario, the damage coefficient can be found exactly. Note that since $T^{\mathrm{T}}T = I$, the last term is simply $(B_l^{\mathrm{T}}\,\phi_{Dj})^{-1}$.

Consider a variation of Eq. (5.4) where B_i is substituted for the known B_l. If B_i is *any* valid element stiffness vector, then

Define: *Estimated Modal Damage Coefficient,* $\widehat{d}_{ij}$,

$$\widehat{d}_{ij} = B_{ci}^{-1}\left[\omega_{Dj}^2\tilde{\phi}_{D1j} - A_1\,\tilde{\phi}_{Dj}\right]\left(B_i^{\mathrm{T}}\,\phi_{Dj}\right)^{-1} \tag{5.5}$$

In order to have a successful detection method, the assumption that the damage location is known must be relaxed. For a given case of damage in a structure, a value of $\widehat{d}_{ij}$ can be calculated for every mode j and every element i. However, only when $B_i = B_l$ does $\widehat{d}_{ij} = d_l$. This introduces the idea that, in order to obtain the correct damage coefficient from Eq. (5.5), one must search through every possible element.

When this postulation is incorrect (ie: $B_i \neq B_l$), Eq. (5.1) can be rewritten

$$\left(M^{-1}K_H - M^{-1}B_i\,\widehat{d}_{ij}B_i^{\mathrm{T}}\right)\widehat{\phi}_{Dj} = \widehat{\omega}_{Dj}^2\widehat{\phi}_{Dj}. \tag{5.6}$$

where $\widehat{\phi}_{Dj} \neq \phi_{Dj}$. Equation (5.5) produces a $\widehat{d}_{ij}$ value which *assigns* the eigenvector $\widehat{\phi}_{Dj}$ in the above equation as close to ϕ_{Dj} as possible in the least squares sense [29].

Note the inner product of B_i and ϕ_{Dj} must be nonzero, otherwise the term $(B_i^{\mathrm{T}}\phi_{Dj})^{-1}$ will approach infinity. This implies that deflections at the frequency ω_{Dj} are unobservable in the element described by B_i. This condition can easily be tested before calculation $\widehat{d}_{ij}$.

To derive the condition in which ϕ_{Dj} is fully assignable, consider Eq. (5.6) which can be written as

$$\phi_{Dj} = \left(\omega_{Dj}^2 I - M^{-1}K_H\right)^{-1}M^{-1}B_l d_l B_l{}^{\mathrm{T}}\phi_{Dj}. \tag{5.7}$$

From this define

$$m_{lj} = d_l B_l{}^{\mathrm{T}}\phi_{Dj}$$

and

$$[\Psi]_{lj} = \left(\omega_{Dj}^2 I - M^{-1}K_H\right)^{-1} M^{-1}B_l.$$

Then Eq. (5.7) is

$$\phi_{Dj} = [\Psi]_{lj}\, m_{lj}. \tag{5.8}$$

Equation (5.8) implies that ϕ_{Dj} is a linear combination of the columns of $[\Psi]_{lj}$ weighted by the entries of m_{lj}. Hence, in order for the desired close loop eigenvector ϕ_{Dj} to be fully assigned, it must lie in the subspace spanned by $[\Psi]_{lj}$ [29]. This can be termed the *achievable* subspace.

However, $[\Psi]_{lj}$ is a vector of dimension $(n \times 1)$ and m_{lj} is a scalar. For ϕ_{Dj} to be completely assignable, it must be equal to $[\Psi]_{lj}$ times a scalar. Since each B_i is unique, this occurs if and only if $[\Psi]_{lj}$ contains B_l. Hence, if any other element stiffness vector is postulated, Eq. (5.8) will not hold and the desired eigenvalue ϕ_{Dj} is only partially assignable [29].

To summarize this section, the estimate modal damage coefficient, $\widehat{d}_{ij}$, was defined as scalar value that is computed via an eigenvector assignment method. The assignment method requires one damaged mode, the mass and healthy stiffness matrices, and some postulated B_i. If the B_i postulated is identical to that of the damage location, then $\widehat{d}_{ij} = d_i$, and the damaged mode is fully assignable.

5.2 DAMAGE LOCATION and ESTIMATION

To locate and estimate damage from Eq. (5.5), consider computing $\widehat{d}_{ij}$ for every mode j and truss element i, and form this data into an array. This array will be called the *estimated modal damage coefficient array* with the symbol $[\widehat{d}]$. Let the rows of $[\widehat{d}]$ be indexed i which correspond to truss element indices, and let the columns be indexed j corresponding to the mode indices. If the number of damaged modes known is N_m, then $[\widehat{d}]$ is a matrix of dimension $(N_m \times N_e)$.

Note that damage is still assumed to exists in element l only. Equation (5.5) has been derived to compute an estimate of d_i. Only when B_l is postulated is this estimate accurate. In this case, the damaged mode shape considered is fully assignable by using $\widehat{d}_{ij}$ in Eq. (5.6). In fact, when B_l is postulated, $\widehat{d}_{ij}$ simultaneously assigns all damaged modes such that $\widehat{\phi}_{Dj} = \phi_{Dj}$ for all j. This results is the same value of $\widehat{d}_{ij}$ for all j, and produces a column of constant values in $[\widehat{d}]$.

The single-element damage location and estimation algorithm can now be proposed:

Step 1. Compute $\widehat{d}_{ij}$ for every element i and every available mode j and arrange into the estimated modal damage coefficient array, $[\widehat{d}]$.

Step 2. Filter out any $\widehat{d}_{ij}$ values outside of the allowable range, $0 \leq \widehat{d}_{ij} \leq 1$, by setting to zero. Notate this matrix with the symbol $[\widehat{d}]_f$.

Step 3. Search the columns of $[\widehat{d}]_f$ for a column of consistent entries. The index of that column is the index of the damaged element. The value in that column are equal to the true damage coefficient.

The last step in the algorithm can be visualized by:

$$[\widehat{d}]_f = \left[\begin{array}{c|c|c|c|c} * & & d_l & & * \\ * & \cdots & d_l & \cdots & * \\ \vdots & & \vdots & & \vdots \\ * & & d_l & & * \end{array}\right], \qquad (5.9)$$

$$\uparrow$$

column l

where l is the index of the damaged element and $*$ represents entries with arbitrary values. This step can be viewed as a pattern recognition problem.

Every entry in the l^{th} column of $[\widehat{d}]_f$ will be equal to d_l with the exception of any unobservable modes. If the mode j is unobservable to element i, $\widehat{d}_{ij}$ will approach infinity. To avoid this, the mode can be tested and rejected before computation. In any other column, the impossibility of full eigenvector assignment produces $\widehat{d}_{ij}$ values that are not all the same, and are often out of the allowable range. Equation (5.9) represents these arbitrary entries by $*$.

Figure 5.1 is a block diagram of the algorithm. The symbols Φ_D and Ω_D represent a set of N_m damaged mode shapes and frequencies, respectively. Note that M and K_H are embedded in the eigenvector assignment routine because they are known a priori and can be stored in the algorithm. The same applies to all element stiffness vectors B_i which do not change with damage.

The primary advantage of this algorithm is that the reduction in stiffness caused by damage is solved for exactly. Contrary to some methods, this exact solution requires no intermediate step of analysis. Locating the damage represented by a column of identical values is a simple pattern recognition problem

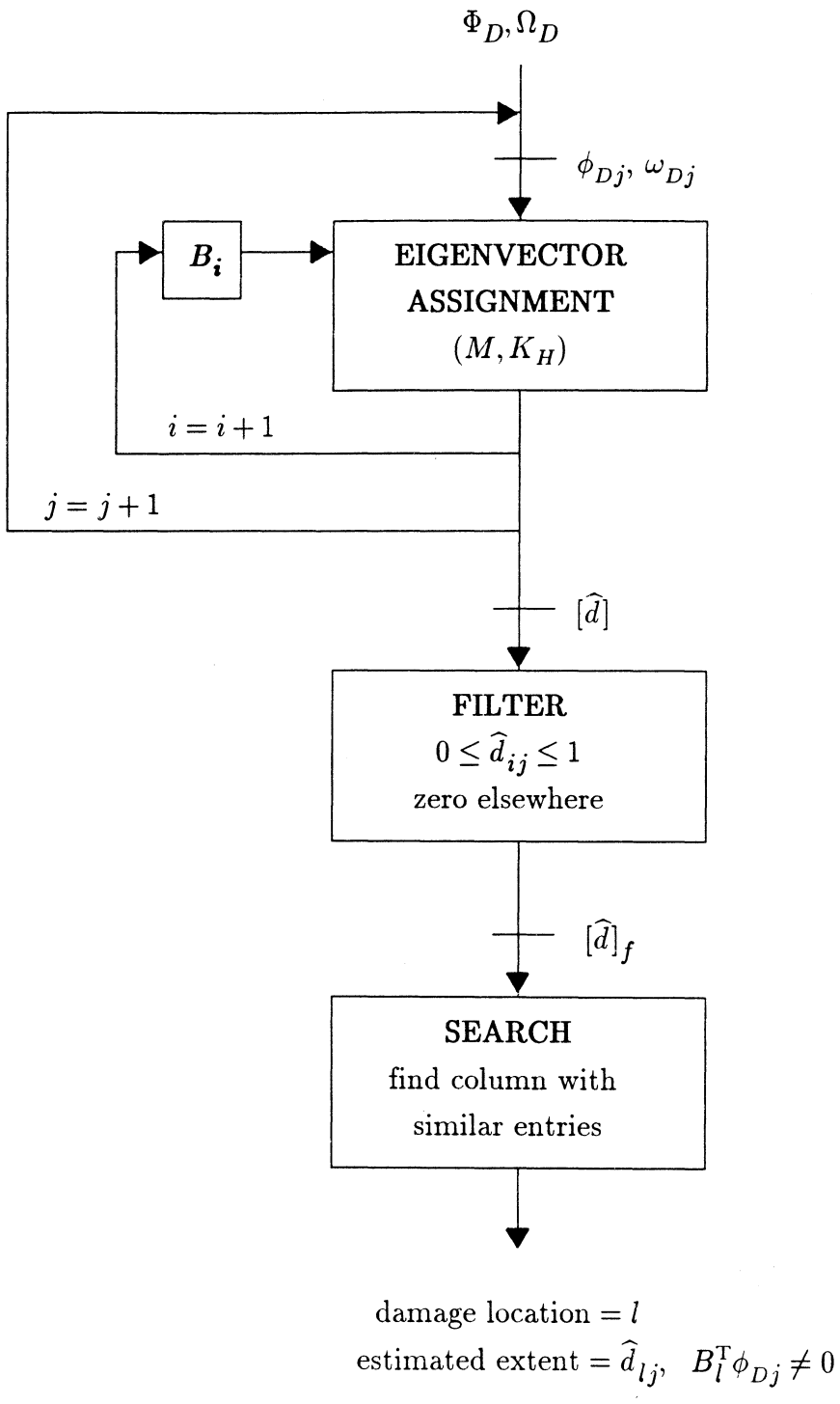

Figure 5.1: Single-Element Damage Location & Estimation Algorithm

and is easily automated in an on-line system. In addition, only one identified mode is required for each $\widehat{d}_{ij}$ value. Only several $\widehat{d}_{ij}$ values are required per element to locate a linear trend in the columns of $[\widehat{d}]_f$, providing $B_i^{\mathrm{T}}\phi_{Dj} \neq 0$. Hence, the small size of a damaged mode set commonly provided from a modal survey does not degrade performance.

The main disadvantage of this detection method is that it is developed around the single-element damage case. This method is generally not able to accurately assess the damage in a truss if more than one element is damaged.

A second disadvantage is the large number of iterations required for large structures. Some proposed space structures have over 500 elements. If three damaged modes are used, over 1500 iterations are required. However, each iteration requires few vector computations. To show this, let T_1 be the first row of the transformation matrix, T, defined in Eq. (5.2). Then Eq. (5.5) can be written as

$$\widehat{d}_{ij} = B_{ci}^{-1}\left(B_i^{\mathrm{T}}\,\phi_{Dj}\right)^{-1}\left[\,\omega_{Dj}^2 T_1 - T_1 M^{-1} K_{Hj}\right]\phi_{Dj}\,. \tag{5.10}$$

Because they only depend on the element stiffness vector, the term B_{ci}^{-1}, T_1 and $T_1 M^{-1} K_H$ can be computed off line and stored in a data base. Hence, the computations required are reduced to one $(n \times 1)$ vector subtraction, two $(n \times 1)$ vector inner products, and three scalar multiplications.

5.3 SIMULATION RESULTS

The single-element damage location and estimation algorithm was exercised with several different scenarios of damage to the 3 bay and the 10 bay trusses. The data from this simulation is presented graphically, rather than numerically. This is done because the primary goal of this section is to illustrate nature of the pattern recognition problem. In addition to verifying expected performance for single element damage, the algorithm was tested with cases of multi-element damage.

The mode shapes and frequencies were computed directly from the mass matrix and the damaged stiffness matrix. All modes are used in the 3 bay simulation, and the lowest ten modes were used for the 10 bay simulation. All $[\widehat{d}]_f$ computed are presented as mesh plots. The z axis indicates the magnitude of $\widehat{d}_{ij}$, the x axis is the column index i of $[\widehat{d}]_f$, and the y axis is the mode index j. All filtered values out of range and all values corresponding to unobservable modes are set to zero.

Damage detection with the 3 bay truss is first examined. Figure 5.2 is the mesh plot of a typical $[\widehat{d}]_f$ of a single-element damage case. The linear trend indicating the damage location is very visible in column 3. The height of this column is exactly 0.5. Other nonzero values outside column 3 have no apparent pattern. Figure 5.3 represents a damaged element with unobservable modes. Seven out of 13 modes are observable for element 10. Noting that the index of any unobservable modes is known, the linear trend is clearly visible.

Beyond the expected performance of the algorithm, cases of multi-element damage produce curious mesh plots. Figure 5.4 shows $[\widehat{d}]_f$ as a result of damage occurring in a diagonal element at each end of the truss. Two trends are very

visible and linear. Their respective magnitudes are 0.7 and 0.3, making damage in this case accurately detectable. These results, however, tend to be the exception, not the rule. A similar case is shown in Figure 5.5, which again represents damage at either end of the truss. Two ridges are again visible at the correct column indices, but the linearity has been degraded. A more advanced pattern recognition approach is required to estimate the extent of the damage in elements 3 and 15. As the two damaged elements become physically closer, linear patterns in the mesh plots are less obvious. Figures 5.6 is the result of damage to two adjacent elements. The location or estimation of damage in these cases is not possible by the simple column searching method.

In analyzing the single-element damage cases of the 10 bay truss, algorithm performance is flawless. Figure 5.7 through 5.9 show results from damage to a horizontal element, a diagonal element, and a vertical element, all in the second bay. In the dynamic behavior of the 10 bay truss, modes 1, 2, 3, 6, 8 and 9 are unobservable to all vertical elements. Hence, damage to any of these elements will produce a $[\widehat{d}]_f$ similar to that in Figure 5.7.

The 10 bay truss is a better platform in which to test possible detection of multi-element damage cases because it more closely approaches the size of a true satellite than does the 3 bay truss. Excellent results are shown in Figure 5.10 where damage is induced in two elements that are separated by five complete bays. As the damaged elements become closer, the damage location becomes less obvious. Figure 5.11 shows the result of two damaged elements separated by one bay. Both columns 14 and 22 have ridges of nonzero values, but do not follow any obvious pattern. In addition, many nonzero values localized around the columns 14 and 22 create the illusion that other elements are damaged as well. It is evident that the

column searching method defined for this algorithm is not adequate to analyze this case.

In conclusion, the single-element damage location and estimation algorithm is very accurate in assessing single-element damage. Although many iterations are required for large structures, each iteration involves only a few computation and the damage parameters can be found exactly. In addition, some specific two-element damage cases can be assessed. However, damage is more likely to occur in adjacent elements making damage assessment poor or impossible. The performance of this algorithm is significantly more accurate than some previously proposed methods, but does not meet the criteria of a flexible and fast method. An ideal detection algorithm will require fewer iterations are will locate and estimate the damage in many elements simultaneously. To that end, Chapter 7 will modify the single-element location and estimation algorithm to closely meet these requirements.

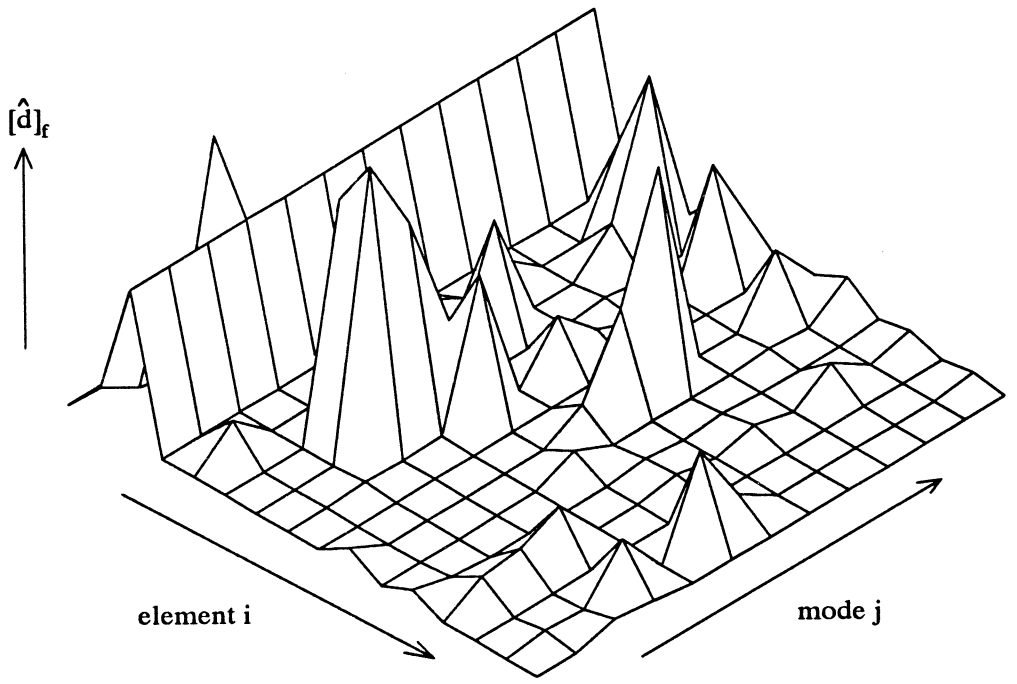

Figure 5.2: $[\widehat{d}]_f$ for 3 Bay Truss - Element 3 Damaged 50%

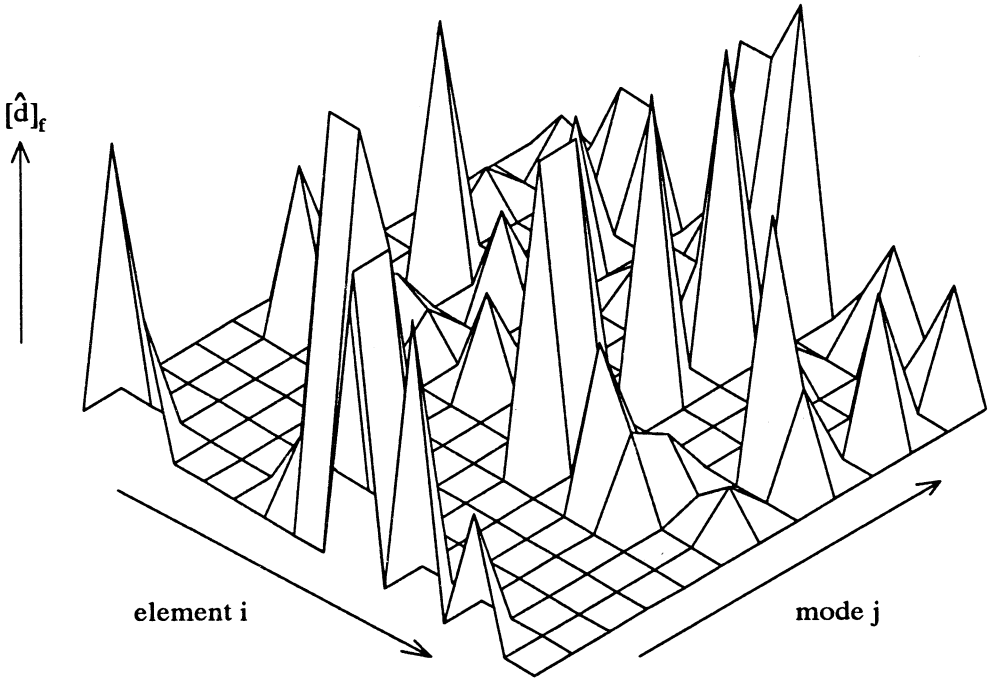

Figure 5.3: $[\widehat{d}]_f$ for 3 Bay Truss - Element 10 Damaged 50%

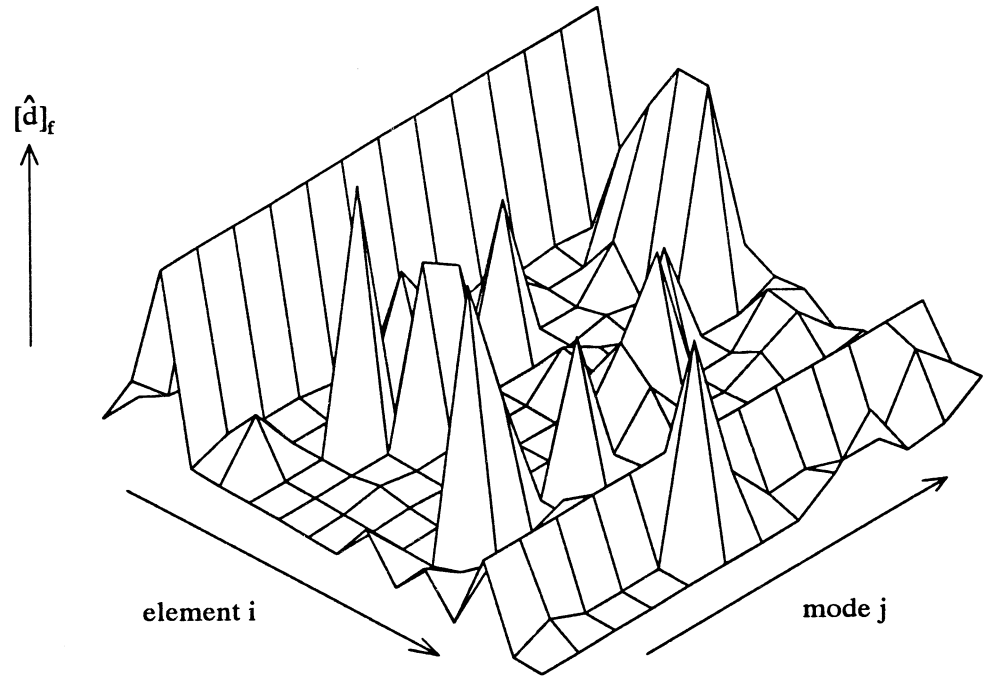

Figure 5.4: $[\widehat{d}]_f$ for 3 Bay Truss - Elements 3, 14 Damaged 70%, 30%.

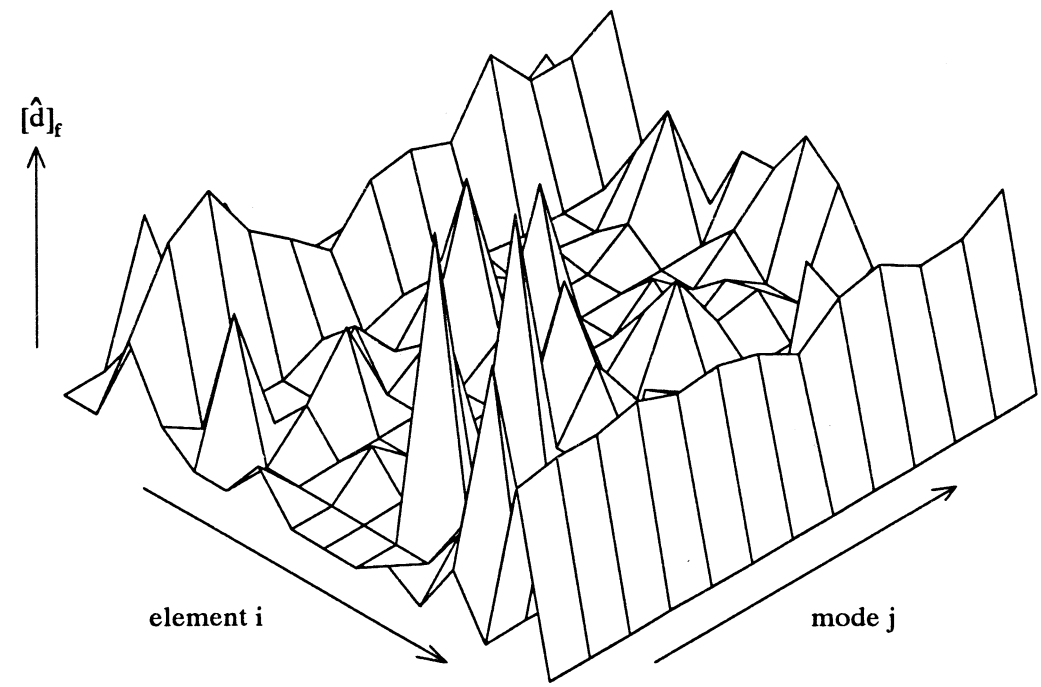

Figure 5.5: $[\widehat{d}]_f$ for 3 Bay Truss - Elements 3, 15 Damaged 40%, 60%

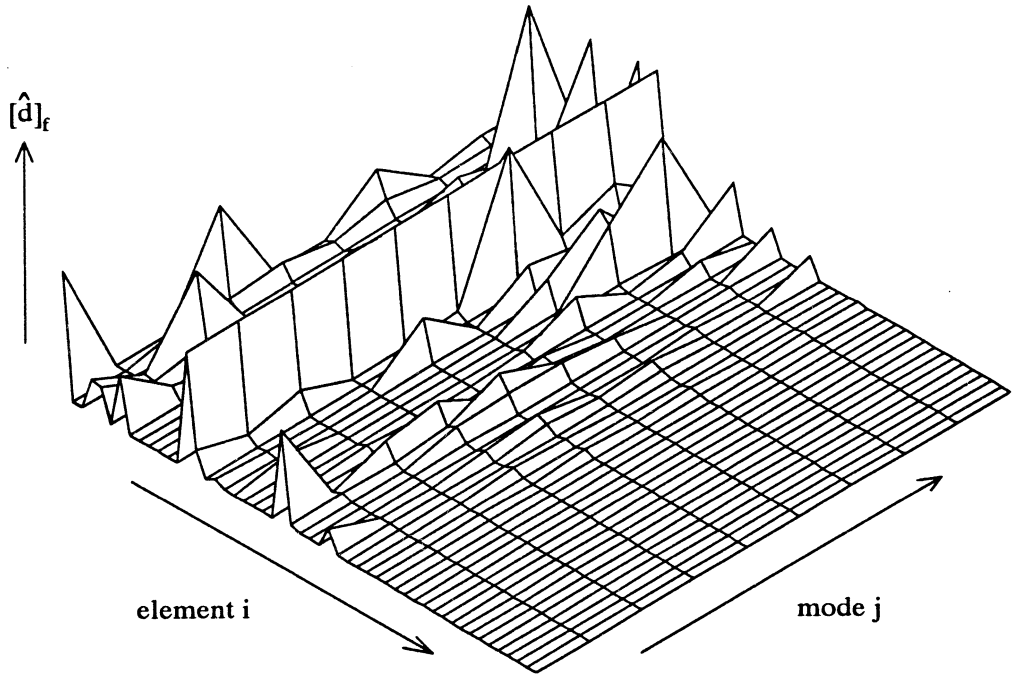

Figure 5.6: $[\widehat{d}]_f$ for 10 Bay Truss - Element 14 Damaged 50%

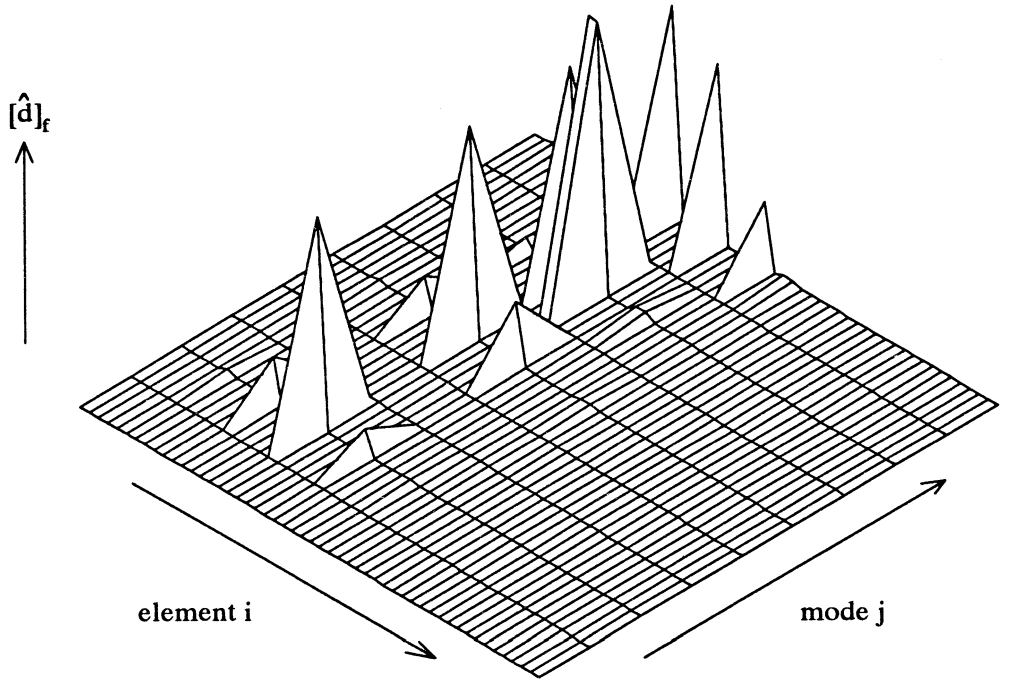

Figure 5.7: $[\widehat{d}]_f$ for 10 Bay Truss - Elements 16 Damaged 50%

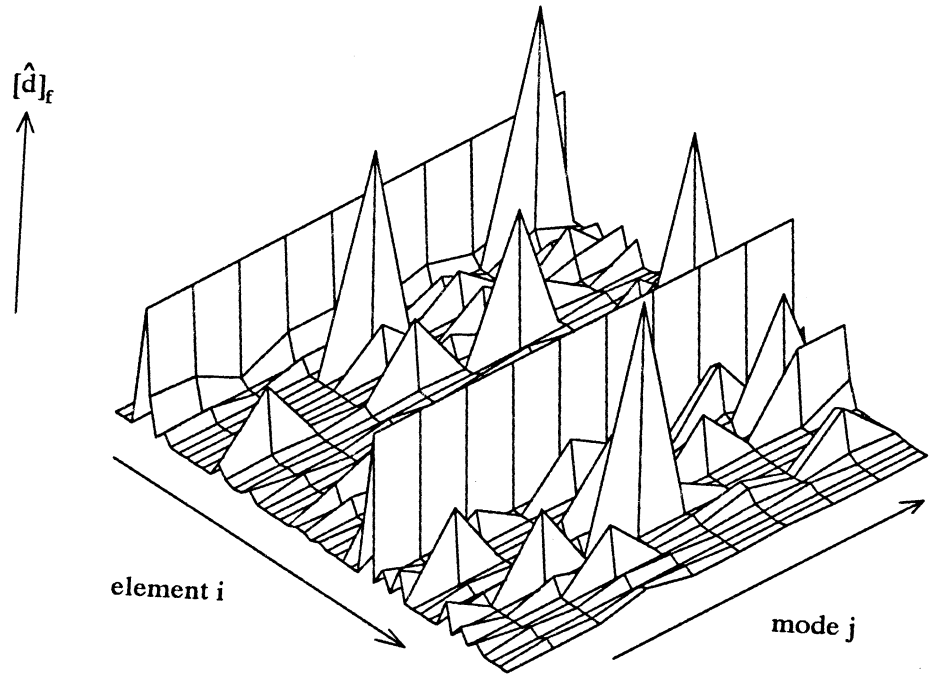

Figure 5.8: $[\widehat{d}]_f$ for 10 Bay Truss - Elements 4, 33 Damaged 40%, 60%

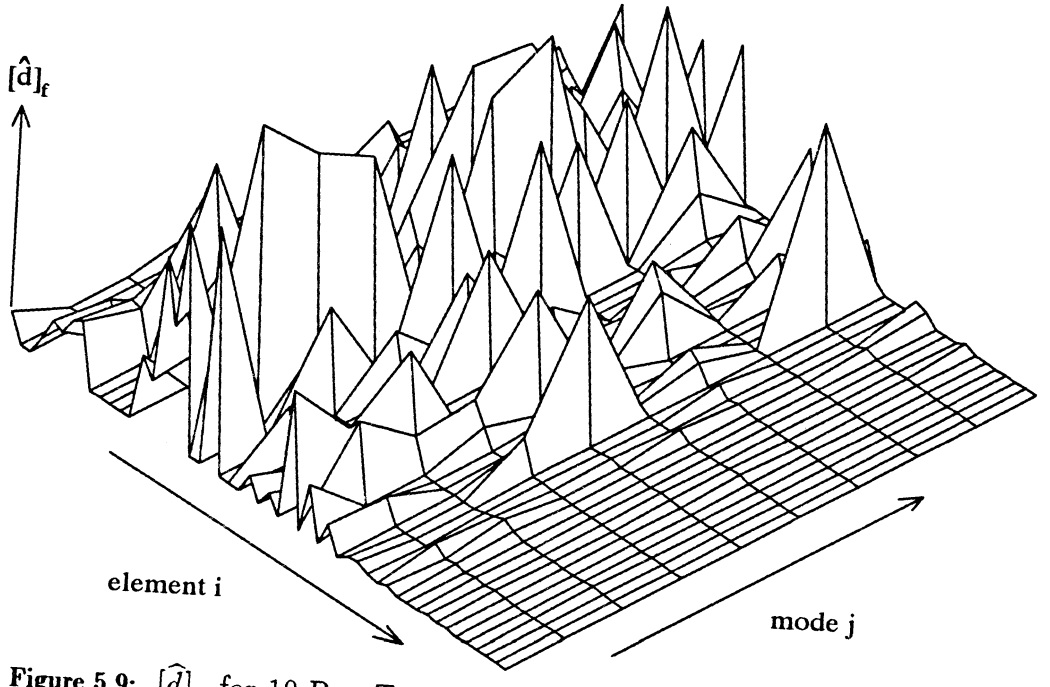

Figure 5.9: $[\widehat{d}]_f$ for 10 Bay Truss - Elements 14, 22 Damaged 60%, 40%

6 STRAIN ENERGY

Strain energy is widely used as a measure of a mode's suitability for damage detection [1,8,10,11,20]. The relationship between strain energy and mode shapes is directly used in the development of all algorithms presented in this thesis. This chapter covers the necessary background material for Chapter 7. Mode sensitivity is also discussed as a criteria for the selection of modes for use in detection algorithms.

6.1 FRACTIONAL MODAL STRAIN ENERGY

In addition to modes, strain energy is second set of data that can describe the dynamic behavior of a structure. For each mode frequency, there is a unique distribution of strain energy over each structural element. Strain energy is a form of potential energy. The use of the word *strain* indicates the case of small deflection in a deformable body who's force-displacement relationship is linear. The most basic example is that of a spring which follows Hooke's law:

$$F = -k\,\Delta q \tag{6.1}$$

where F is the force acting on the spring with spring constant k resulting in a

deflection of Δq. The spring constant k is always positive. The potential energy stored in the spring due to the deflection is

$$V = \tfrac{1}{2} F \Delta q = \tfrac{1}{2}\, k \Delta q^2. \tag{6.2}$$

Potential energy is a positive semidefinite function which implies $V \geq 0$. Expressing Eq. (6.1) in relation to the basic one dimensional truss element in Fig. 3.1

$$f'_2 = -f'_1 = \frac{E_i A_i}{h_i} (q'_1 - q'_2) \tag{6.3}$$

which holds for static deformation (kinetic energy is zero). In matrix form, Eq. (6.3) is

$$\begin{bmatrix} F_1 \\ F_2 \end{bmatrix} = \frac{E_i A_i}{h_i} \begin{bmatrix} 1 & -1 \\ -1 & 1 \end{bmatrix} \begin{bmatrix} q'_1 \\ q'_2 \end{bmatrix} = K'_i \{q'\}. \tag{6.4}$$

In local and global coordinates, Eq. (6.2) is then

$$V_i = \tfrac{1}{2} \{q'\}^{\mathrm{T}} K'_i \{q'\} = \tfrac{1}{2} \{q\}^{\mathrm{T}} K_i \{q\}. \tag{6.5}$$

Because this is a function of stiffness and displacement only, the assumption of zero kinetic energy can be ignored. Since K_i has nonzero entries at only the degrees of freedom element i connects, only the components of $\{q\}$ at those indices contributes to V_i. Hence, strain energy is defined here as a function of K_i and the

deflections acting on the nodes the element connects.

Mode shapes describe the relative amplitude of oscillation at a specific frequency for all degrees of freedom. The oscillation of each DOF during free oscillation is exactly described as a linear combination of the mode shapes and frequencies such that

$$\{q(t)\} = \begin{bmatrix} q_1(t) \\ q_2(t) \\ \vdots \\ q_{N_e}(t) \end{bmatrix} = \sum_j C_j \phi_j cos(\omega_j t + \psi_j). \tag{6.6}$$

Both the phase angle ψ_j and scaling constant C_j are functions of initial displacement $\{q(0)\}$ and velocity $\{\dot{q}(0)\}$ where

$$C_j \, cos \, \psi_j = \phi_j^{\mathrm{T}} \, M \, \{q(0)\}, \text{ and} \tag{6.7}$$

$$C_j \, sin \, \psi_j = \frac{1}{\omega_j} \phi_j^{\mathrm{T}} \, M \, \{\dot{q}(0)\}.$$

In viewing these complex distortions of the structure, it becomes evident that for each mode frequency, each truss element is subject to a time varying amount of deformation. This produces a measure of strain energy that is a function of time. *Modal strain energy* represents the maximum possible strain energy in an element over one period of oscillation of the mode considered. That is let

$$V_{ij}(t) = \tfrac{1}{2} \, v_j^{\mathrm{T}}(t) \, K_i \, v_j(t) \tag{6.8}$$

where

$$v_j(t) = C_j\, \phi_j \sin(\omega_j t + \psi_j).$$

Modal strain energy for mode j and element i is then

$$\overline{SE}_{ij} = \max_t\{V_{ij}(t)\} = \tfrac{1}{2}\, v_j{}^{\mathrm{T}}\, K_i\, v_j \tag{6.9}$$

where $v_j = C_j\phi_j$. Because C_j is usually not available from a modal survey, $\overline{SE}_{ij}$ from Eq. (6.9) is not computable from the modal data provided. Rather, the magnitude of $\overline{SE}_{ij}$ can be expressed in relation to other elements as a fraction of the total strain energy [20]. Formally, *Fractional Modal Strain Energy* for mode j and element i is

$$SE_{ij} = \frac{\phi_j^{\mathrm{T}}\, K_i\, \phi_j}{\phi_j^{\mathrm{T}}\, K\, \phi_j} = \frac{\overline{SE}_{ij}}{\overline{SE}_{Tj}} \tag{6.10}$$

where K is the global stiffness matrix. The denominator is equal to the sum of strain energy over all elements for mode j. From Eq. (3.25), the total strain energy for mass orthonormal mode shapes is identical to the square of the mode frequency, or ω_j^2.

Strain energy SE_{ij} is defined by its respective mode shape j and the stiffness of element i, so it too changes with damage. For a damaged element, the damaged stiffness modulus must also be considered in computing strain energy. The equation $E_{Di} = (1 - d_i)E_{Hi}$ is applied to the definition of K_i in Eq. (6.10) giving

$$SE_{Dij} = \frac{\phi_{Dj}^{\mathrm{T}}\,(1-d_i)K_i\,\phi_{Dj}}{\phi_{Dj}^{\mathrm{T}}\,K_D\,\phi_{Dj}} = \frac{\overline{SE}_{Dij}}{\omega_{Dj}^2}. \tag{6.11}$$

Note that even if $d_i = 0$, this equation still holds because ϕ_{Dj} can represent damage in elements other than i. Similarly, the healthy fractional modal strain energy is

$$SE_{Hij} = \frac{\phi_{Hj}^{\mathrm{T}}\,K_i\,\phi_{Hj}}{\phi_{Hj}^{\mathrm{T}}\,K_H\,\phi_{Hj}} = \frac{\overline{SE}_{Hij}}{\omega_{Hj}^2} \tag{6.12}$$

Because strain energy is a quadratic function that is always non-negative, SE_{ij} is a positive semidefinite function. An interpretation of SE_{ij} is that it gives a relative value of element i's participation in the mode j with respect to the participation of the other elements. For the largest value of SE_{ij} for a given mode j, element i oscillates with a larger amplitude at frequency ω_j than any other element in the structure. If SE_{ij} has a zero value, element i exhibits rigid body motion, which is much the same as rigid body motion for the global structure. Here, either the element does not move at all in that frequency, or both ends of the element move the same displacement in the same direction with respect to the element's local axis resulting in overall element movement but no change in length.

Figures 6.1 through 6.10 are plots of the fractional modal strain energy of the 10 bay truss for the first ten modes. Note SE_{ij} for all vertical elements is zero in modes 1, 2, 4, 5, 7, 9, and 10. For these mode shapes, the vertical displacement of the even nodes is equal to that of the odd nodes. Also notable is the symmetry of the plots since the structure is symmetrical about element 26.

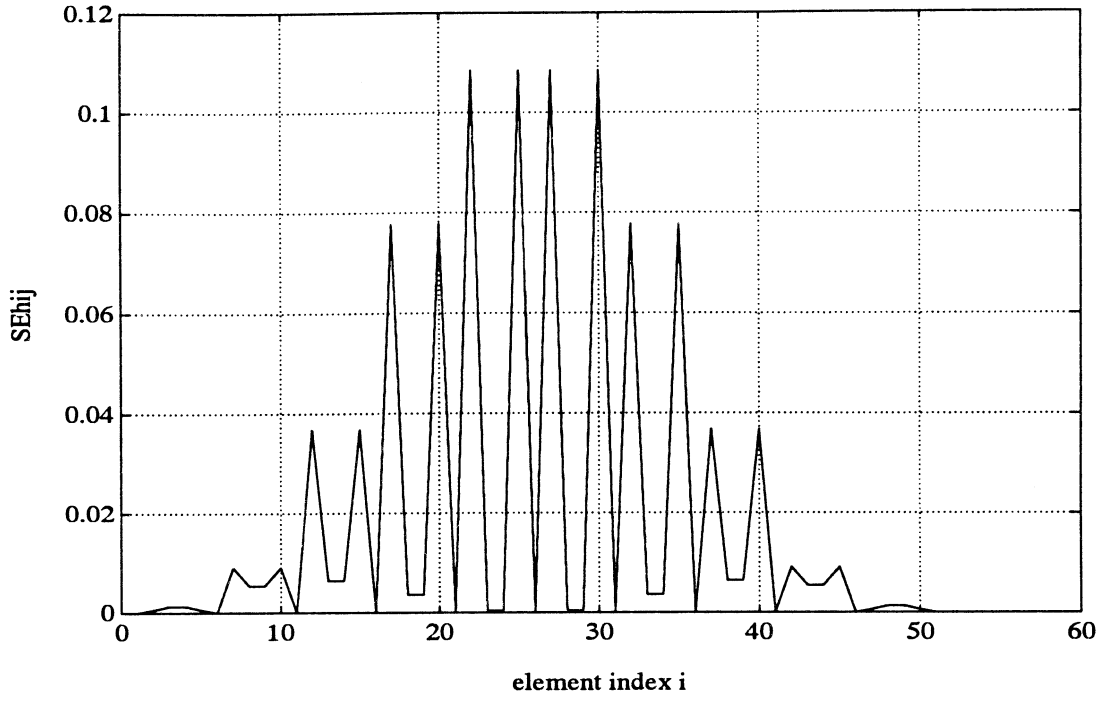

Figure 6.1: SE_{Hi1} for the 10 Bay Truss

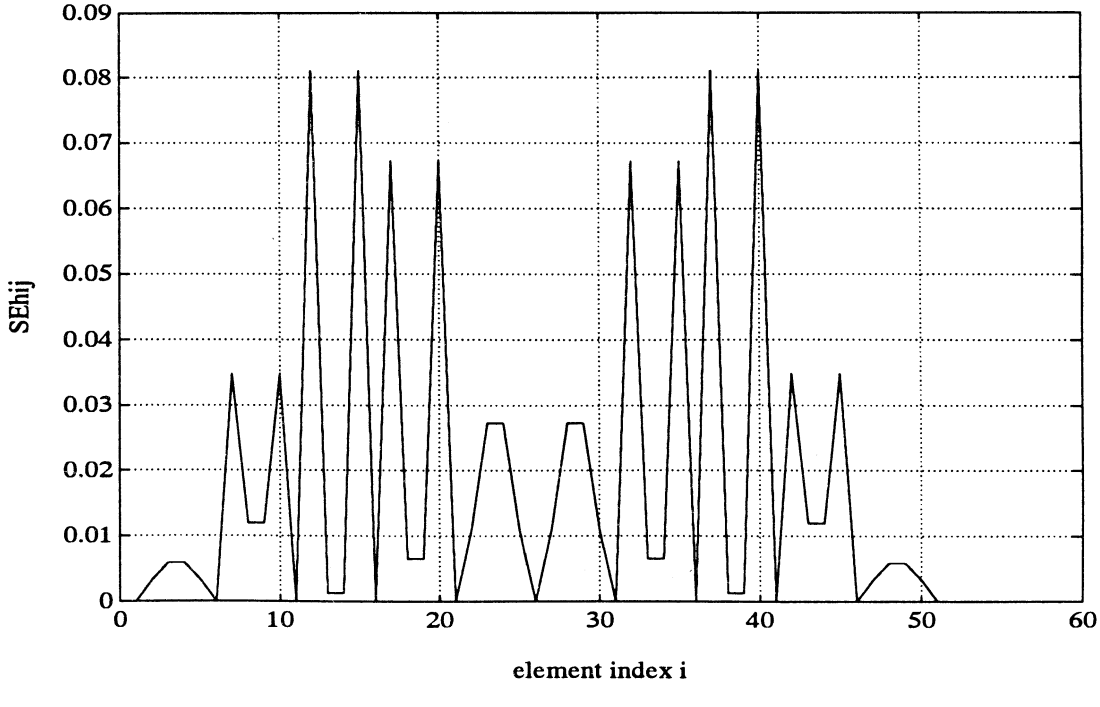

Figure 6.2: SE_{Hi2} for the 10 Bay Truss

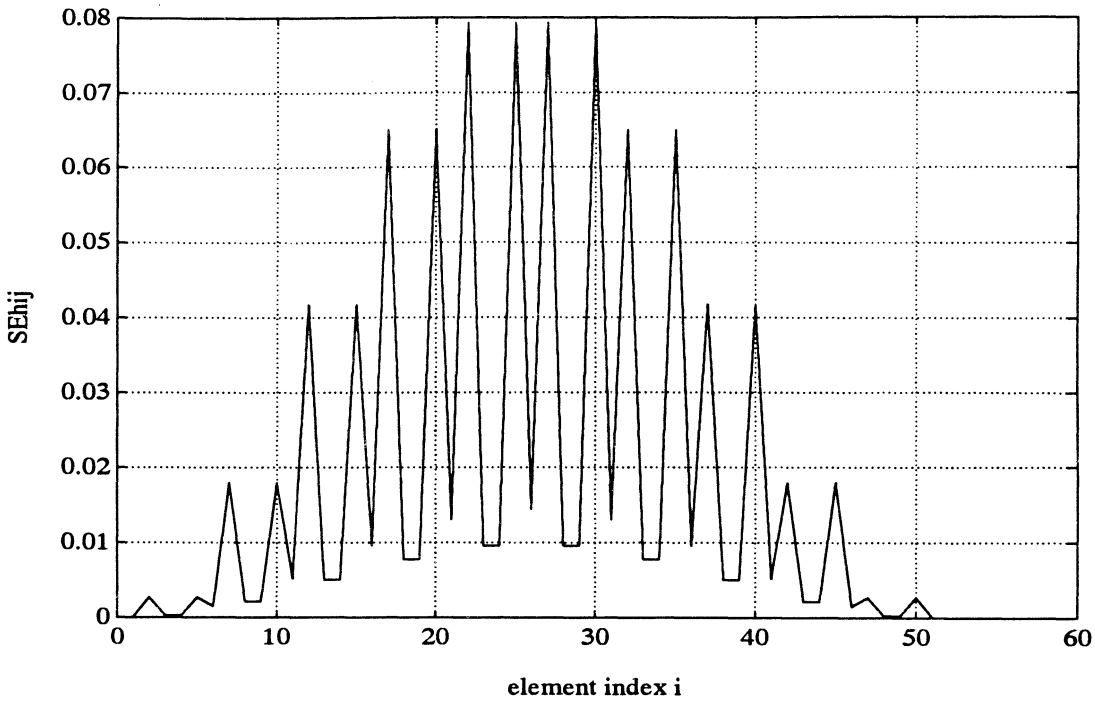

Figure 6.3: SE_{Hi3} for the 10 Bay Truss

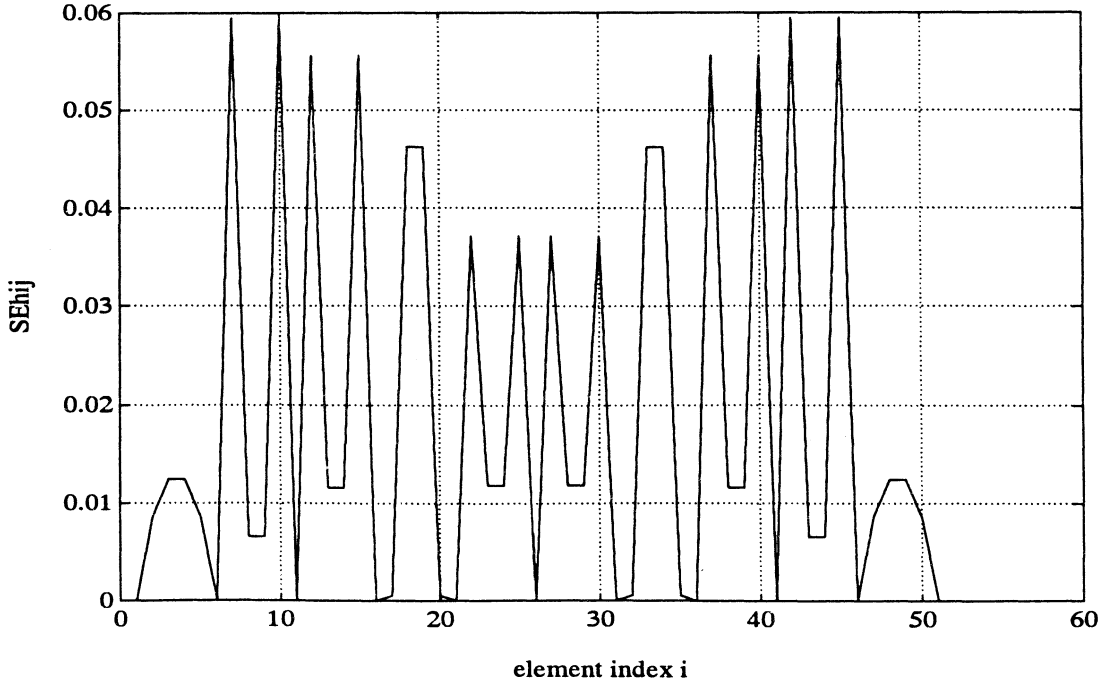

Figure 6.4: SE_{Hi4} for the 10 Bay Truss

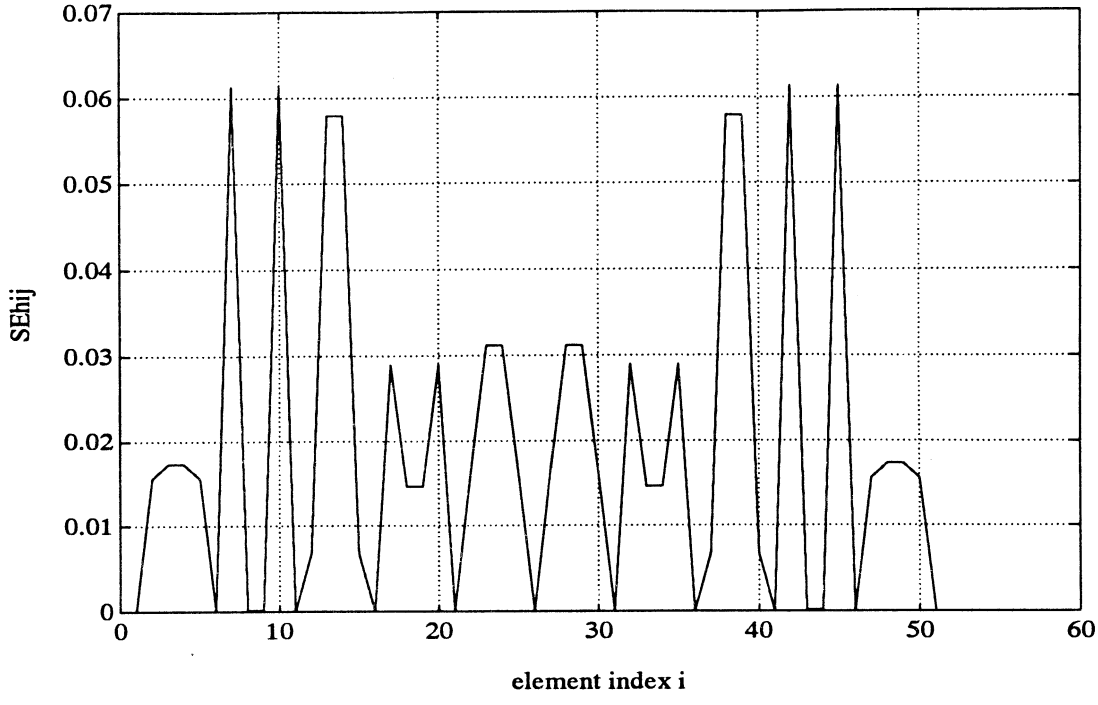

Figure 6.5: SE_{Hi5} for the 10 Bay Truss

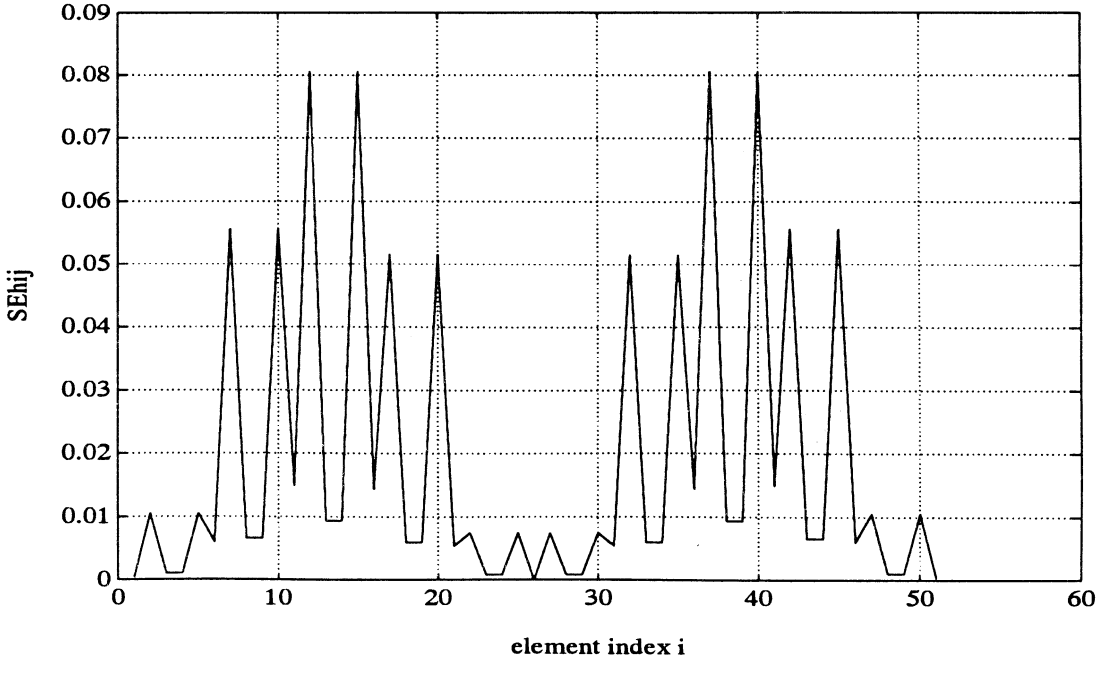

Figure 6.6: SE_{Hi6} for the 10 Bay Truss

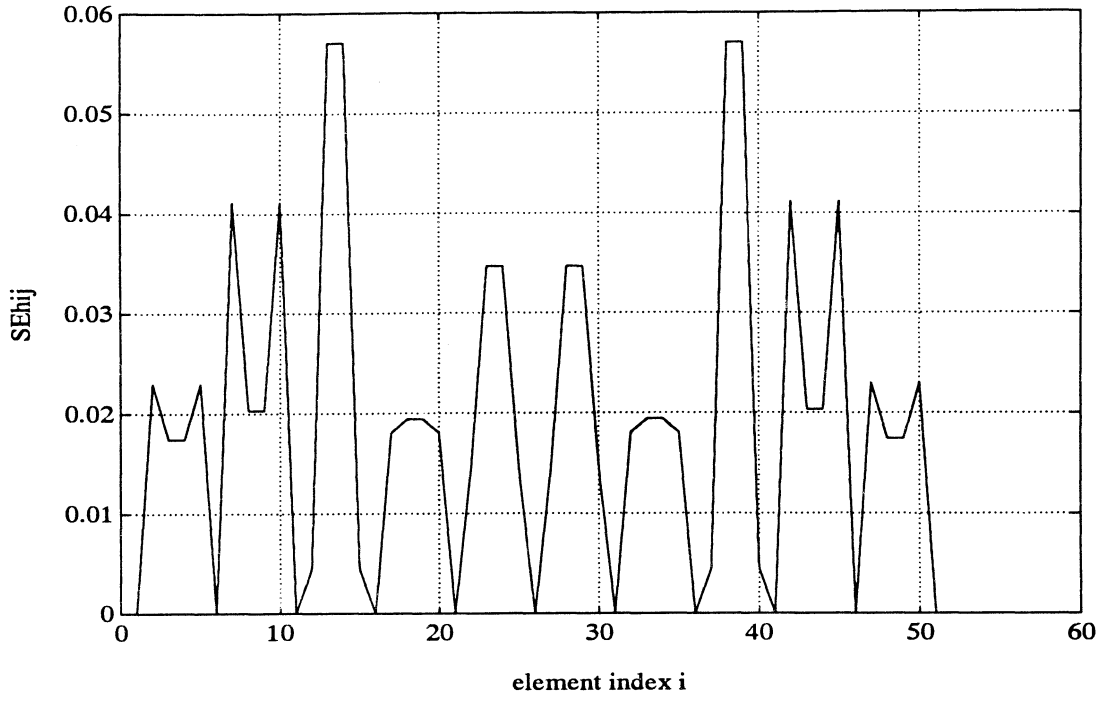

Figure 6.7: SE_{Hi7} for the 10 Bay Truss

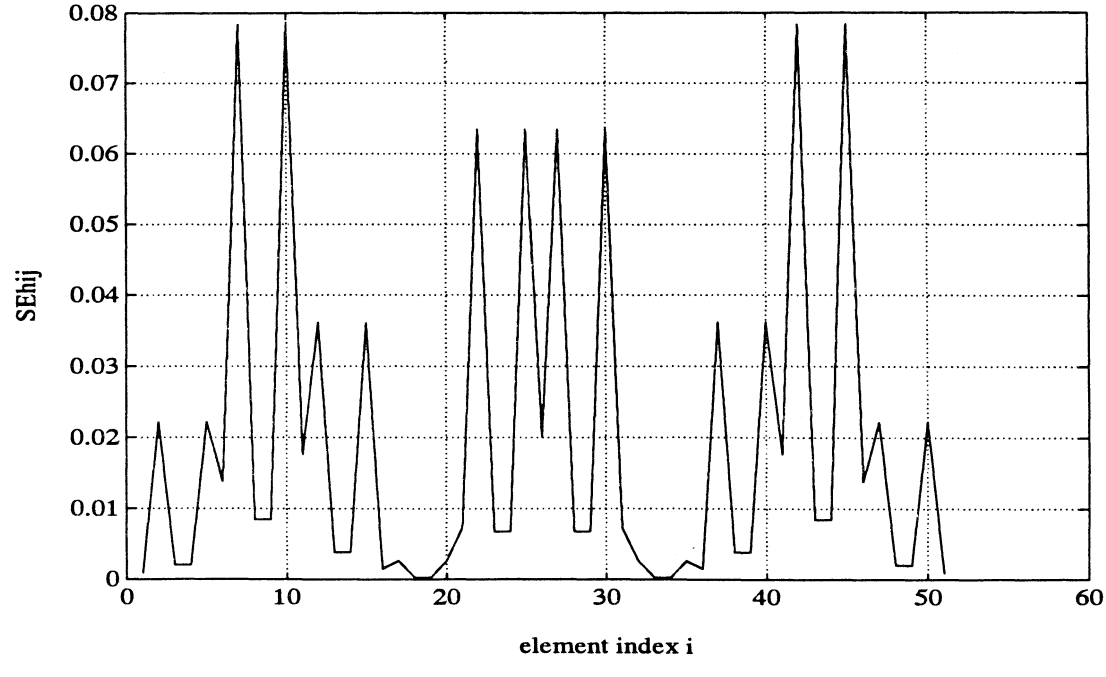

Figure 6.8: SE_{Hi8} for the 10 Bay Truss

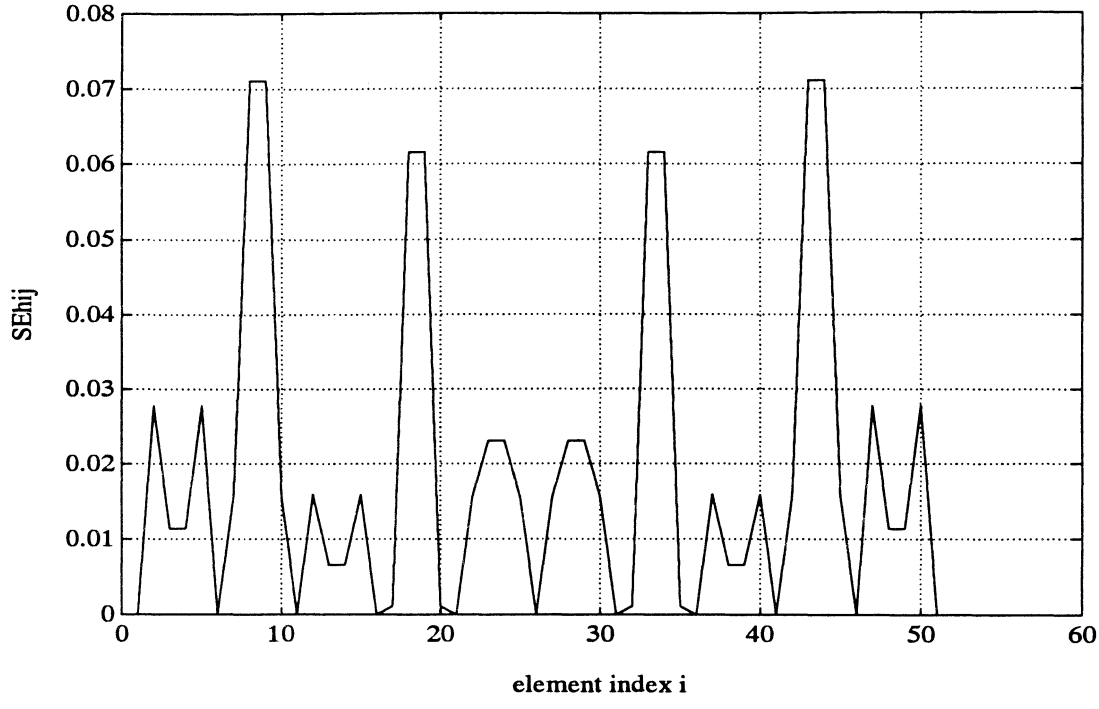

Figure 6.9: SE_{Hi9} for the 10 Bay Truss

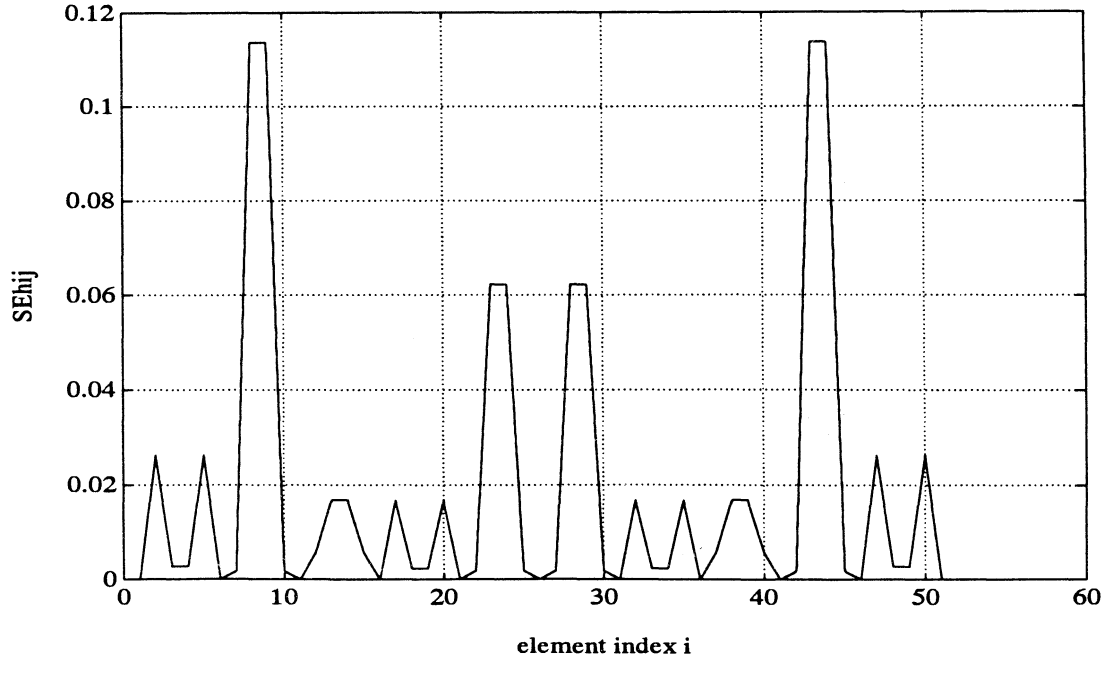

Figure 6.10: SE_{Hi10} for the 10 Bay Truss

6.2 MODE SHAPE – STRAIN ENERGY RELATIONSHIP

Strain energy holds a direct relationship, through information contained in the stiffness matrix, with its corresponding mode shape. This relationship is derived here as background material required for the development of the algorithms in Chapter 7.

First apply the definition of the element stiffness vector, B_i, to Eq. (6.12) to get

$$SE_{ij} = \frac{\phi_j^{\mathrm{T}} B_i B_i^{\mathrm{T}} \phi_j}{\omega_j^2}. \tag{6.13}$$

In this light, the following is offered

Define: *Healthy Element Modal Deflection*, ϵ_{Hij},

$$\epsilon_{Hij} = B_i^{\mathrm{T}} \phi_{Hj} \tag{6.14}$$

where $\epsilon_{Hij}^2 = \omega_{Hj}^2 SE_{Hij}$.

As with fractional modal strain energy, damaged and healthy states of the element modal deflection must be defined. For simplification of notation, let

$$s_i = \sqrt{1 - d_i}. \tag{6.15}$$

Then

Define: *Damaged Element Modal Deflection,* ϵ_{Dij},

$$\epsilon_{Dij} = s_i B_i^{\mathrm{T}} \phi_{Dj} \tag{6.16}$$

where $\epsilon_{Dij}^2 = \omega_{Dj}^2 SE_{Dij}$.

The element modal deflection holds a square law relationship with fractional modal strain energy. During a square transformation, the modal deflection looses its sign. The sign of the element modal deflection defines the direction of deflection (compression or tension) for a given mode in the considered element. This sign contains information of how the structure oscillates and it is vital in this derivation.

Both the healthy and damaged element modal deflection measures have a physical meaning similar to that of the fractional modal strain energy. When $\epsilon_{ij} = 0$, element i undergoes rigid body motion at frequency ω_j. This is identical to the condition of mode unobservability defined in the single-element detection algorithm developed in Chapter 5. Note in that development, that unobservability was defined as

$$B_i^{\mathrm{T}} \phi_{Dj} = \frac{\epsilon_{Dij}}{s_i} = 0. \tag{6.17}$$

If this equation is true, it is impossible to detect damage in element i with mode j regardless of the method, because the element has no influence on mode j.

The mode-strain energy relationship will now be derived. Plugging Eq. (6.11) into the eigenvalue equation Eq. (3.39) yields

$$\omega_{Hj}^2 M\phi_{Hj} = \sum_{i=1}^{N_e} B_i B_i^{\mathrm{T}} \phi_{Hj}$$

$$= \sum_{i=1}^{N_e} B_i \epsilon_{Hij} \tag{6.18}$$

By multiplying both sides by M^{-1} , it is apparent that the mode shape j is represented as a linear combination of vectors related to B_i.

$$\omega_{Hj}^2 \phi_{Hj} = \left[\begin{array}{c|c|c|c} M^{-1}B_1 & M^{-1}B_2 & \cdots & M^{-1}B_{N_e} \end{array}\right] \begin{bmatrix} \epsilon_{H1j} \\ \epsilon_{H2j} \\ \vdots \\ \epsilon_{HN_ej} \end{bmatrix} \tag{6.19}$$

This gives an exact relationship between the modal strain energy and the corresponding mode shape by using the structural geometry and stiffness information. The mode shape can be viewed as lying in the range space of the vectors $M^{-1}\, B_i$. Elements that exhibit rigid body motion in mode j, or $\epsilon_{Hij} = 0$, do not influence the formation of the mode shape. The stiffness of these elements has no effect on the structure's response in the frequency ω_j.

Similar to the mode shapes, the element modal deflections can be computed directly from the FEM model. By multiplying Eq. (6.19) by B_i^{T}, a relationship between the scalar ϵ_{Hij} and the vector $\{\epsilon_{Hj}\}$ is drawn:

$$\omega_{Hj}^2 B_i^{\mathrm{T}} \phi_{Hj} =$$

$$\omega_{Hj}^2 \epsilon_{Hij} = \left[\begin{array}{c|c|c|c} B_i^{\mathrm{T}} M^{-1} B_1 & B_i^{\mathrm{T}} M^{-1} B_2 & \cdots & B_i^{\mathrm{T}} M^{-1} B_{N_e} \end{array}\right] \begin{bmatrix} \epsilon_{H1j} \\ \epsilon_{H2j} \\ \vdots \\ \epsilon_{HN_ej} \end{bmatrix}. \quad (6.20)$$

By considering this equation for every element, $i = \{1,2,\ldots,N_e\}$, and arranging as a series of linear equations, a matrix representation can be formed:

$$\omega_{Hj}^2 \begin{bmatrix} \epsilon_{H1j} \\ \epsilon_{H2j} \\ \vdots \\ \epsilon_{HN_ej} \end{bmatrix} = \begin{bmatrix} B_1^{\mathrm{T}} M^{-1} B_1 & B_1^{\mathrm{T}} M^{-1} B_2 & \cdots & B_1^{\mathrm{T}} M^{-1} B_{N_e} \\ B_2^{\mathrm{T}} M^{-1} B_1 & B_2^{\mathrm{T}} M^{-1} B_2 & \cdots & B_2^{\mathrm{T}} M^{-1} B_{N_e} \\ \vdots & \vdots & \ddots & \vdots \\ \mathrm{B}_{N_e}^{\mathrm{T}} M^{-1} B_1 & B_{N_e}^{\mathrm{T}} M^{-1} B_2 & \cdots & B_{N_e}^{\mathrm{T}} M^{-1} B_{N_e} \end{bmatrix} \begin{bmatrix} \epsilon_{H1j} \\ \epsilon_{H2j} \\ \vdots \\ \epsilon_{HN_ej} \end{bmatrix}. \quad (6.21)$$

Define the matrix above as $[BB]_H$. This equation holds the form of an eigenvector equation. By forming $[BB]_H$ from element stiffness vectors, the element modal deflection vectors fall out as the eigenvectors. All entries in $[BB]_H$ are real by definition, and $[BB]_H$ is symmetric. Hence, it qualifies as a hermitian matrix who's eigenvectors and eigenvalues are real. The eigenvalues produced are identical to the square of the mode frequencies. Because the number of elements is usually greater that the number of degrees of freedom, Eq. (6.21) produces more eigenvalues than there exists mode frequencies. The additional eigenvalues that are not equal to ω_{Hj}^2 are all identically zero.

The mode shape-strain energy relationship can be formed for a damaged structure as well. For arbitrary damage Eq. (6.20) can be expressed as

$$\omega_{Dj}^2 M\phi_{Dj} = \sum_{i=1}^{N_e} s_i B_i s_i B_i^{\mathrm{T}} \phi_{Dj},$$

or

$$\omega_{Dj}^2 \phi_{Dj} = \left[s_1 M^{-1} B_1 \;\middle|\; \cdots \;\middle|\; s_i M^{-1} B_i \;\middle|\; \cdots \;\middle|\; s_{N_e} M^{-1} B_{N_e} \right] \begin{bmatrix} \epsilon_{D1j} \\ \epsilon_{D2j} \\ \vdots \\ \epsilon_{DN_e j} \end{bmatrix}. \quad (6.22)$$

This is a key equation derived for use specifically in Chapter 7.

For simplicity of notation, let $\tilde{b}_{ij} = B_i^{\mathrm{T}} M^{-1} B_j$. Multiply both sides by a damage element stiffness vector $s_i B_i^{\mathrm{T}}$, then

$$\omega_{Dj}^2 \epsilon_{Dij} = \left[s_1 s_i \tilde{b}_{1i} \;\middle|\; \cdots \;\middle|\; s_i^2 \tilde{b}_{ii} \;\middle|\; \cdots \;\middle|\; s_{N_e} s_i \tilde{b}_{NN_e i} \right] \begin{bmatrix} \epsilon_{D1j} \\ \epsilon_{D2j} \\ \vdots \\ \epsilon_{DN_e j} \end{bmatrix}. \quad (6.23)$$

Arranging Eq. (6.23) into a matrix equation similar to Eq. (6.0),

$$\omega_{Dj}^2 \begin{bmatrix} \epsilon_{D1j} \\ \epsilon_{D2j} \\ \vdots \\ \epsilon_{DN_e j} \end{bmatrix} = \begin{bmatrix} s_1^2 \tilde{b}_{11} & s_1 s_2 \tilde{b}_{12} & \cdots & s_1 s_{N_e} \tilde{b}_{1N_e} \\ s_2 s_1 \tilde{b}_{21} & s_2^2 \tilde{b}_{22} & \cdots & s_2 s_{N_e} \tilde{b}_{2N_e} \\ \vdots & \vdots & \ddots & \vdots \\ s_{N_e} s_1 \tilde{b}_{N_e 1} & s_{N_e} s_2 \tilde{b}_{N_e 2} & \cdots & s_{N_e}^2 \tilde{b}_{N_e N_e} \end{bmatrix} \begin{bmatrix} \epsilon_{D1j} \\ \epsilon_{D2j} \\ \vdots \\ \epsilon_{DN_e j} \end{bmatrix} \quad (6.24)$$

Again, the damaged element modal displacements are the eigenvectors of the matrix above. This matrix will be called $[BB]_D$. The nonzero eigenvectors of $[BB]_D$ are identical to ω_{Dj}^2.

6.3 MODE SENSITIVITY

The use of fractional modal strain energy in mode selection for damaged detection is discussed by several researchers. The modes with the largest SE_{ij} in elements suspected of damage are the most suitable for damaged detection in those elements [8,9,15,20]. This is because the magnitude of SE_{ij} holds a direct relationship with mode j's sensitivity to damage in element i. The more a particular mode changes per increment in d_i, the better damage is represented in that mode. This section will prove this relationship using eigenvalue and eigenvector derivatives.

The change in a mode with respect to change of a finite element model parameter can be represented as eigensystem sensitivity, or a partial derivative. Consider first the sensitivity of a mode frequency to some physical parameter p. The partial derivative of the square of the mode frequency is

$$\frac{\partial \omega_j^2}{\partial p} = \phi_j^{\mathrm{T}} \left(\frac{\partial K}{\partial p} - \omega_j^2 \frac{\partial M}{\partial p} \right) \phi_j. \tag{6.25}$$

Here, p represents a physical parameter subject to change [22]. The only parameter that changes from damage in the finite element model is element stiffness. The derivative of the mass matrix is zero. Hence, $p = d_i$. Consider the case of single element damage to element i. The derivative of the damaged stiffness matrix is

$$\frac{\partial K_D}{\partial p} = \frac{\partial \left(K_H - d_i K_i \right)}{\partial d_i} = K_i. \tag{6.26}$$

Then substituting into Eq. (6.25), the derivative is

$$\frac{\partial \omega_{Dj}^2}{\partial d_i} = -\phi_{Dj}^{\mathrm{T}} K_i \phi_{Dj}. \tag{6.27}$$

This equation is independent of damage in other elements, and is only accurate for small changes in d_i.

Except for the scaling factor $1/\omega_{Dj}^2$, this is the exact definition of fractional modal strain energy. Hence, modal strain energy holds a direct relationship with how damage in that element effects mode frequencies. Since $SE_{ij} \geq 0$, the mode frequencies are always decreased by damage. If $SE_{ij} = 0$, element i has rigid body motion in frequency j, and any damage in that element will not effect mode j. Hence, damage is not detectable in element i if only mode j is considered. To choose a mode that is suitable for damage detection in all elements, the vector $\{SE_j\}$ must contain no zeros. In addition, since the location of damage is unknown, the best mode for detection is the one with the most even distribution of modal strain energy over all elements. Noting Figures 6.1 through 6.10, there is no single mode that meets these criteria. Rather, several modes must be used to represent all elements.

Not only is Eq. (6.27) useful in determining mode suitability, but direct application to damage detection can be considered [20]. Since the frequency sensitivity is related to the fractional modal strain energy, one approach is to view Eq. (6.27) as a mapping of how damage affects mode frequencies. Equation (6.27) implies that changes in the mode frequencies after identification are an indication of damage. However, the fact that a symmetric structure produces a symmetric distribution of fractional modal strain energy values limits the use of this approach

for damage location. That is, damage in one element has the identical effect on all mode frequencies as that element's symmetric counterpart. An example are the four diagonal elements located in bays 1 and 10 in the planar 10 bay truss. A 50% reduction in the stiffness of element 4 has the identical effect on frequencies as a 50% reduction in the stiffness of element 48, etc.

This method of damage detection was investigated by Kashingaki et. al. showing the frequency sensitivity magnitude to be important in mode selection [20]. Because Eq. (6.27) is only accurate for small changes in stiffness, an iterative method was used to map the changes in frequency over the entire range of d_i. Because identified modes typically are 5% in error, frequencies that changed less than 5% over this range are viewed as unsuitable for damage detection in the corresponding element. Though this maximum frequency change is not computable from Eq. (6.27), the most suitable modes from a given set can be selected by comparing the fractional modal strain energy values.

To expand on mode sensitivity, eigenvector derivatives can be analyzed to illustrate the effect of damage on mode shapes. The mode shape derivative is given by

$$\left(K - \omega_j^2 M\right)\frac{\partial \phi_j}{\partial p} = -\left(\frac{\partial K}{\partial p} - \frac{\partial \omega_j^2}{\partial p}M - \omega_j^2\frac{\partial M}{\partial p}\right)\phi_j. \tag{6.28}$$

For the case of damage to element i only

$$\left(K_D - \omega_{Dj}^2 M\right)\frac{\partial \phi_{Dj}}{\partial d_i} = -\left(K_i - \frac{\partial \omega_{Dj}^2}{\partial d_i}M\right)\phi_{Dj}. \tag{6.29}$$

Since the matrix $(K_D - \omega_{Dj}^2 M)$ is not full rank, there are several non-exact methods for solving for $\partial\phi / \partial d$ [21,22]. These include pseudo-inverse using singular value decomposition, and implicit and explicit methods solving for a perturbation S such that

$$\frac{\partial \phi_{Dj}}{\partial p} = c_j \phi_{Dj} + S. \tag{6.30}$$

Noting that mode shapes are orthonormal with respect to the mass matrix and Eqs. (6.27) and (6.16), Eq. (6.29) can be written

$$\left(K_D - \omega_{Dj}^2 M\right) \frac{\partial \phi_{Dj}}{\partial d_i} = B_i \epsilon_{Dij} + SE_{Dij}\, \phi_{Dj}. \tag{6.31}$$

Clearly, this relationship is a function of strain energy of element i and mode j. Applications of Eq. (6.31) to damage detection are currently being addressed by some researchers [20].

6.4 SIMULATED HEALTHY-DAMAGED MODE COMPARISON

This section offers a graphical view of how damage effects a structure's dynamics. The 10 bay truss is damaged in two different single-element cases. Both damage cases were chosen from bay 3 at a 70% stiffness reduction. A large damage value was chosen to exaggerate the difference between healthy and damaged modes. Of the first 10 modes, the two modes most visually effected by the damage were chosen for the comparison.

Figures 6.11 through 6.14 are arranged in pairs and correspond to a single mode from one damage case. The figures' (a) portion consists of three deformed trusses. The top truss is deformed by a healthy mode, the bottom truss is deformed by the corresponding damaged mode, and the middle truss is the healthy deformation superimposed over the damaged deformation for comparison. The element damaged is marked in bold in the damaged deflection figure. The figures' (b) portion is the comparison of healthy and damaged fractional modal strain energy.

In viewing both comparisons, it is evident that damage to one element usually changes the truss's dynamics over the entire structure. A good example is Figure 6.11, where the damage disrupts mode 6 so that it is no longer purely an axial mode. An exception to this occurs when a vertical element is damaged. Of the first 10 modes, three axial modes are the only modes observable to any vertical element. Damage in these elements do not disrupt the symmetry of the structure's stiffness, and change the mode shape and fractional modal strain energy mostly in a local area. Figures 6.13 and 6.14 illustrate this.

Figure 6.13 compares healthy mode 6 with damaged mode 5. Because

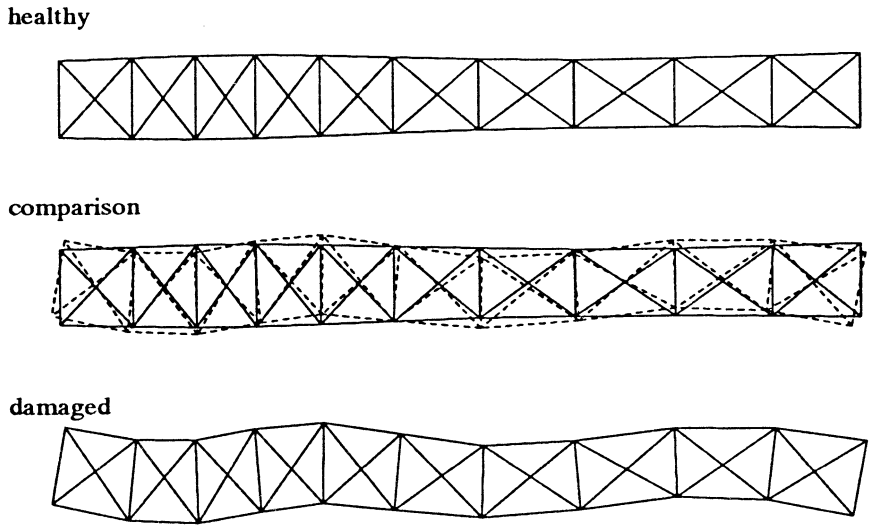

Figure 6.11a: ϕ_{H6} vs. ϕ_{D6} for Element 14 Damaged 70%

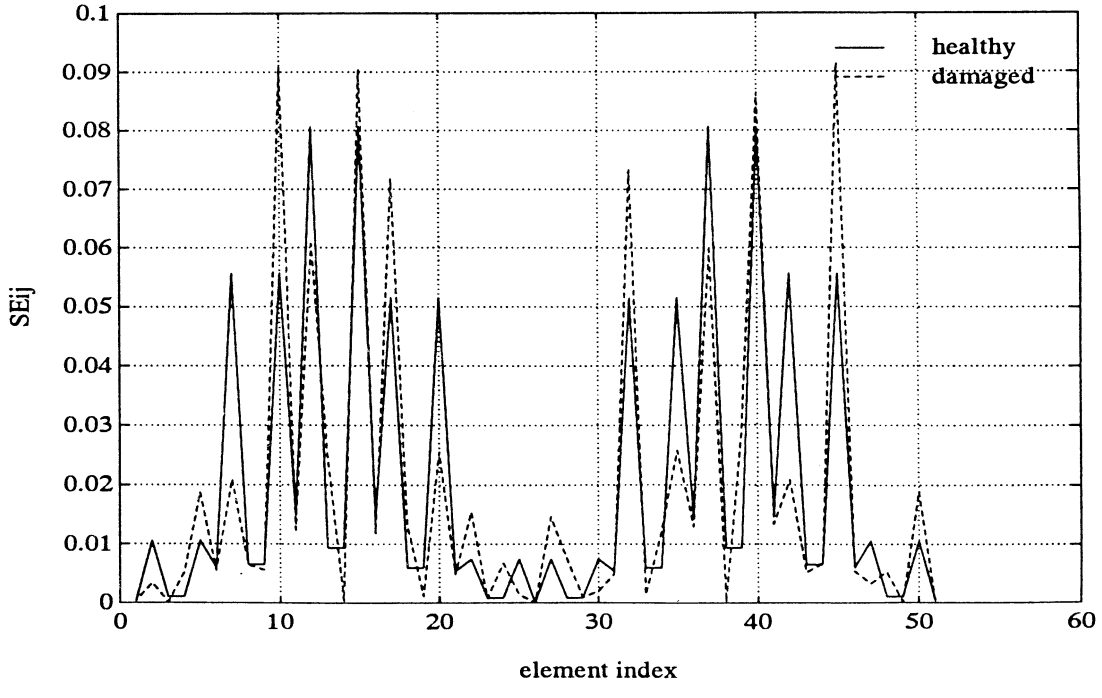

Figure 6.11b: SE_{Hi6} and SE_{Di6} for Element 14 Damaged 70%

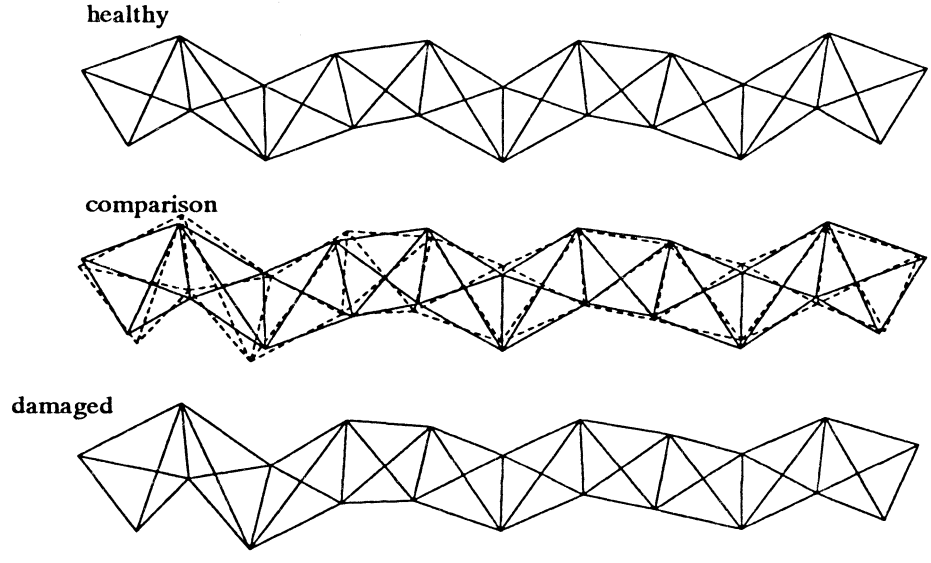

Figure 6.12a: ϕ_{H10} vs. ϕ_{D10} for Element 14 Damaged 70%

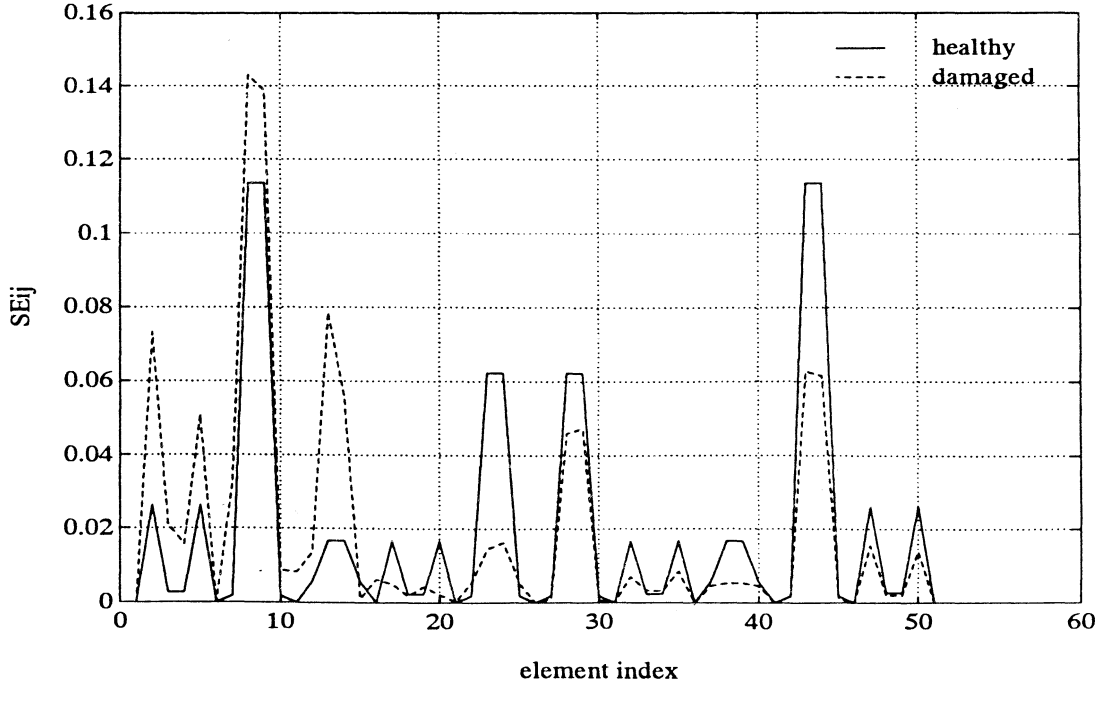

Figure 6.12b: SE_{Hi10} and SE_{Di10} for Element 14 Damaged 70%

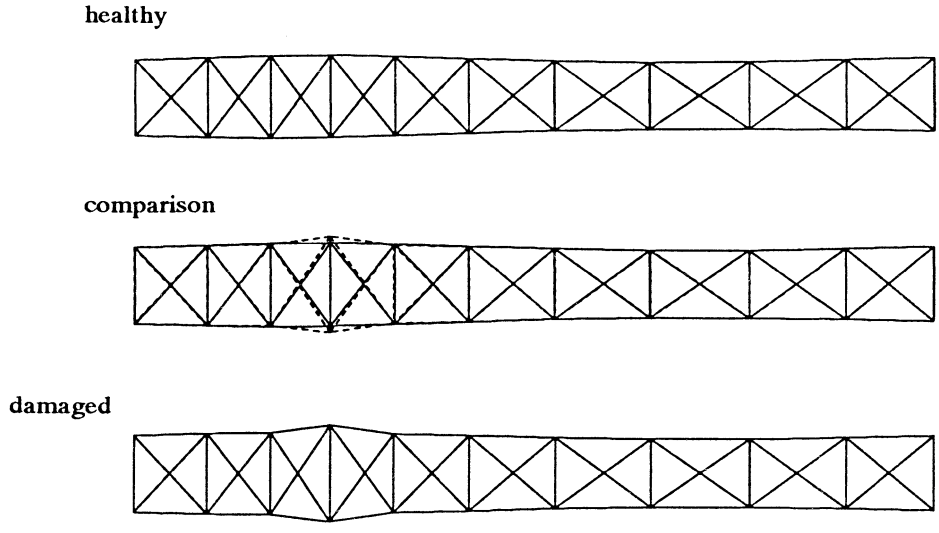

Figure 6.13a: ϕ_{H6} vs. ϕ_{D6} for Element 16 Damaged 70%

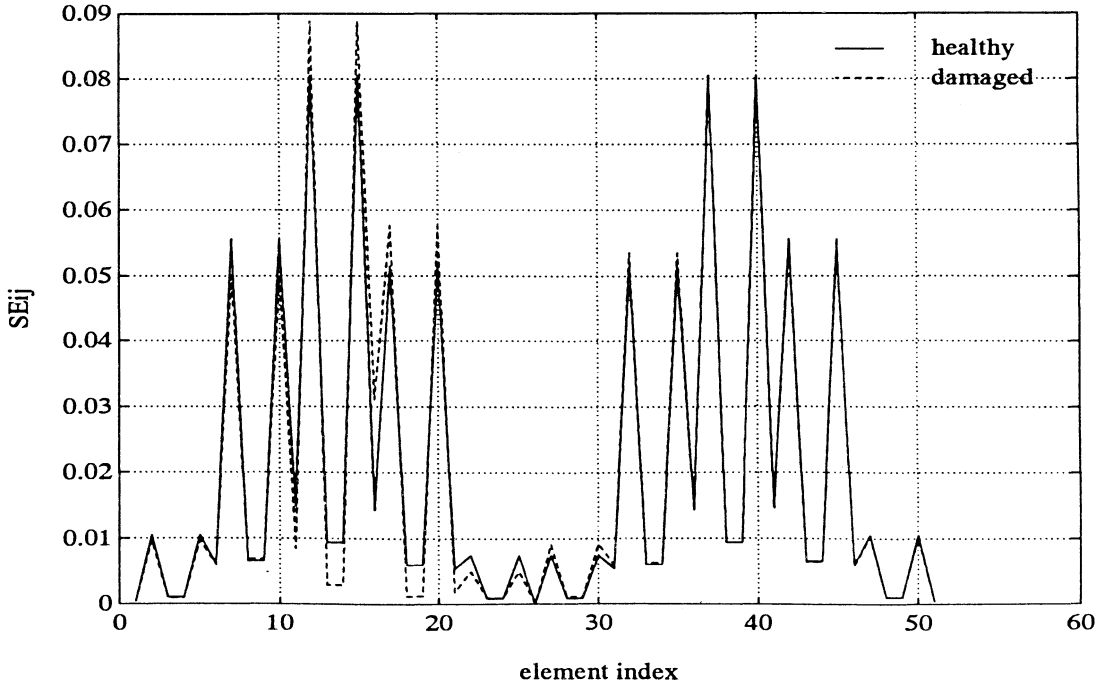

Figure 6.13b: SE_{Hi6} and SE_{Di6} for Element 16 Damaged 70%

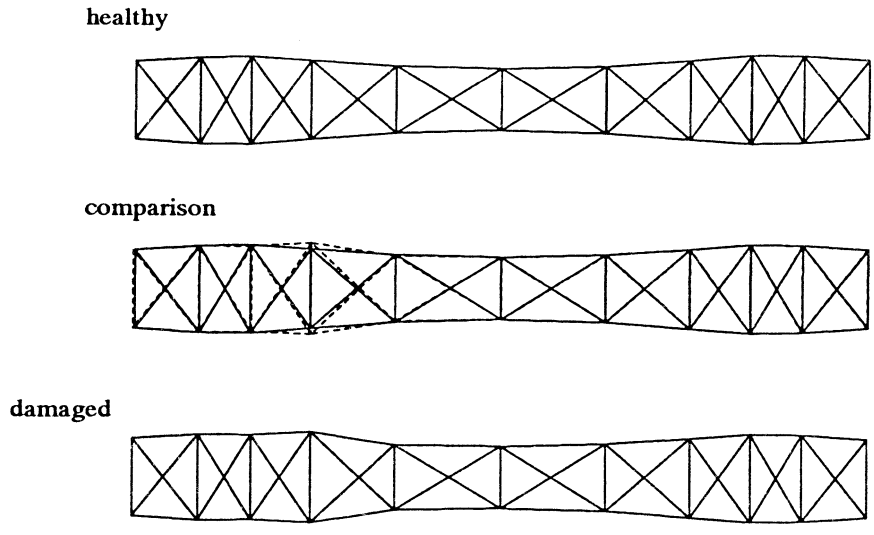

Figure 6.14a: ϕ_{H8} vs. ϕ_{D8} for Element 16 Damaged 70%

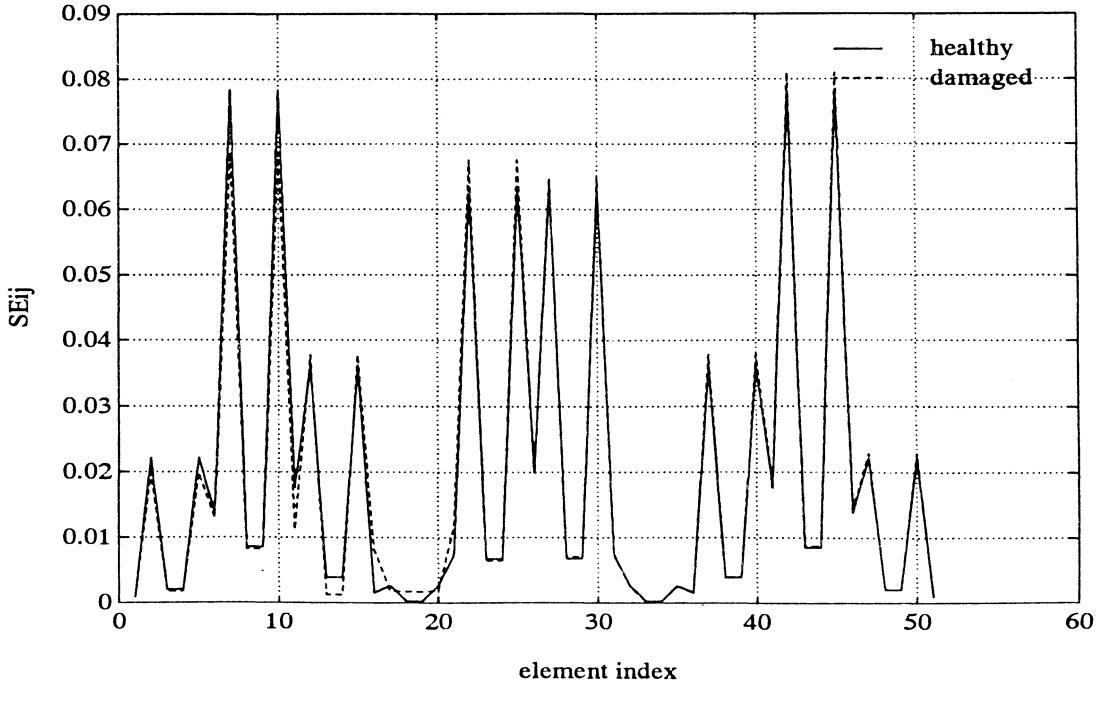

Figure 6.14b: SE_{Hi8} and SE_{Di8} for Element 16 Damaged 70%

healthy mode 5 is unobservable by all vertical elements, it does not change with damage in element 16 (ie: $\omega_{H5} = \omega_{D5}$ for small damage). However, damage does decrease the frequency of mode 6. At $d_{16} = 0.7$, frequency 6 has decreased below the value of healthy mode 5, and thus changes the order of these two modes. Hence, at this level of damage, $\omega_{H5} = \omega_{D6}$. This reordering is verified by the fact that the deflections produced by ϕ_{H6} are visually similar to those of ϕ_{D5} at $d_{16} = 0.7$.

The change in frequency these two damage cases produce is listed in Tables 6.1 and 6.2. These tables show the resulting damaged mode frequency, the percent change from the original healthy mode frequency, and the corresponding damaged fractional modal strain energy. Without exception, the mode with the largest frequency change is the mode with the largest fractional modal strain energy . The second largest change occurs to the mode with the second largest fractional modal strain energy, and so on. This verifies the relationship of SE_{ij} to mode sensitivity. Recall that the percent change in Table 6.2 for mode 5 is computed using healthy mode 6.

Table 6.1: Frequency Sensitivity for Element 14 damaged 70%

mode j	ω_{Dj}	% change	$SE_{H(14)j}$
1	7.6158	0	0.0064
2	19.2094	0.1352	0.0013
3	25.3969	0.3854	0.0050
4	33.7787	0.9077	0.0116
5	48.2908	4.7984	0.0579
6	51.2152	0.1332	0.0094
7	65.8103	3.5947	0.0571
8	77.3240	0.2250	0.0038
9	85.4225	0.4695	0.0066
10	100.2447	2.1106	0.0160

Table 6.2: Frequency Sensivity - Element 16 damaged 70%

mode j	ω_{Dj}	% change	$SE_{H(16)j}$
1	7.6158	0	0
2	19.2354	0	0
3	25.2982	0.7722	0.0096
4	34.0881	0	0
5	50.5964	1.3398	0.0143*
6	50.7247	0	0
7	68.2642	0	0
8	77.3240	0.2250	0.0015
9	85.8254	0	0
10	102.4061	0	0

$*$ computed using ω_{H6}

7 MULTI-ELEMENT DAMAGE DETECTION

In Chapter 5, a damage detection algorithm was developed which estimates damage location and the extent of stiffness reduction caused by damaged. The of iterations required for very large structures becomes very cumbersome. Even more important, this algorithm is reliable only for damage involving one element.

The goal of this chapter is to present a detection algorithm capable of locating and estimating damage anywhere in a truss with only a few iterations, regardless of the number of elements damaged. The algorithm is divided into two sub-algorithms, both of which are derivatives of the single-element damage location and estimation algorithm. The first two chapter sections will each develop one sub-algorithm. The last section will present a detection algorithm using the two sub-algorithms sequentially.

7.1 DETECTING DAMAGE in ELEMENT GROUPS

7.1.1 Defining Element Groups

The goal of the sub-algorithm presented here is to dramatically reduce the number of computations required to detect the presents of damage in a large structure. This is accomplished by dividing a structure into a small number of

element groups. Rather than accurately locating and estimating damage, this method will detect the presents of damage in each element group independently of damage outside of that group. For a pre-defined group, damage in any combination of elements is detectable. In addition, very few iterations are required for each group.

First consider the following notation:

$$P^m = M^{-1}P \tag{7.1}$$

where P is any matrix or vector.

The function of this sub-algorithm is built around the idea of defining groups of elements from some larger structure. In this sub-algorithm, each element group must be represented by a vector that satisfies two conditions.

Define: *Element Group Vector*, G_p^m, must satisfy two conditions:

A1) $$G_p^{m\mathrm{T}} B_i^m = 0, \quad \forall\, i \neq \{i_1, i_2, \ldots, i_{N_p}\}$$

A2) $$G_p^{m\mathrm{T}} B_i^m \neq 0, \quad \forall\, i = \{i_1, i_2, \ldots, i_{N_p}\}$$

where $\{i_1, i_2, \ldots, i_{N_p}\}$ are the indices of the elements **in** group p and B_i^m is computed from the element stiffness vector B_i. The subscript p indicates a specific element group where $p = \{1, 2, \ldots, N_g\}$. For full coverage of the structure, all truss elements are divided up into N_g groups. Each element, however, should not be a member of more than one group.

7.1.2 Eigenvector Assignment Decomposition

The basic relationship in which this sub-algorithm is developed around will now be derived, starting from an approach similar to that used in Chapter 5. Consider the following linear system:

$$\dot{x} = \left[M^{-1}K_H - M^{-1}G_p f_{pj} G_p^{\mathrm{T}} \right] x. \tag{7.2}$$

where M, K_H and G_p are fixed matrices, and f_{pj} is a scalar subject to change. Let the eigenvectors of this system be $\widehat{\phi}_{Dj}$ for $j = \{1, 2, \ldots, n\}$.

Since the eigenvectors are affected by change in f_{pj}, an eigenvector assignment method presented by Andry et al. can be used to compute a value of f_{pj} that will place one eigenvector, $\widehat{\phi}_{Dj}$, as close to a chosen damaged mode shape, ϕ_{Dj}, as possible in the least squares sense [29]. Because f_{pj} has significance here, it will be called the *damage indicator*. Note that for a given group p, there is a different damage indicator of each damaged mode, ϕ_{Dj}.

To apply eigenvector assignment, first let T be a transformation used to partition all matrices in Eq. (7.2) such that

$$TG_p^m = \begin{bmatrix} G_{cp} \\ 0 \\ \vdots \\ 0 \end{bmatrix} \qquad \text{where} \qquad T = \left[\begin{array}{c} T_1 \\ \hline T_2 \end{array}\right].$$

Note T_1^{T} is a $(n \times 1)$ vector. Without loss of generality, let

$$T_1^{\mathrm{T}} = \frac{G_p^m}{\|G_p^m\|}. \tag{7.3}$$

For T to be a valid transformation, it must have full rank. All columns in T_2^{T} must be orthoginal to T_1^{T} and G_p^m. By normalizing these columns, T becomes a unitary matrix where $T^{-1} = T^{\mathrm{T}}$ and $T^{\mathrm{T}}T = I_n$. Note that

$$G_{cp} = T_1 G_p^m = \|G_p^m\|. \tag{7.4}$$

The eigenvector assignment equation becomes

$$f_{pj} = \frac{1}{\|G_p^m\|}\left[\omega_{Dj}^2 \tilde{\phi}_{D1j} - A_1\,\tilde{\phi}_{Dj}\right]\left(\tilde{G}_p^{\mathrm{T}}\,\tilde{\phi}_{Dj}\right)^{-1} \tag{7.5}$$

where

$$A = TM^{-1}K_H T^{\mathrm{T}} = \left[\begin{array}{c} A_1 \\ \hline A_2 \end{array}\right],$$

$$\tilde{G}_p = TG_p, \qquad \text{and} \qquad \tilde{\phi}_{Dj} = T\phi_{Dj} = \left[\begin{array}{c} \tilde{\phi}_{D1j} \\ \hline \tilde{\phi}_{D2j} \end{array}\right].$$

The vector A_1 can be expressed as

$$A_1 = T_1 M^{-1} K_H T^{\mathrm{T}}.$$

Using Eq. (7.3) and since $T^{\mathrm{T}}T = I_n$,

$$A_1\tilde{\phi}_{Dj} = \frac{1}{\|G_p^m\|} G_p^{m\mathrm{T}} M^{-1} K_H \phi_{Dj}. \tag{7.6}$$

Also from Eq. (7.3),

$$\tilde{\phi}_{D1j} = T_1\phi_{Dj} = \frac{1}{\|G_p^m\|} G_p^{m\mathrm{T}}\phi_{Dj}. \tag{7.7}$$

These relationships can be substituted into Eq. (7.5) to yield

$$f_{pj} = \frac{\left(G_p^{\mathrm{T}}\,\phi_{Dj}\right)^{-1}}{\|G_p^m\|^2}\; G_p^{m\mathrm{T}}\left[\,\omega_{Dj}^2\phi_{Dj} - M^{-1}K_H\,\phi_{Dj}\right]. \tag{7.8}$$

Using a summation of element stiffness vectors to represent the healthy stiffness matrix and using Eqs. (6.19) and (6.17), the last term in Eq. (7.8) can be decomposed further to yield

$$M^{-1}K_H\,\phi_{Dj} = M^{-1}\sum_{i=1}^{N_e} B_i B_i^{\mathrm{T}}\phi_{Dj}$$

$$= \left[\begin{array}{c|c|c|c} \frac{1}{s_1} M^{-1}B_1 & \frac{1}{s_2} M^{-1}B_2 & \cdots & \frac{1}{s_{N_e}} M^{-1}B_{N_e} \end{array}\right] \begin{bmatrix} \epsilon_{D1j} \\ \epsilon_{D2j} \\ \vdots \\ \epsilon_{DN_ej} \end{bmatrix}. \tag{7.9}$$

The second term in Eq. (7.8) can be expressed using Eq. (6.22). Substituting these two equations into Eq. (7.8) and collecting terms gives

$$f_{pj} = \frac{\left(G_p^{\mathrm{T}}\,\phi_{Dj}\right)^{-1}}{\left\|G_p^m\right\|^2} \sum_{i=1}^{N_e} (s_i - \tfrac{1}{s_i}) G_p^{m\mathrm{T}}\, M^{-1} B_i \epsilon_{Dij} \tag{7.10}$$

where

$$f_{pj} = \begin{cases} = 0 & \text{if } d_i = 0 \ \ \forall \ \ i = \{i_1, i_2, \ldots, i_{N_p}\}. \\ \\ \neq 0 & \text{if } d_i \neq 0 \quad \text{for any } i = \{i_1, i_2, \ldots, i_{N_p}\}. \end{cases}$$

This equation is the primary relationship between the damage coefficients, the healthy model, one damaged mode, and the damage indicator, f_{pj}. One way to view the relationship is that f_{pj} is *sensitive* to damage occurring to any elements within the group p, and *insensitive* to damage elsewhere.

7.1.3 Damaged Group Location sub-algorithm

Equation (7.10) provides a powerful relationship between the damage locations, the group element vector, and the damage indicator. That is for $f_{pj} \neq 0$, the sets $\{i_1, i_2, \ldots, i_{N_g}\}$ and $\{l_1, l_2, \ldots, l_R\}$ have **at least one** common value, and $f_{pj} = 0$ otherwise. For $f_p = 0$, every term in the summation must meet at least one of four conditions:

B1) the damage coefficient is unity for any $G_p^{m\mathrm{T}} M^{-1} B_i \epsilon_{Dij} \neq 0$

B2) the innerproduct of G_p^m and B_i^m is zero

B3) ϵ_{Dij} is zero

B4) two terms in the summation of Eq. (7.10) are equal but opposite in sign such that

$$(s_i - \tfrac{1}{s_i})\, G_p^{m\mathrm{T}}\, B^m{}_i \epsilon_{Dij} \;=\; -\; (s_r - \tfrac{1}{s_r})\, G_p^{m\mathrm{T}}\, B^m{}_r \epsilon_{Drj}. \tag{7.11}$$

Because ϵ_{Dij} is a function of damage, Eq. (7.11) represents a situation that is difficult to evaluate. However, it seems very improbable that elements i and r will be damaged the exact amount required for this equation to hold. In addition, since the distribution of ϵ_{Dij} changes for every mode, Eq. (7.11) will never hold for more than one mode.

Of the three conditions, condition (B2) is the only one that is not previously defined by the structure model. Hence, it can be controlled, or defined by the user. This leads to the definition of G_p that was stated at the beginning of this section: conditions (A1) and (A2) must be met. Consider a plot of the inner product of G_p^m and B_i^m. Conditions (A1) and (A2) describe a "window" of nonzero values over the elements in the group p. All other values are zero.

This relationship can also be expressed in matrix form. Consider substituting $\omega_j^2 \phi_j = M^{-1} K_D \phi_j$ into Eq. (7.8). Then a conditional equation can be created:

$$G_p'^{\mathrm{T}}\, M^{-1} K_D \phi_{Dj} \;\stackrel{?}{=}\; G_p'^{\mathrm{T}}\, M^{-1} K_H \phi_{Dj}. \tag{7.12}$$

The question mark indicates that this equation only holds when damage is located **outside** the element group p. Hence, Eq. (7.12) does not hold when damage is located in group p.

Define the vector

$$\{\psi\} = \begin{bmatrix} \frac{\epsilon_{D1j}}{s_1} \\ \vdots \\ \frac{\epsilon_{DN_ej}}{s_{N_e}} \end{bmatrix}. \tag{7.13}$$

The damaged stiffness matrix can be written as

$$K_D = \begin{bmatrix} B_1 & B_2 & \cdots & B_{N_e} \end{bmatrix} \begin{bmatrix} d_1 & & & \\ & d_2 & & \\ & & \ddots & \\ & & & d_{N_e} \end{bmatrix} \begin{bmatrix} B_1^{\mathrm{T}} \\ B_2^{\mathrm{T}} \\ \vdots \\ B_{N_e}^{\mathrm{T}} \end{bmatrix}, \tag{7.14}$$

and the healthy stiffness matrix can be written as

$$K_H = \begin{bmatrix} B_1 & B_2 & \cdots & B_{N_e} \end{bmatrix} I_{N_e} \begin{bmatrix} B_1^{\mathrm{T}} \\ B_2^{\mathrm{T}} \\ \vdots \\ B_{N_e}^{\mathrm{T}} \end{bmatrix}. \tag{7.15}$$

Substituting in these three equations into Eq. (7.12) yields

$$\begin{bmatrix} 0 \cdots 0 & * * * & 0 \cdots 0 \end{bmatrix} \begin{bmatrix} \\ \psi \\ \\ \end{bmatrix} \stackrel{?}{=} \begin{bmatrix} 0 \cdots 0 & * * * & 0 \cdots 0 \end{bmatrix} \begin{bmatrix} d_1 & & \\ & \ddots & \\ & & d_{N_e} \end{bmatrix} \begin{bmatrix} \\ \psi \\ \\ \end{bmatrix}$$

The zeros produced in the transposed vector are created by the orthoginality of G_p^m to B_i^m. The symbol "$*$" represents the "window" of nonzero inner products for the group elements. Assuming $\{\psi\}$ has no zeros, this equation only holds when the damage coefficients within the window are all unity. That is, elements within the group are not damaged.

In reality, it is not uncommon for some elements to have zero modal strain energy for a given mode. In this case, $\{\psi\}$ will have some zeros. Hence, the use of one mode may not be sufficient to cover all elements. It is recommended that a small set of modes is used.

Rather than using Eq. (7.8), a more efficient algorithm can be can be built around Eq. (7.15). To minimize the number and size of the computations, it can be written as

$$e_{pj} = G^{m\mathrm{T}}_p \left[\lambda_{Dj} I - M^{-1} K_H\right] \phi_{Dj}. \tag{7.16}$$

The steps of the sub-algorithm are as follows:

Step 1. Divide the truss into desired element groups. Each element should be included in one, and only one, element group.

Step 2. Compute the element group vectors, G_p^m, for each group.

Step 3. Compute e_{pj} with Eq. (7.16), for all groups p and all chosen modes j.

Arrange all results into the array. Call this array $[E]$, where j is the row index and p is the column index.

Step 4. Search each column for nonzero values. Damage is located in the group whose column has at least one nonzero entry.

In application, computational error will prevent e_{pj} from being exactly zero. This requires the use of some threshold for comparison.

Note that K_H, M, and G_p^m are all computed before space structure deployment and can be stored in a data base. By storing $M^{-1}K_H$ as one matrix, this sub-algorithm only requires one matrix addition and two vector multiplications per iteration.

This sub-algorithm follows the same form as the single-element damage detection algorithm. Figure 7.1 illustrates the sub-algorithm in a block diagram. The matrix Φ_D represents the set of damaged mode shapes to be used, and Λ_D is a vector of the corresponding mode frequencies.

The power of this sub-algorithm is its flexibility in defining the element groups. A structure can be broken up into a small number of groups each with a large number of elements. This would provide course damage location, and would require few iterations. In contrast, many small groups providing fine damage location can be created. These two types of groups can be used to quickly narrow the number of suspected elements down to a small size.

As an example, consider a truss constructed with 1000 elements. If damage is found to exist somewhere in one of 10 groups containing 100 elements, that group can then be searched using smaller groups, each containing 10 elements. This requires searching through only 20 separate groups.

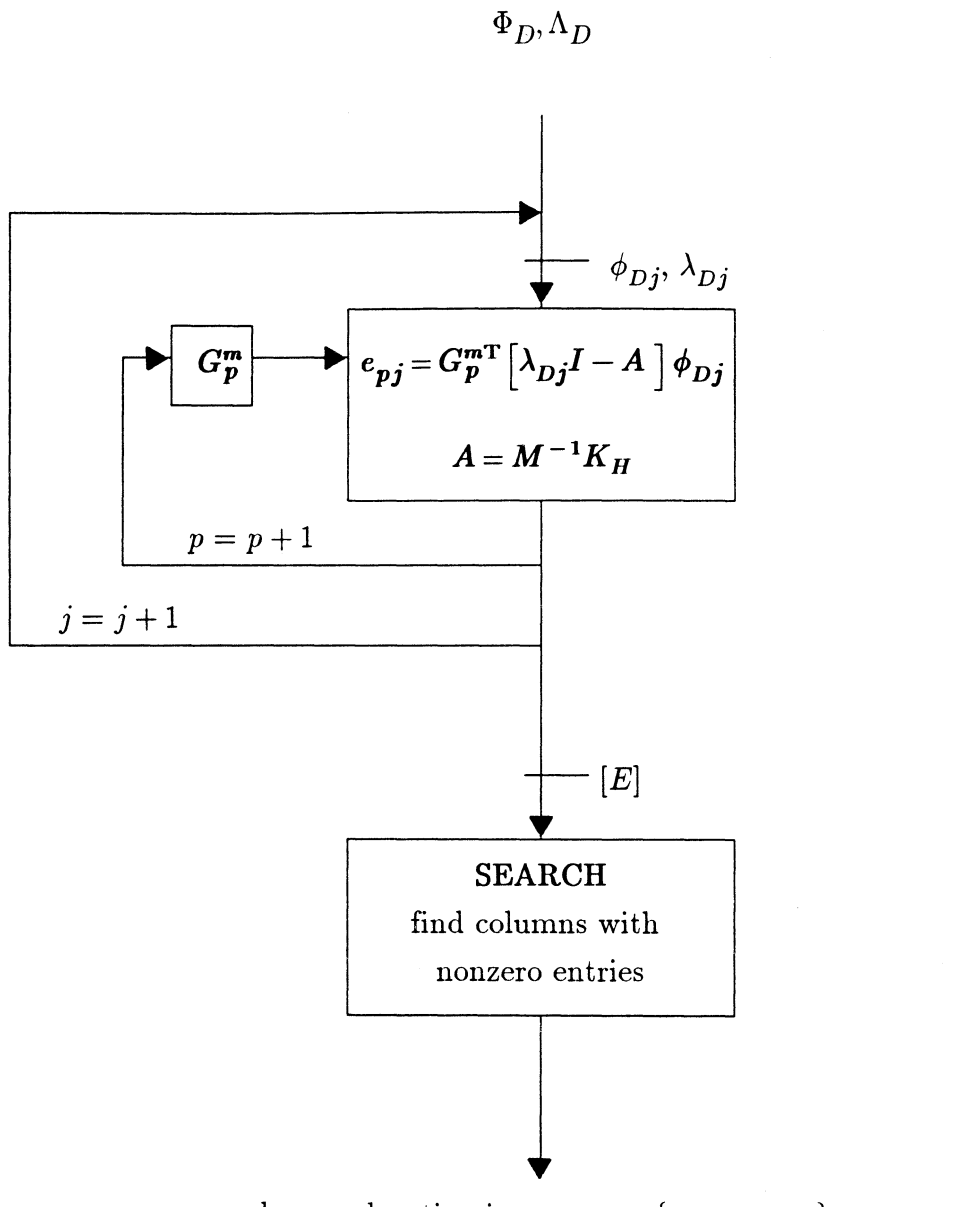

Figure 7.1: Damaged Group Location Sub-Algorithm

7.1.4 RESULTS

This section presents simulations of the damaged group location sub-algorithm using the 10 bay truss model. Because the operation of this sub-algorithm is similar to the one simulated in Chapter 5, the results will be offered in the same mesh plot format.

7.1.4.1 Computing Element Group Vectors

The first step discussed is the computation of the element group vectors. The method used for computing G_p^m involves iteration through a routine with a least square error solution. Consider iteration j. First a $(N_e \times 1)$ vector, called N_j, with random entries is generated where each entry has a Gaussian probability density function.

Second, a window vector is formed such that

$$L_p = \begin{bmatrix} 0 \\ \vdots \\ 0 \\ 1 \\ \vdots \\ 1 \\ 0 \\ \vdots \\ 0 \end{bmatrix}. \tag{7.17}$$

This vector represents the target or ideal inner product $(G_p^m, B_i)\ \forall\ i$, where the 1's

exist at the indices of the elements in group p. With this window vector, a bias is introduced to produce the random window vector

$$R_{pj} = L_p \odot (N_j + 1). \tag{7.18}$$

The symbol $\odot$ represents entry-by-entry multiplication. A least squares solution for iteration j can be computed by use of the pseudo-inverse signified by # in the equation

$$\widehat{G}^m_{pj} = \left[M^{-1}K_H\right]^{\#} R_{pj}. \tag{7.19}$$

For the final element group matrix, the sum of all $\widehat{G}^m_p$ is taken

$$G^m_p = \sum_{j=1}^{m} \widehat{G}^m_{pj} \tag{7.20}$$

The 10 bay truss is divided into five bay pairs. The element indices are

Bays 1 & 2:	p=1, $i = \{1$ through $10\}$
Bays 3 & 4:	p=2, $i = \{12$ through $20\}$
Bays 5 & 6:	p=3, $i = \{22$ through $30\}$
Bays 7 & 8:	p=4, $i = \{32$ through $40\}$
Bays 9 & 10:	p=5, $i = \{42$ through $51\}$

Plots of the inner products of G^m_p and B^m_i are shown in Figures 7.2 through 7.6.

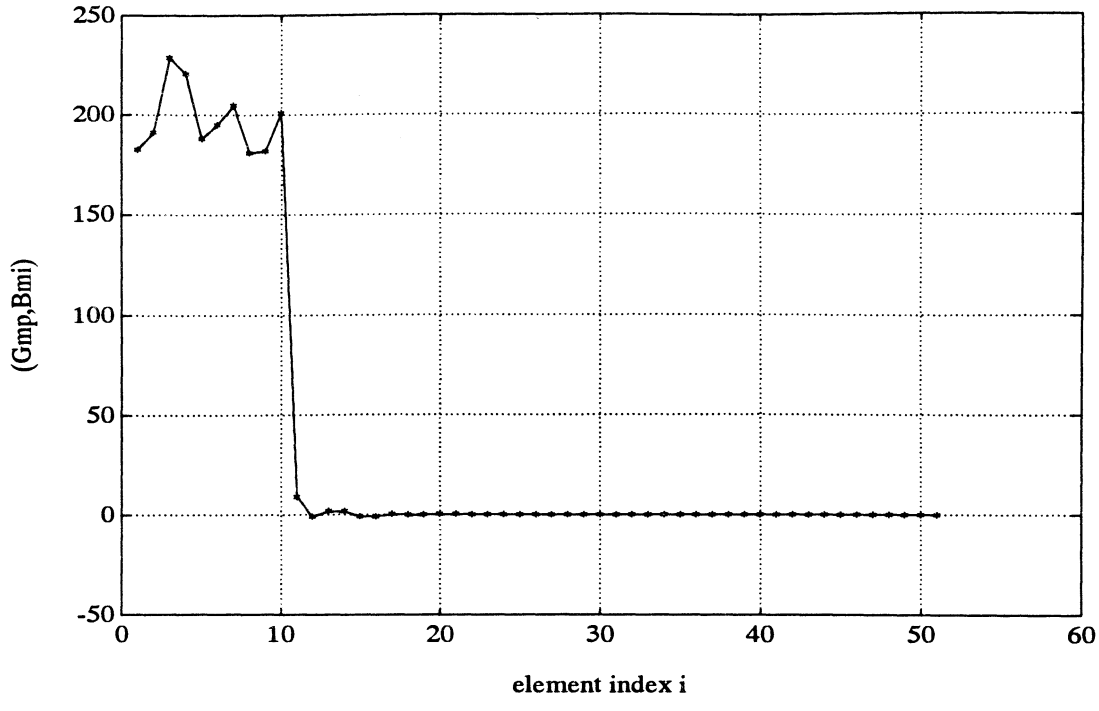

Figure 7.2: Inner Product of G_1^m and B_i^m for all i.

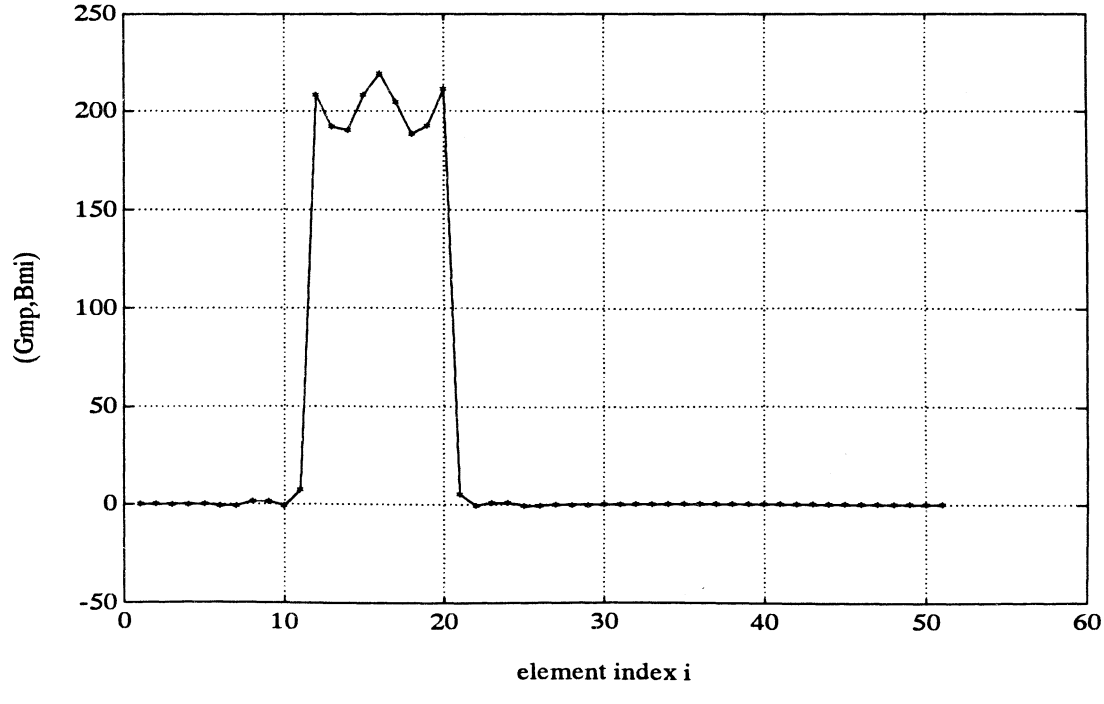

Figure 7.3: Inner Product of G_2^m and B_i^m for all i.

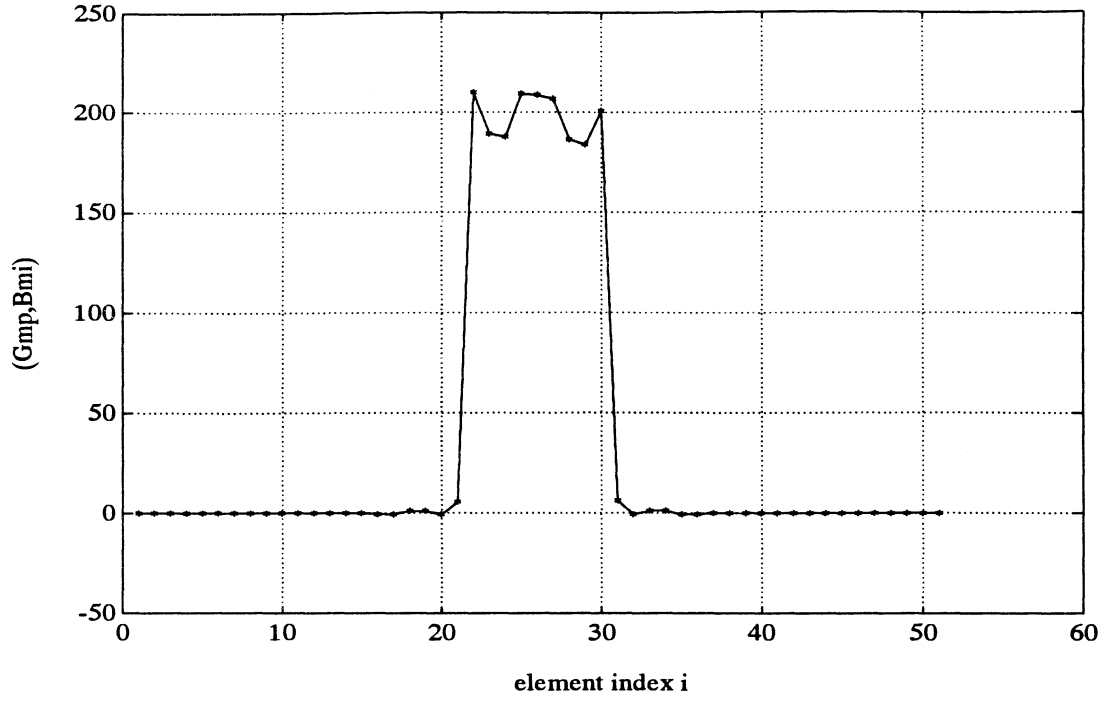

Figure 7.4: Inner Product of G_3^m and B_i^m for all i.

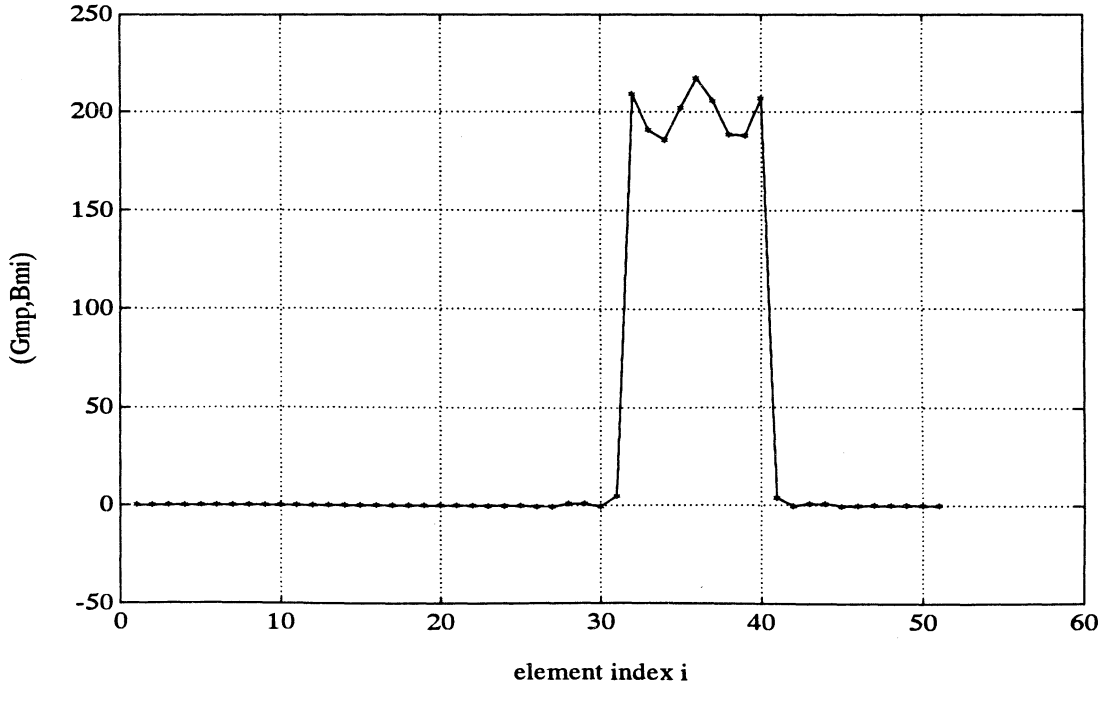

Figure 7.5: Inner Product of G_4^m and B_i^m for all i.

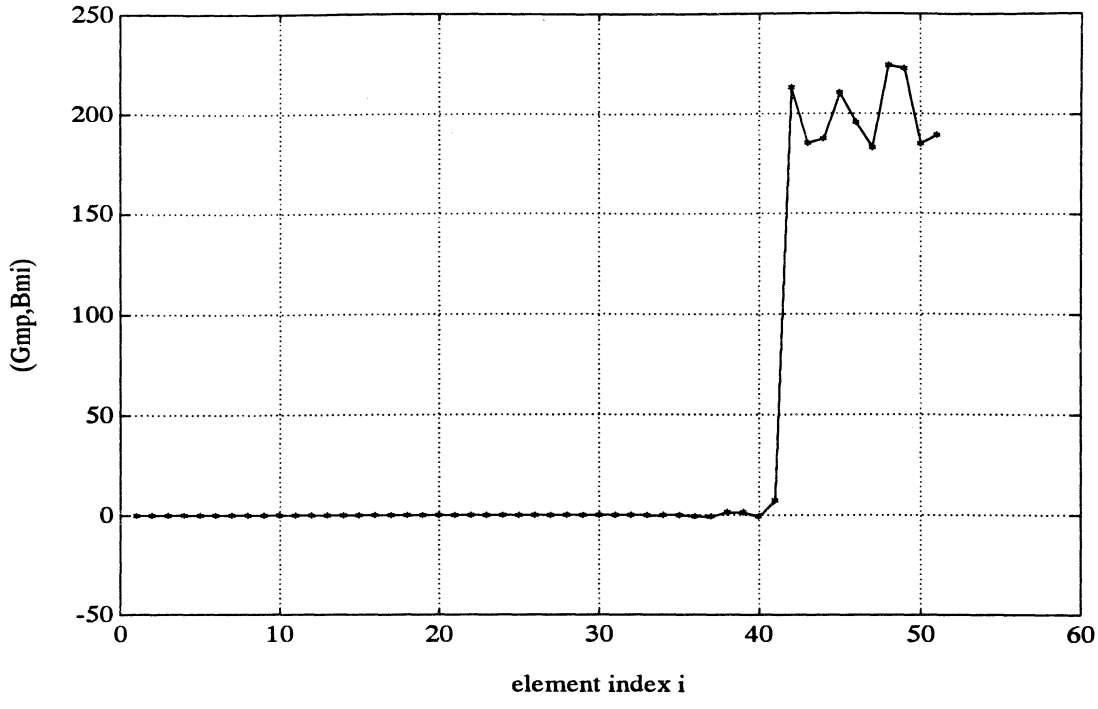

Figure 7.6: Inner Product of G_5^m and B_i^m for all i.

Elements 11, 21, 31 and 41 are not represented in this grouping. The inclusion of these elements in groups 2, 3 or 4 would disrupt the clean window functions produced by this particular iteration method. For simplicity of the presentation, these elements will be ignored.

7.1.4.2 Locating Damaged Groups

To illustrate the performance of this sub-algorithm, the absolute value of $[E]$ will be presented in the form of mesh plots for various damage scenarios. Because the maximum magnitudes of e_{pj} vary greatly for every damage case, their magnitudes relative to the largest entry are plotted. To test the sensitivity of the algorithm for small damage, $[E]$ was computed for 10% damage in element 8 (Figure 7.7). Figures 7.8 through 7.10 are mesh plots of the array $[E]$ produced by analyzing complex damage scenarios in element groups 1, 2 and 3, respectively. Each scenario includes three damaged elements, and is tested with the first 10 damaged modes. All entries in the columns outside the damaged group are zero. This proves that detection in each group is independent of all other groups.

Detecting damage in much more complex scenarios is illustrated in Figures 7.11 and 7.12. The first of these plots clearly shows damage in groups 1 and 4. All entries in columns 2, 3 and 5 are zero. The latter plot correctly shows damage in groups 1, 3 and 5.

The sub-algorithm appears easy to automate. Detection of damage to each group is performed by a simple threshold comparison. Only one mode is needed if it is observable to all elements. However, the fractional modal strain energy plots in Chapter 6 show that this not the case for any of the first ten modes.

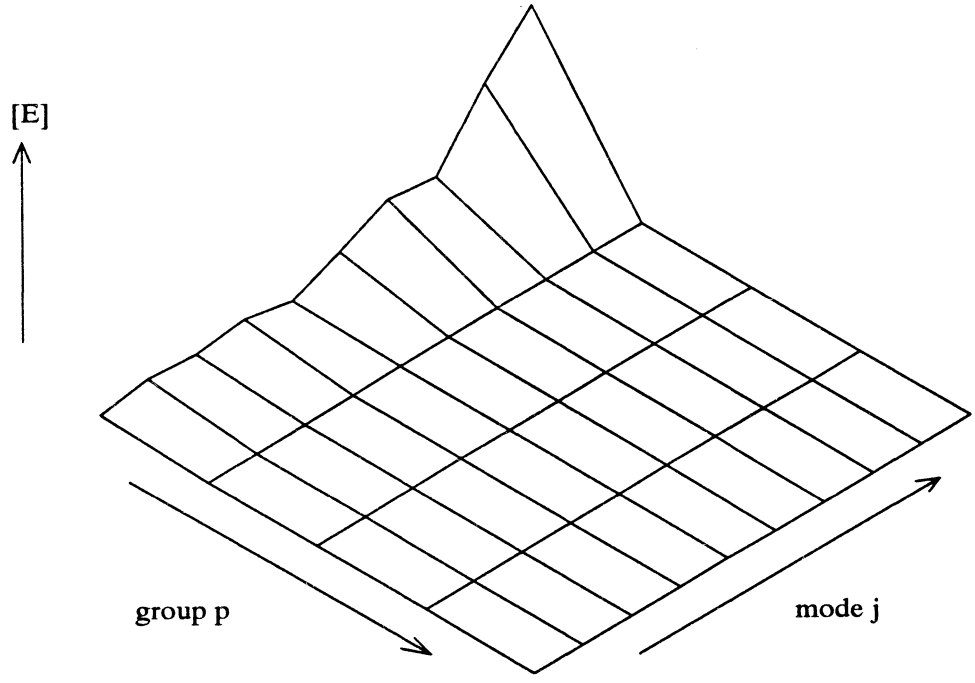

Figure 7.7: $[E]$ for Elements 8 Damaged 10%

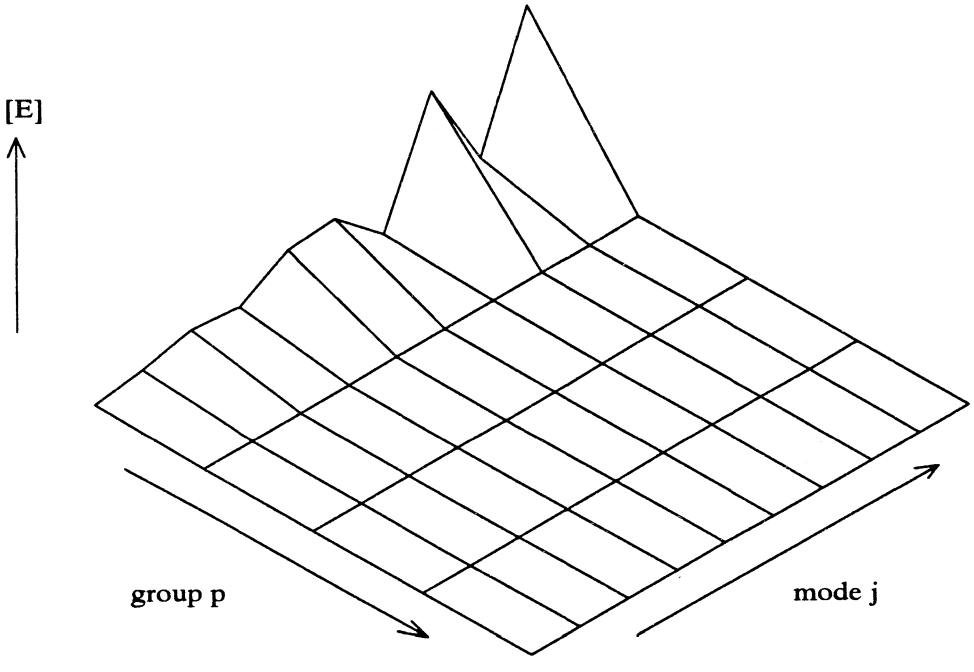

Figure 7.8: $[E]$ for Elements 2, 3, 10 Damaged 30%, 40%, 50%

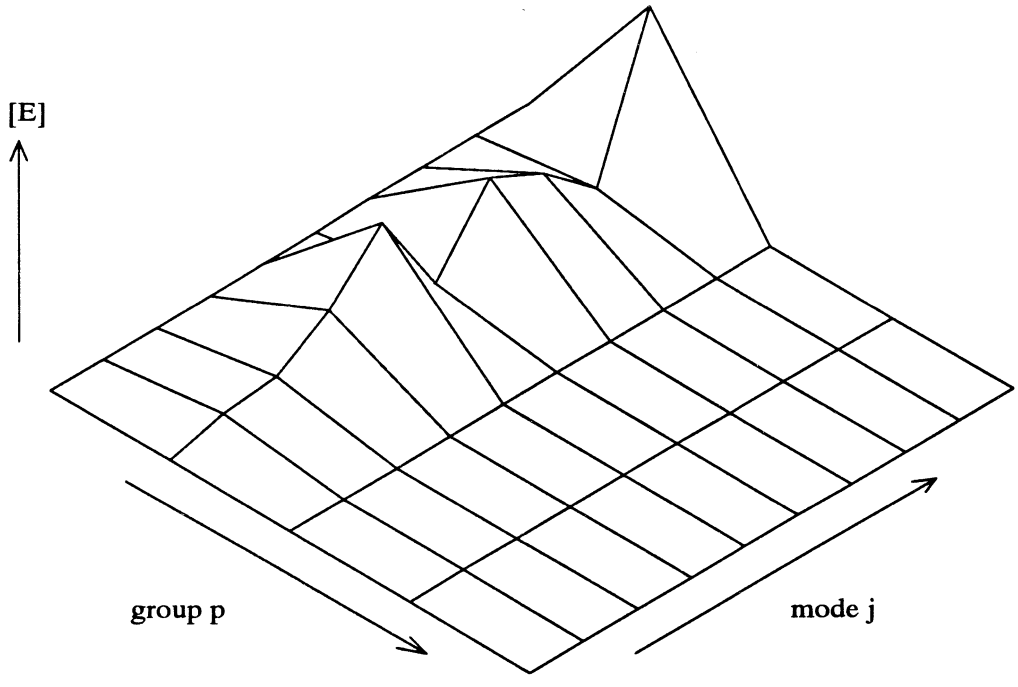

Figure 7.9: $[E]$ for Elements 12, 14, 16 Damaged 30%, 40%, 50%

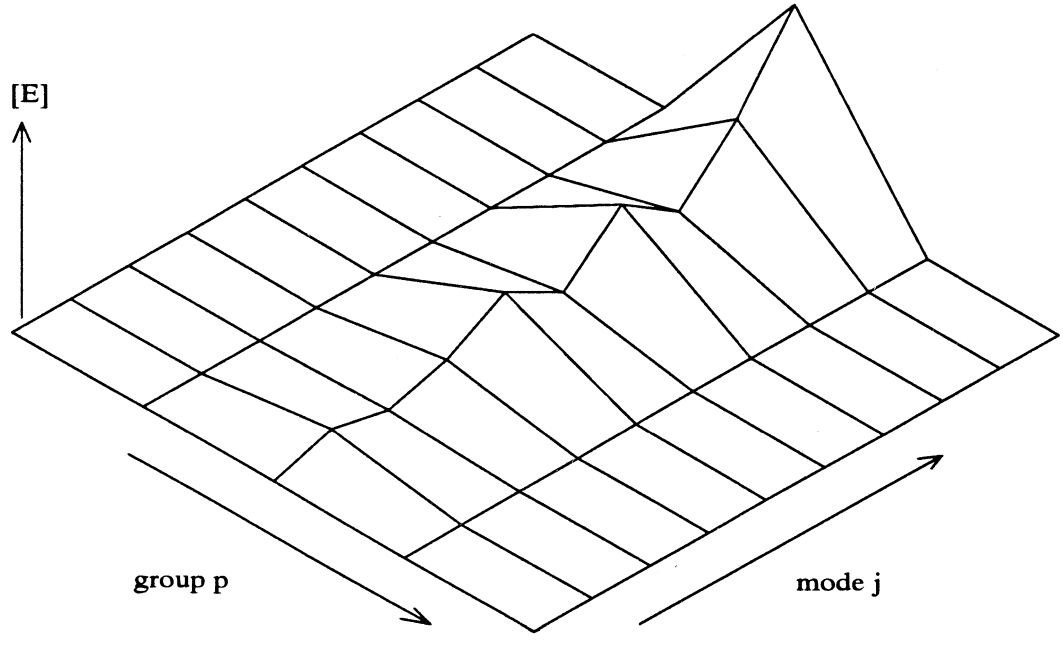

Figure 7.10: $[E]$ for Elements 22, 24, 26 Damaged 50%, 30%, 40%.

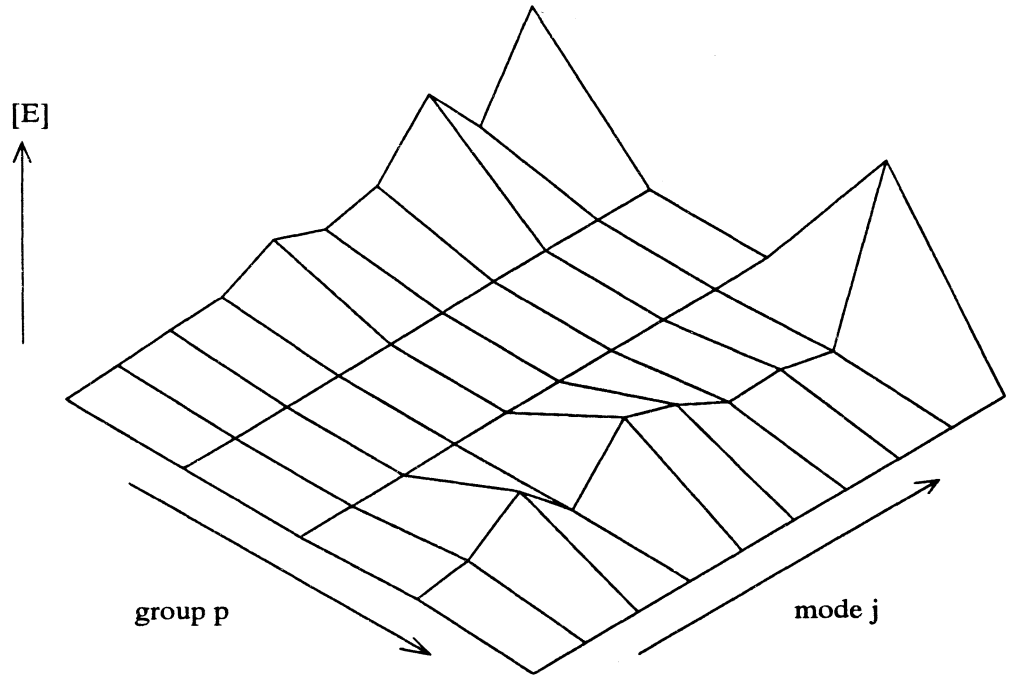

Figure 7.11: $[E]$ for Elements 2, 4, 5, 35, 32, Damaged 40%, 20%, 50%, 40%, 60%.

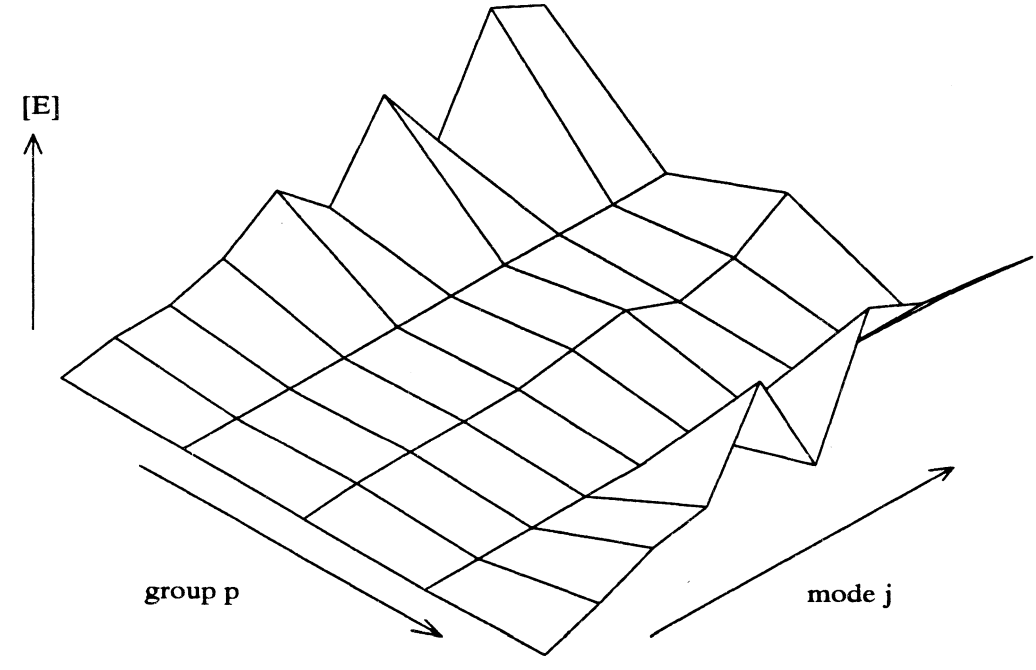

Figure 7.12: $[E]$ for Elements 4, 5, 23, 44, 45 Damaged 40%, 50%, 30%, 50%, 60%

7.2 LOCATION and ESTIMATION of MULTI-ELEMENT DAMAGE

7.2.1 Multi-Element Damage Model

The damage location and estimation algorithm developed in Chapter 5 is built around a single-element damage model. The inability of this algorithm to accurately asses scenarios involving damage to multiple elements is caused by the inability of the damage model to represent multi-element damage. To remedy this, the damage model will be modified and substituted into the development in Chapter 5. The result is a detection technique that can locate and estimate damage in any scenario with the same accuracy.

To represent multi-element damage in terms of a mode frequency and mode shape, a general form of Eq. (5.1) is

$$\left(M^{-1}K_H - M^{-1}\sum_{i=1}^{N_e} B_i d_i B_i^{\mathrm{T}}\right)\phi_{Dj} = \omega_{Dj}^2 \phi_{Dj}. \tag{7.21}$$

Define the indices of a set of damaged elements as $i = \{l_1, l_2, \ldots, l_R\}$, where R is the number of elements damaged. Then the only damage coefficients that are nonzero are d_i, $i = \{l_1, l_2, \ldots, l_R\}$. The summation term in Eq. (7.21) can be represented by the triple product $B_R D_R B_R^{\mathrm{T}}$ such that

$$D_R = \begin{bmatrix} d_{l_1} & 0 & \cdots & 0 \\ 0 & d_{l_2} & \cdots & 0 \\ \vdots & \vdots & \ddots & \vdots \\ 0 & 0 & \cdots & d_{l_R} \end{bmatrix},$$

and

$$B_R = \left[\begin{array}{c|c|c|c} B_{l_1} & B_{l_2} & \cdots & B_{l_R} \end{array} \right].$$

The multi-element damage model can be rewritten as

$$\left(M^{-1}K_H - M^{-1}B_R D_R B_R^{\mathrm{T}}\right)\phi_{Dj} = \omega_{Dj}^2 \phi_{Dj}. \tag{7.22}$$

This equation holds for all modes j. The known terms are M and K_H, ω_{Dj} and ϕ_{Dj}. The unknown terms are the matrices D_R and B_R. These unknowns imply that the number of damaged elements as well as the damage locations and extent are unknown. The goal of the multi-element damage detection sub-algorithm is to estimate D_R.

As a temporary step, the damage locations, and hence B_R, are assumed known. The problem is now reduced to solving for D_R. As with the single-element detection algorithm, the matrix in the eigenvalue equation above can be viewed as a closed loop system where the feedback gain, D_R, is unknown. Again, an eigenvector assignment algorithm can be applied to solve for D_R [29]. Computing multi-variable feedback will require more than one eigenvector.

The first step in solving for D_R is defining the transformation

$$TM^{-1}B_R = \left[\begin{array}{c} B_{Ro} \\ \hline 0 \\ \vdots \\ 0 \end{array} \right] \tag{7.23}$$

where B_{Ro} is an $(R \times R)$ matrix. Next, apply this transformation to all other components of Eq. (7.22), resulting in

$$A = TM^{-1}K_H T^{-1},$$

$$\tilde{B}_R^{\mathrm{T}} = B_R^{\mathrm{T}}\, T^{-1}, \qquad \text{and} \qquad \tilde{\phi}_{Dj} = T\phi_{Dj}.$$

Define a matrix $\tilde{\Phi}_{D\zeta}$ who's columns are the R different eigenvectors, $\tilde{\phi}_{Dj}$, where $j = \{k_1, k_2, \ldots, k_R\}$, and a $(R \times R)$ matrix $\Lambda_{D\zeta}$ with the corresponding eigenvalues ω_{Dj}^2 on the diagonal.

To make dimensionally compatible with Eq. (7.23), the following partitions are made:

$$A = \left[\begin{array}{c} A_1 \\ \hline A_2 \end{array}\right], \quad \text{and} \qquad \tilde{\Phi}_{D\zeta} = \left[\begin{array}{c} \tilde{\Phi}_{D1\zeta} \\ \hline \tilde{\Phi}_{D2\zeta} \end{array}\right]$$

where A_1 is the first R rows of A and $\tilde{\Phi}_{D1\zeta}$ is a $(R \times R)$ matrix. Substitute these transformations into Eq. (7.22) and solve for D_R. Then

$$D_R \;=\; B_{Ro}^{-1}\left[\,\Lambda_{D\zeta}\tilde{\Phi}_{D1\zeta} \;-\; A_1\,\tilde{\Phi}_{D\zeta}\right]\left(\tilde{B}_R^{\mathrm{T}}\,\tilde{\Phi}_{D\zeta}\right)^{-1} \tag{7.24}$$

Note that since $T^{\mathrm{T}}T = I$, the last term is simply $(B_R^{\mathrm{T}}\,\Phi_{D\zeta})^{-1}$. For Eq. (7.24) to be computable, the inverse of B_{Ro} and $B_R^{\mathrm{T}}\Phi_{D\zeta}$ must exist. In order for both of these $(R \times R)$ matrices to have full rank, all columns of B_o and $\Phi_{D\zeta}$ must be

independent. This requires that no one mode can be used twice, and that the substructure defined by the columns in B_R is not over determined. That is no one element connects two nodes that are already connected by at least two elements.

Now that an equation for computing the damage coefficients has been derived, the assumption that the damage locations are known is dropped. Similar to single-element detection, the locations must be *postulated.* This increases the number of unknown variables in the damage model to include the number of damaged elements R, the damage locations $\{l_1,l_2,\ldots,l_R\}$, and the extent of the damage to each element $\{d_{l_1},d_{l_2},\ldots,d_{l_R}\}$. To delineate this large set of unknowns from Eq. (7.24), the following notation is offered:

Define: *Estimated Modal Damage Coefficient Matrix*

$$\widehat{D}_{\xi\zeta} = B_{R'\xi}^{-1}\left[\Lambda_{D\zeta}\widetilde{\Phi}_{D1\zeta} - A_1\,\widetilde{\Phi}_{D\zeta}\right]\left(\widetilde{B}_{\xi}^{\mathrm{T}}\,\widetilde{\Phi}_{D\zeta}\right)^{-1} \tag{7.25}$$

where R' is the postulate number of elements damaged

$\zeta = \{k_1,k_2,\ldots,k_{R'}\}$ is the set of R' mode indices

$\xi = \{l'_1,l'_2,\ldots,l'_{R'}\}$ is the set of R' postulated element indices

B_{ξ} is an $(n \times R')$ matrix who's columns are the postulated element stiffness vectors

$B_{R'\xi}$ is an $(R' \times R')$ matrix computed with Eq. (7.23)

$\Phi_{D\zeta}$ is an $(n \times R')$ matrix who's columns are the selected mode shapes

$\Lambda_{D\zeta}$ is an $(R' \times R')$ matrix who's diagonal entries are the corresponding eigenvalues, ω_{Dj}^2

$\widehat{D}_{\xi\zeta}$ is an $(R' \times R')$ matrix of gain values.

Only when the correct elements are postulated, does $\widehat{D}_{\xi\zeta} = D_R$.

In the context of eigenvector assignment, Eq. (7.25) attempts to assign the eigenvectors in $\Phi_{D\zeta}$ to the matrix $\left(M^{-1}K_H - M^{-1}B_\xi\ \widehat{D}_{\xi\zeta}\ B_\xi^{\mathrm{T}}\right)$. If the eigenvectors are not fully achievable, they are assigned in the least squares sense [29]. Let $\widehat{\Phi}_{D\zeta}$ be the set of achievable eigenvectors, then

$$\left(M^{-1}K_H - M^{-1}B_\xi\ \widehat{D}_{\xi\zeta}\ B_\xi^{\mathrm{T}}\right)\widehat{\Phi}_{D\zeta} = \widehat{\Lambda}_{D\zeta}\widehat{\Phi}_{D\zeta}. \tag{7.26}$$

Only when the correct postulations are made is $\widehat{\Phi}_{D\zeta} = \Phi_{D\zeta}$.

The conditions of full assignability (or $\widehat{\Phi}_{D\zeta} = \Phi_{D\zeta}$) must be analyzed to determine the conditions for a correct postulation. Consider

$$\phi_{Dj} = [\Psi]_{\xi j}\ m_{\xi j} \tag{7.27}$$

where

$$[\Psi]_{\xi j} = \left(\omega_{Dj}^2 I - M^{-1}K_H\right)^{-1} M^{-1}B_\xi,$$

and

$$m_{\xi j} = \widehat{D}_{\xi\zeta}B_\xi^{\mathrm{T}}\ \phi_{Dj}.$$

For the eigenvector ϕ_{Dj} to be fully assignable, it must lie in the space spanned by $[\Psi]_{\xi j}$. This implies the size of the achievable subspace is directly proportional to R', the number of elements postulated. Hence, increasing the number of postulated elements increases the size of the subspace. Because the set of damaged mode shapes considered are defined exactly by the damaged structure, if one mode shape

lies in the achievable subspace, then all other damaged modes will lie exactly in the subspace as well. This implies that every mode is equally suitable for use in Eq. (7.25), as long as its modal strain energy is not zero for all elements in B_ξ.

7.2.2 Multi-Element Damage Location and Estimation Sub-algorithm

When all damage elements are represented in B_ξ, only then are all mode shapes fully assignable. The gain matrix that can assign all mode shapes is the diagonal matrix D_R. When a postulation set does not contain all damged elements, a gain matrix is computed to partially assign only the eigenvectors in $\Phi_{D\zeta}$. The result is a gain matrix that is not diagonal. This is the condition in to test for.

A multi-element damage detection sub-algorithm then is the following:

Step 1. Create some set of postulated elements and form B_ξ.

Step 2. Select a set of damaged modes $\Phi_{D\zeta}$ and $\Lambda_{D\zeta}$.

Step 3. Compute $\widehat{D}_{\xi\zeta}$. Three possible outcomes follow:

Case 1. If B_ξ contains the exact set of damaged elements, the diagonal of $\widehat{D}_{\xi\zeta}$ will contain the corresponding damage coefficients defined by the multi-damage model.

Case 2. If B_ξ contains the exact set of damaged elements, plus additional elements such that B_ξ is of full rank, the diagonal of $\widehat{D}_{\xi\zeta}$ will contain the corresponding damage coefficients. Hence, any elements not damaged in that set produce a zero on the diagonal of $\widehat{D}_{\xi\zeta}$.

Case 3. If B_ξ does not contain the full set of damaged elements, then $\widehat{D}_{\xi\zeta}$ is not a diagonal matrix, but contains arbitrary nonzero values. That is, B_ξ can contain some or none of the damaged elements.

Step 4. Noting Case 3, if $\widehat{D}_{\xi\zeta}$ is not a diagonal matrix, return to Step 1 and create a different postulation set. If Case 1 or 2 occur, extract the damage coefficients from the diagonal entries. Their indices corresponds to the order of the postulation set in B_ξ.

This sub-algorithm is outlined as a block diagram in Figure 7.13. In contrast to the single-element detection method, there is no fixed number of iterations required for full detection. From this figure, it is evident that the number of iterations required depends on the rules used to make each postulation.

Case 2 above shows there is no disadvantage to choosing a large postulation set. This gives a greater probability of including all damaged elements, and hence correct detection. However, the selection of a postulation set is not completely arbitrary since B_ξ must have full rank. The size of the postulation set is also limited by the number of damaged modes available.

This exposes a disadvantage of this damage detection method. Damage may be located such that B_R is not full rank. In this case, damage is not dectable with this sub-algorithm.

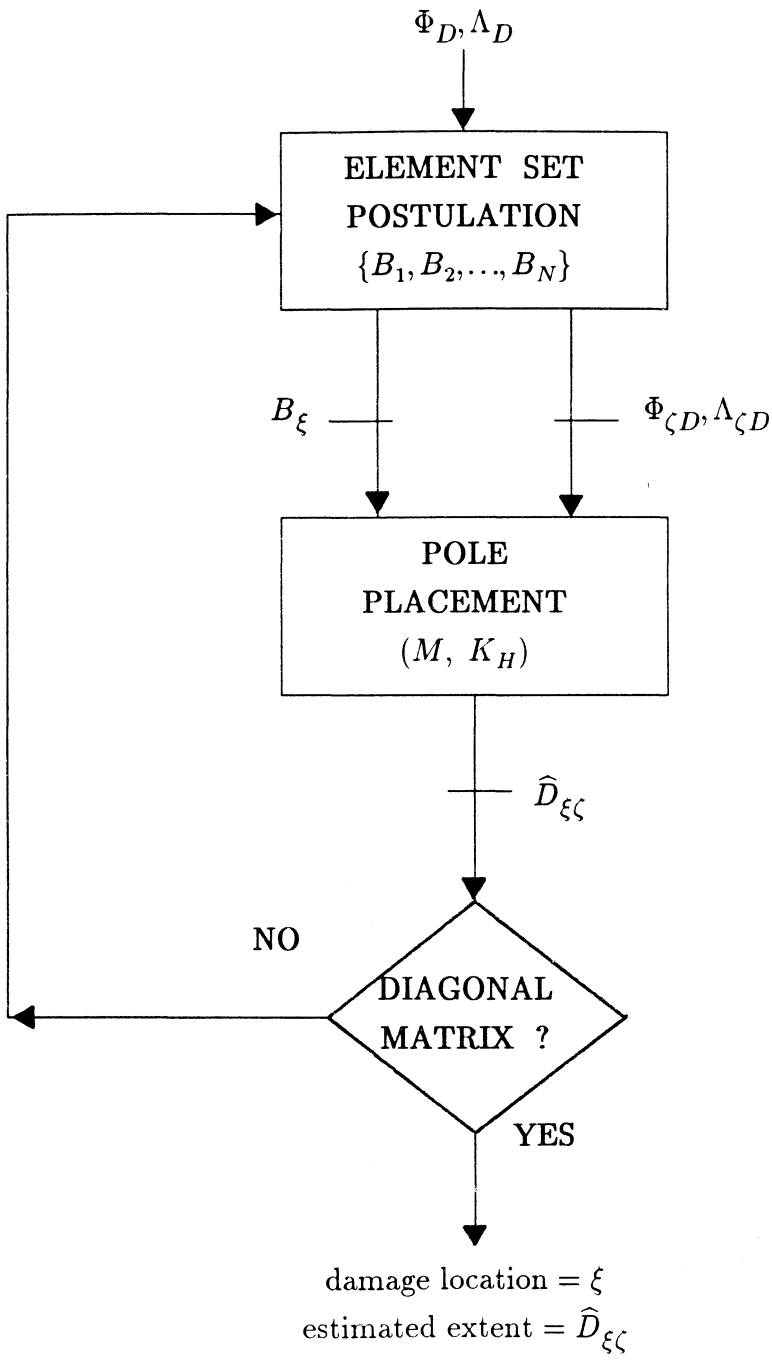

Figure 7.13: Multi-Element Damage Location & Estimation Sub-algorithm

7.3 A SEQUENTIAL DAMAGE DETECTION ALGORITHM

This section brings together the advantages of the two sub-algorithms developed in Sections 7.1 and 7.2 to form one larger sequential algorithm that can accurately locate and estimate damage with a minimum of computations. The damaged group location sub-algorithm is first used to quickly search through a structure to find an element group in which damage is located. This algorithm will be called Sub-algorithm 1. Then, the multi-element damage location and estimation sub-algorithm is used to pinpoint the damage within the group of suspect elements, and to estimate the extent of the damage. This will be called Sub-algorithm 2.

Figure 7.12 illustrates the sequential algorithm in a block diagram. Sub-algorithm 1 performs two functions. It screens the truss for damage. If no damage is detected, the next step is to wait some time step for the next iteration. The other function is the location of damage. If damage does exists, Sub-algorithm 1 will define one or more element groups where the damage is located. Together, all damaged groups form a set of suspected elements.

The indices of the suspected elements is then passed to Sub-algorithm 2. Here, some search procedure is required to form a postulation set from the set of suspected elements. If the resulting estimated modal damage coefficient matrix, $\widehat{D}_{\xi\zeta}$, holds the desired form of a diagonal matrix, the damage locations and extents can be extracted. If not, then a new postulation is made and the process is repeated.

Compared with other damage detection methods, this sequential algorithm requires few computations. The number of iterations required is dependant upon

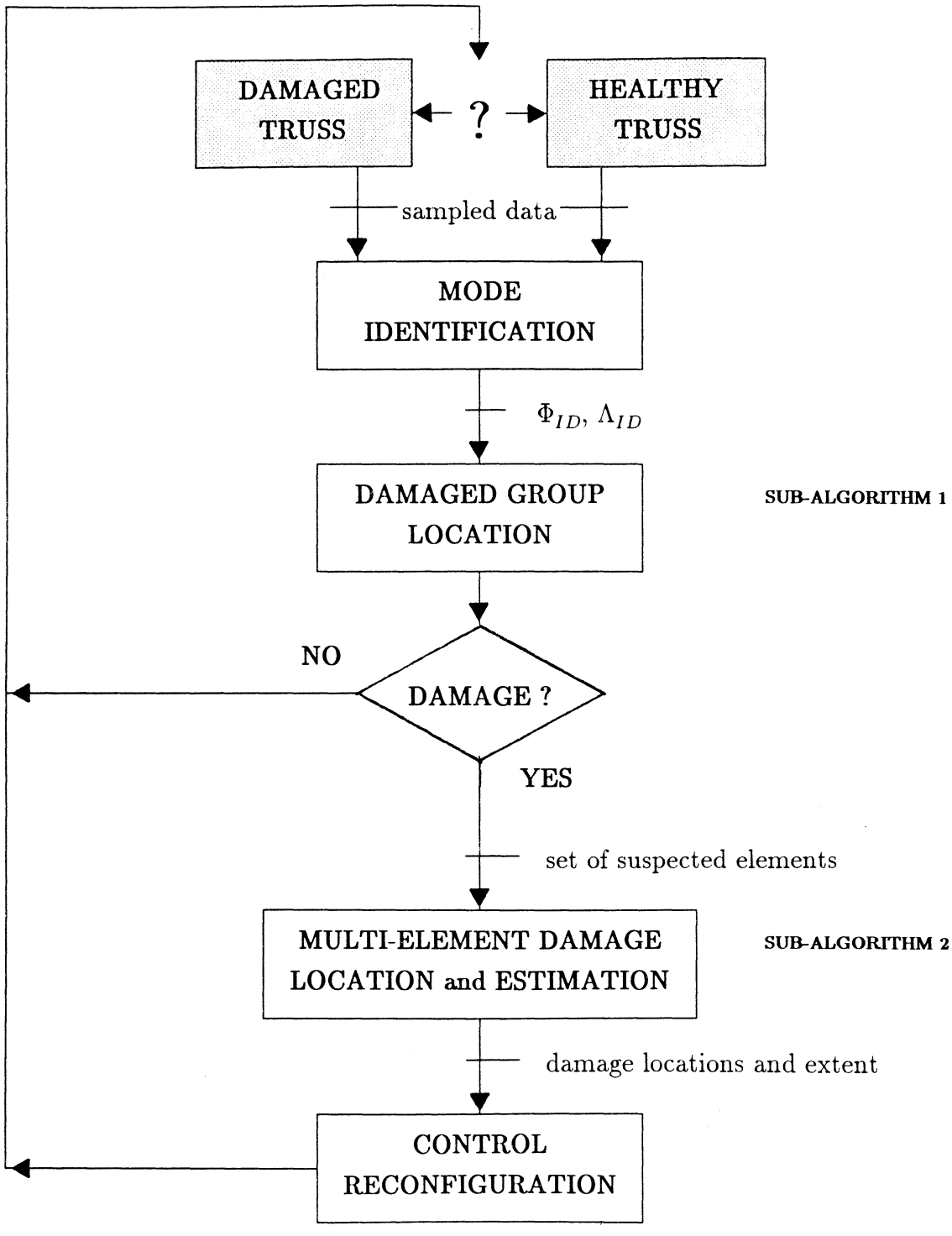

Figure 7.14: Sequential Damage Detection Algorithm

the number of elements damaged and the size of the element groups defined. One possible source of a large number of computations is Sub-algorithm 2. If the set of suspected elements is large, many postulations may be made before the damage is located. The size of the postulation set is limited by the number of damaged modes available and by the redundancy of the structure (recall that the rank of the matrix B_ξ is dependent upon structure redundancy).

Hence, it is advantageous to provide Sub-algorithm 2 with the smallest possible set of suspect elements. One approach is to divide the truss evenly into a few large element groups, and then into a large number of small element groups. This would produce two sets of element group vectors, G_p^m. Once damage is located within a large group, only a few iterations using the small groups is needed to reduce the number of suspected elements.

For maximum efficiency, this sequential algorithm must be tuned for a specific truss. Section 7.1.4.1 illustrated that the selection of element groups is not entirely arbitrary. The element groups must be chosen with care in order to be able to compute a G_p^m that satisfies the condition of orthoginality to all B_i^m outside the group. In addition, a method for making postulations must be created for Sub-algorithm 2. The approach taken to search through a set of suspected elements depends on the size of the set and the number of available damage modes.

The performance of the sequential damage detection algorithm is limited by several factors. As mentioned above, the geometry of the structure may limit the selection of element groups and the selection of postulation sets. The number of damaged modes available from a modal survey also limits the size of the postulation set. Hence, it is possible that the smallest suspect set Sub-algorithm 1 can produce is much larger than the maximum size of the postulation set. In this

case, many iteration would be required. In addition, if the number of damaged elements is greater than the number of available damaged modes, Sub-algorithm 2 would fail. In this case, the suspect set would be the only information of the damage available. Hence, the sequential algorithm's performance is dependent on the physical situation: the structure's geometry and the all factors that limit the number of modes supplied by a modal survey.

8 CONCLUSIONS

This research has addressed several key issues involved in the damage detection problem for large space structures. The major goals stated for the algorithms that were developed are computational efficiency, accuracy, and the ability to address cases of multi-element damage. The sequential algorithm developed meets all three goals.

Reviewing current published literature, Chapter 2 identified several approaches made by other detection techniques. Most algorithms in these categories are complex and difficult to automate, computationally intensive, or inaccurate in the estimation of stiffness reduction. Many of these methods are unable to detect damage if several elements are damaged.

The two detection algorithms developed in this thesis are based on a damaged truss model which is expressed in terms of the healthy stiffness matrix, a damage coefficient, and a vector representation of the damage element's contribution to the truss's stiffness. Because each element stiffness matrix has the rank of one, it was shown that singular value decomposition could be used to compute a vector that contains all stiffness and geometry information.

The damaged truss model expresses a change in the healthy stiffness matrix as a product of a scalar and two vectors, enabling the use of an eigenvector assignment method to exactly solve for the unknown damage coefficient. Chapter

5 first exploited this procedure to develop a detection method that is accurate in assessing single-element damage, and requires a minimum number of damaged modes. Compared with other detection methods, this algorithm requires relatively few computations. Though simple to automate, the algorithm performs poorly for most multi-element damage cases. However, possible use of advanced pattern recognition methods may extend the function of this algorithm.

Chapter 6 presented the definition of fractional modal strain energy. This measure was shown to be directly related to the effect damage to a particular element has on a particular mode frequency. When this measure is zero, it was shown that detection is not possible, and corresponds to an unobservability condition. In this chapter, element modal deflection was defined as having a square law relationship with strain energy. This definition and its relationship to mode shapes was developed as background material for Chapter 7.

Building upon the damaged truss model and the eigenvector assignment method used in Chapter 5, two sub-algorithms were developed in Chapter 7. The first sub-algorithm used material from Chapter 6 and the element stiffness vector to detect damage within a set of predetermined element groups. To fully represent all elements, this method requires two or three damaged modes. The goal of this method is to reduce the number of elements suspected of damage to a manageable size. From this set of suspect elements, damage can be exactly located and estimated using the second sub-algorithm.

The second sub-algorithm was developed using the same process described in Chapter 5, but using a truss model built around multi-element damage. The speed of this sub-algorithm is directly dependent on the number of suspected elements, and the number of damaged modes available. The complexity of iterating through

postulations makes this sub-algorithm unattractive for use individually. Chapter 7 finally forms a sequential algorithm from both sub-algorithms. The result is a detection method that requires few computations and can search through large structures efficiently. This sequential algorithm can accurately assess damage to many elements, which is a task no other current method can perform.

To determine a detection method's suitability for application to a physical structure, all of the assumptions made in this thesis must be addressed. These areas of future study would involve a wide range of disciplines. Damage is assumed to be a linear reduction in stiffness. This implies a damaged element has the same stiffness in both compression and tension. It may be possible to address nonlinear effects of damage in the interpolation functions used to form the finite elements. The finite element method is assumed to exactly describe the stiffness and mass properties, and the dynamics of the truss. Model refinement methods attempt to address the inherent inaccuracy of the finite element method by performing adjustments on the mass and stiffness matrices. However, all algorithms in this thesis require the use of element stiffness vectors, which are not common to refinement methods. This prompts the need for analysis of the effects of element stiffness vector accuracy on the algorithm's performance and possible development of a refinement method to improve such accuracy. Finally, no error was considered to exist in the mode identification process. There are several methods for approximating error incurred during identification. Because this error is induced with any modal survey, studying the effects of this error on the detection algorithms should be an important goal of any future research.

REFERENCES

1. Zimmerman, D. C. and S. W. Smith, "Model Refinement and Damage Location for Intelligent Structures," *Intelligent Structural Systems,* H. S. Tzou, editor, Kluwer Academic Publishers, 1991.

2. Kirchner, C. A., "Ambient and Forced Vobration Analysis of Full Scale Structures," PhD Dissertation, Stanford University, 1976.

3. Yao, J. T. P., "Damage Evaluation for Structural Reliability Assessment," *Nuclear Engineering Design,* Vol. 1, No. 2, pp. 141-149, 1983.

4. Coppolino, R.N. and S. Rubin, "Detection of Structural Failures in Offshore Platfroms by Ambient Vibration Monitoring," *Proceedings of the 12th Offshore Technology Conference,* Houston, Texas, pp. 101-110, 1980.

5. West, W.M., Jr., "Single Point Random Modal Test Technology Application to Failure Detection," *Shock and Vibration Bulletine,"* No. 52, pp. 25-31, 1982.

6. Pacia, A. B., "Using Modal Testing to Identify Dynamic Changes in Battle Damaged F-16 Wings," *Proceedings of the 59th Shock and Vibration Symposium,* Albuquerque, New Mexico, 1988, pp. 337-359.

7. Hajela, P. and F. J. Soeiro, "Structural Damage Detection Based on Static and Modal Analysis," *AIAA Journal,* Vol. 28, No. 6, June 1990, pp. 1110-1115.

8. Lim, T. W., "Structural Damage Detection Using Modal Test Data," *AIAA Journal,* Vol. 29, No. 12, December 1991, pp. 2271-2274.

9. Smith, S. W., "Damage Detection and Location in Large Space Trusses," PhD Dissertation, Virginia Polytechnic Institute and State University, April 1988.

10. Zimmerman, D. C. and M. Kaouk, "Structural Damage Detection Using a Subspace Rotation Algo", AIAA paper, AIAA-92-2521-CP, 1992.

11. Zimmerman, D. C. and M. Kaouk, "Eigenstructure Assignment Approach for Structural Damage Detection," *AIAA Journal,* Vol. 30, No. 7, July 1992, pp. 1848-1885.

12. Grantham, W. L. and R. A. Laskin, "NASA CSI Technology Program Focus Mission and Benefit Studies," *Proceedings of the 4th NASA/DoD CSI Technology Conference,* January 1991, pp 1-29.

13. Kabe, A. M., "Stiffness Matrix Adjustment Using Modal Data," *AIAA Journal,* Vol. 23, 1985, No. 9, pp. 251-259.

14. White, C. W. and B. D. Maytum, "Eigensolution Sensitivity to Parametric Modal Perturbations," *Shock and Vibration Bulletin,* Bulletin 46, Aug 1976, pp 193-198.

15. Ricles, J. M. and J. B. Kosmatka, "Damage Detection in Elastic Structures Using Vibratory Residual Forces and Weighed Sensitivity," *AIAA Journal,* Vol. 30, No. 9, September 1992, pp 2310-2316.

16. Edwins, D. J., *Modal Testing: Theory and Practice,* Wiley, New York, 1984.

17. Lim, T. W., "A Submatrix Approach to Stiffness Matrix Correction Using Modal Test Data," *AIAA Journal,* Vol. 28, No. 6, June 1990, pp. 1123-1130.

18. Chen, J. Y. and J. A. Garba, "On-Orbit Damage Assessment for Large Space Structures," *AIAA Journal,* Vol. 26, No. 9, September 1988, pp. 1119-1126.

19. Meirovitch, L. S, *Elements of Vibration Analysis,* McGraw-Hill, Inc., New York, NY, 1986.

20. Kashangaki, T. A. L., S. W. Smith, and T. W. Lim, "Underlying Modal Data Issues for Detecting Damage in Truss Structures," AIAA paper, No. AIAA-92-2264-CP

21. Nelson, R. B., "Simplified Calculation of Eigenvector Derivatives," *AIAA Journal,* Vol. 14, No. 9, September 1976, pp. 1201-1205.

22. Wang, B.P., "Improved Approximate Methods for Computing Eigenvector Derivatives in Structural Dynamics," *AIAA Journal,* Vol. 29, No. 6, June 1991, pp. 1018-1020.

23. Creamer, N. G., "Identification of Linear Structural Models," DhD Dissertation, Virginia Polytechnique Institute and State University, March 1987.

24. Juang, J. N. and R. S. Pappa, "An Eigensystem Realization Algorithm for Modal Parameter Identification and Model Reduction," *Journal of Guidance, Control and Dynamics,* Vol. 9, No. 3, May-June 1986, pp. 294-303.

25. Ibrahim, S. R., and E. C. Mikulcik, "A Method for the Direct Identification of Vibration Parameters from the Free Response," *Shock and Vibration Bulleting,* No. 43, pp. 21-37, 1973.

26. EE 6714 System Identification class notes, Professor Dr. S. P. Bingulac, Virginia Polytecnique Institute and State University, Sring 1992.

27. Sinha, N. K. and B. Kuszta, *Modeling and Identification of Dynamic Systems,*Van Nostrand Reinhold Company, New York, NY, 1983.

28. Chen, C. T., *Linear System Theory and Design,* Holt, Rinehart and Winston, New York, NY, 1970.

29. Andry, A. N., Jr., E. Y. Shapiro and J. C. Chung, "Eigenstructure Assignment for Linear Systems," *IEEE Transactions on Aerospace and Electronic Systems,* Vol. AES-19, No. 5, September 1983.

The vita has been removed from the scanned document